

Reconstructing the middle to late Pleistocene explosive eruption histories of Popocatepetl, Iztaccíhuatl and Tláloc-Telapón volcanoes in Central México

Ivan Sunyé-Puchol^{1,2*}, Alastair G.E. Hodgetts³, Sebastian F.L. Watt³, José L. Arce⁴, Dan N. Barfod⁵, Darren F. Mark⁵, Giovanni Sosa-Ceballos⁶, Claus Siebe⁷, Ross C. Dymock⁵, Maarten Blaauw⁸ and Victoria C. Smith¹

¹ Research Laboratory for Archaeology and the History of the Art (RLAHA), School of Archaeology, University of Oxford, Oxford, UK

² Department of Earth Sciences, University of Rome - La Sapienza, P. le Aldo Moro 5, 00185 Roma, Italy

³ School of Geography, Earth and Environmental Sciences, University of Birmingham, Edgbaston, Birmingham, UK

⁴ Instituto de Geología, Universidad Nacional Autónoma de México, Cd. de México, México

⁵ NEIF Argon Isotope Laboratory, Scottish Universities Environmental Research Centre (SUERC), East Kilbride, UK

⁶ Unidad Michoacán del Instituto de Geofísica, Universidad Nacional Autónoma de México, Ciudad de México, México

⁷ Departamento de Vulcanología, Instituto de Geofísica, Universidad Nacional Autónoma de México, Cd. de México, México

⁸ The ¹⁴CHRONO Centre for Climate, the Environment and Chronology, School of Natural and Built Environment, Queen's University Belfast, Belfast, UK.

* Corresponding author (e-mail: ivan.sunyepuchol@uniroma1.it)

Abstract

The Sierra Nevada Volcanic Range (SNVR), which includes Popocatepetl, Iztaccíhuatl and Tláloc-Telapón volcanoes, has been the source of multiple large explosive eruptions that have dispersed tephra across central México. Several eruptions since 40 ka have previously been described, particularly from Popocatepetl, the southernmost volcano of the range. However, the longer-term eruption history of the SNVR is poorly understood, due to challenges with correlating limited exposures of older pyroclastic sequences, and in discriminating between tephra derived from different sources. Here we describe two extensive exposures located between Popocatepetl and Iztaccíhuatl volcanoes, which provide a more complete and longer-term explosive eruption record of the SNVR: the Nepopualco and Xalitxintla tephra sequences. A detailed tephrostratigraphic survey, together with new ⁴⁰Ar/³⁹Ar geochronological analyses and glass geochemistry, has permitted the characterization of identified eruption units further leading to the determination of geochemical fields for each volcano and the subsequent discernment of volcanic sources. Our results show that, since the collapse of Los Pies Cone, which destroyed the Paleo-Iztaccíhuatl edifice at 631 ± 44 ka (2σ), Iztaccíhuatl has produced

at least 6 explosive rhyolitic eruptions. After coeval activity with Popocatepetl, between ~600 and ~500 ka, Iztaccíhuatl's explosive activity ceased while Popocatepetl's continued until present day. Popocatepetl has produced at least 27 medium to large explosive eruptions (inferred VEI 4-6), commonly of andesitic to dacitic compositions. Some of these eruptions deposited pumice fallout of >1 m thick in both the Nepopualco and Xalitlintla sequences (e.g. the 339 ± 16 ka [2 σ] NT-23/WRT-7 eruption), suggesting that Popocatepetl has produced several eruptions similar in magnitude to well-known the ~14 ka Tutti Frutti Pumice (a VEI 6 eruption with a ~5 km³ tephra volume). The Popocatepetl and Iztaccíhuatl tephras are interbedded with deposits from more distal volcanoes, including some mafic to intermediate products of unknown sources (possibly from nearby monogenetic cones) and tephras related to the late Pleistocene eruptions of Tláloc-Telapón (including the tephra layer produced by the San Valentin Ignimbrite, recently ⁴⁰Ar/³⁹Ar dated in this study at ~102 ka; 2 σ). Our new chemical, stratigraphic and geochronologic investigations of these pyroclastic deposits, predominantly from Popocatepetl and Iztaccíhuatl, provide information on the scale and frequency of medium to large magnitude explosive eruptions over a longer-time period than currently known and that have had potential to disperse tephra across central México since the middle to late Pleistocene. This new data can be used to determine the source of further unknown tephras in the region as well as to better assess the volcanic hazard to the densely populated megalopolis of México City.

Keywords: Chronostratigraphy, glass chemistry, México, Popocatepetl, tephra, volcanic history

1. Introduction

The metropolitan area of México City and its ~25 million inhabitants sit within the México Basin, which is surrounded by several Pleistocene-Holocene volcanoes of the Trans-Mexican volcanic belt (TMVB; **Fig. 1**). These volcanoes include Popocatepetl, Iztaccíhuatl, and Tláloc-Telapón, which constitute the Sierra Nevada Volcanic Range (SNVR) to the east of the city. Their explosive activity, as well as those of volcanoes west of the México Basin, is fairly well-constrained for the last 30 ka, as the associated deposits are clearly visible in some accessible exposures (e.g. [Ortega-Guerrero et al., 2018](#); [Arce et al., 2003](#); [Sosa-Ceballos et al., 2012](#); [Rueda et al., 2013](#); [Siebe et al., 2017](#)). However, their longer-term eruption history is poorly understood, due to burial and erosion of older deposits, and challenges with correlating the available isolated exposures based on the deposit physical characteristics alone. These isolated

exposures have not been studied in detail but contain valuable information that permits reconstruction of a longer and more complete record of explosive volcanism from the SNVR. This is important for evaluating the frequency of large-magnitude explosive eruptions in the region, and for improving our knowledge of the temporal and spatial development of the major volcanic centres in the area.

Here we present detailed chronostratigraphic logs and the glass chemical composition of tephtras recorded in two extensive exposures (Nepopualco and Xalitizintla sites), supplemented by a small number of shorter sequences, along the SNVR (**Fig. 1b and c**). We use these to characterize the proximal pyroclastic products of Iztaccíhuatl, Popocatepetl and Tláloc-Telapón volcanoes (the three main edifices of the SNVR), and to extend and develop our understanding of their explosive eruption histories. These SNVR volcanoes have been the most active stratovolcanoes near the México basin during the middle to late Pleistocene (Cadoux et al., 2011; Macías et al., 2012). Our geochemical and geochronological data from Nepopualco and Xalitizintla constrain the range of magma compositions erupted from Popocatepetl and Iztaccíhuatl, and the timing of their eruptions over the last ~600 thousand years (ka), and constitute the first step to establishing a long-term record of the medium to large explosive eruptions from the volcanoes surrounding México City.

2. Geological framework and volcanic evolution of the Sierra Nevada Volcanic Range

The México Basin (**Fig. 1b**) is an endorheic basin closed by the Sierra de Las Cruces Volcanic Range (SLCVR, Mora-Alvarez et al., 1991; Arce et al., 2017) to the west, the SNVR to the east (Nixon, 1989; Cadoux et al., 2011; Macías et al., 2012), and the Sierra Chichinautzin Volcanic Field (SCVF, Siebe et al., 2004; Jaimes-Viera et al., 2018) to the south. The basin closed ~1 Ma ago, when monogenetic cones and lavas of the SCVF blocked drainage to the south resulting in the lower México Basin gradually filling with water (Mooser, 1963; Arce et al., 2013), and facilitating the rapid accumulation of lake sediments (e.g., Martínez-Abarca et al., 2021). The magmatism around the México Basin is related to the 3rd phase of the TMVB (**Fig. 1a**), a 1000 km-long Neogene continental arc related to the subduction of the Cocos and Rivera plates beneath the North American plate (Ferrari et al., 2012), active since 20 Ma. The locus of the TMVB migrated towards the trench at ~7 Ma, coinciding with an increase in silicic volcanism along the arc (Gómez-Tuena et al., 2007).

99 2.1. Sierra Nevada Volcanic Range (SNVR)

100 The SNVR forms a N-S oriented range (**Fig. 1c**) that divides drainage between the México
101 Basin to the west and the Puebla basin to the east (**Fig. 1b**). There are four large volcanic
102 edifices in the range (**Fig. 1b and c**); from north to south they are: Tláloc (the “Aztec's God of
103 Rain” in the Náhuatl language) - Telapón (“flat mountain” in Spanish), Iztaccíhuatl (“the
104 woman in white” in Náhuatl), and Popocatepetl (“smoking mountain” in Náhuatl). In this paper
105 we group Tláloc and Telapón volcanoes following the criteria of [Macías et al. \(2012\)](#), as they
106 are perceived to be a single volcanic complex (i.e., compound volcano; **Fig. 1c**). Minor
107 monogenetic vents are also present along the SNVR, such as El Papayo that emitted lava flows
108 ~118 ka ago ([Macías et al., 2012](#)). The volcanic activity of the SNVR is thought to have
109 commenced at its northern tip at Tláloc-Telapón volcano at ~1.82 Ma ([García-Palomo et al.](#)
110 [2002](#); [Cadoux et al. 2011](#); [Macías et al., 2012](#)). This age is based on dated lavas, which occur
111 as blocks within pyroclastic density current (PDC) deposits, inferred to have originated from a
112 Paleo-Tláloc edifice ([Cadoux et al., 2011](#)). Subsequent activity migrated to the south and
113 emplaced the Paleo-Iztaccíhuatl volcano (Llano Grande, ~1.09 Ma; [Cadoux et al., 2011](#)) and
114 then further south again, at the Paleo-Popocatepetl volcano (Tlamacas/Nexpayantla, ~538 ka;
115 [Robin and Boudal, 1987](#); [Conte et al., 2004](#); [Sosa-Ceballos et al., 2015](#); [Delgado-Granados et](#)
116 [al., 2017](#)). Although Tláloc-Telapón is the site of the oldest activity of the SNVR, its eruptive
117 history has continued until the very late Pleistocene, evidenced by deposits of ignimbrite-
118 forming eruptions that are < 50 ka (e.g., [Macías et al., 2012](#)), indicating possible coeval activity
119 with Iztaccíhuatl and Popocatepetl volcanoes ([Rueda et al., 2013](#)).

120 2.1.1. Tláloc-Telapón

121 This volcanic complex comprises the lowest elevation edifices of the SNVR, at 4,120 (Tláloc
122 crater) and 4,080 (Telapón crater) meters above sea level (m.a.s.l.). Located ~40 km east from
123 the centre of México City, Tláloc-Telapón is primarily composed of dacitic domes and lava
124 flows, and surrounded by ignimbrites and lahar deposits ([Cadoux et al., 2011](#)). Radiometric
125 dates of Paleo-Tláloc lavas yield ages that extend to 1.82 Ma ([González and Huddart, 2004](#);
126 [Rueda et al., 2007](#); [García-Tovar and Martínez-Serrano, 2011](#); [Cadoux et al., 2011](#) [Macías et](#)
127 [al., 2012](#)). The modern Tláloc-Telapón volcano began its construction at ~0.94 Ma by the
128 effusion of dacitic lavas. This constructional phase ended with the extrusion of the summit lava
129 flows and domes between 0.64 – 0.27 Ma ([Cadoux et al., 2011](#); [Macías et al., 2012](#)). Activity
130 at the Tláloc crater appears to have resumed at 129 ka with the emission of rhyolitic lava flows

and domes, that are distributed to the east of the present summit dome and within a 2.5-km-wide horseshoe-shaped collapse structure (Macías et al., 2012; Rueda et al., 2013).

Several authors have identified and characterized numerous pyroclastic deposits exposed proximally to Tláloc-Telapón, which have been ascribed to that volcano (e.g., Cornwall, 1971; Huddart and González, 2004; Rueda et al., 2006; Meier et al. 2007; Macías et al., 2012). The youngest deposits include at least five Plinian eruptions that produced PDCs ranging in age from 44,000 to 21,000 14C yr BP (Macías et al., 2012). They are, from oldest to youngest: San Valentín (45,990-46,895 cal. yr BP, 95% probability [2 σ]; 44,195 + 2020/-1615 yr BP), La Joya (40,668-42,807 cal. yr BP, 2 σ ; 37,220 \pm 890 yr BP), P-Mex (36,498-39,375 cal. yr BP, 2 σ ; 33,180 \pm 550 yr BP), Multilayered White Pumice (MWP, 35,578-36,137 cal. yr BP, 2 σ ; 31,490 +1995/-1595 yr BP) and Cuauhtémoc (29,909-30,065 cal. yr BP, 2 σ ; 25,640 +275/-265 yr BP) ignimbrites. A relatively recent lava covers the crater at the summit of Tláloc (Rueda et al. 2013), and this is overlain by the ~5.4 cal. ka BP Ochre Pumice eruption deposit from Popocatepetl volcano (Siebe et al., 1996; Arana-Salinas et al., 2010). This indicates that the last known activity at the volcano was pre-5 ka but given the occurrence of multiple late-Pleistocene explosive eruptions and limited exposure in the region, Tláloc-Telapón should still be considered an active volcano.

2.1.2. Iztaccíhuatl

The morphology of Iztaccíhuatl volcano has been likened to a woman lying on her back along a NNW–SSE direction with her head to the north (Figs. 1c and 2a; Macías et al., 2012). This volcano is located ~47 km ESE from the international airport of México City (Fig. 1b), and consists of four peaks (Macías et al., 2012): La Cabeza (the head), El Pecho (the breast), Las Rodillas (the knees) and Los Pies (the feet). El Pecho is the highest peak and reaches 5286 m.a.s.l. The evolution of Iztaccíhuatl is divided into two main phases of cone growth: first, the Older Volcanic Series, including the activity of Paleo-Iztaccíhuatl and the construction of Llano Grande, a shield volcano ~1.09 Ma (Nixon, 1989; Cadoux et al., 2011); and second, the Younger Volcanic Series, represented by lavas and domes emplaced between 600 and 80 ka (e.g., the El Solitario or Téyotl dacite flow; Nixon et al. 1988; Nixon, 1989; Macías et al., 2012).

A major event in the evolution of modern Iztaccíhuatl involved a sector collapse of the Los Pies cone (Siebe et al., 1995; García-Tenorio, 2008). The volume of the debris avalanche deposit is estimated to be ~1.5 km³, and the deposits cover an area of 550 km² on the SE flank

of the volcano (**Fig. 1c**). Los Pies Debris Avalanche Deposit (LPDAD) is overlain by a sequence of PDCs – block & ash-flow type deposits associated with an eruption that followed the sector collapse (Macías et al., 2012; García-Tenorio et al., 2012). An $^{40}\text{Ar}/^{39}\text{Ar}$ date on plagioclase from juvenile pumices of these PDCs yielded an age of 440 ± 190 ka for the LPDAD (Macías et al., 2012). All of these deposits are towards the base of Nepopualco gully, a key outcrop in this study and site of preliminary description by García-Tenorio et al. (2015).

2.1.3. Popocatepetl

Popocatepetl is the most active volcano of the SNVR and considered one of México's most dangerous volcanoes (e.g., Macías et al., 2020), posing significant risk to the densely populated region as more than 25 million people who live within 100 km of its vent. Located ~45 km SE from México City, Popocatepetl volcano is 5452 m.a.s.l, forming the highest peak of the SNVR, and the second highest in México. After ~70 years of inactivity, Popocatepetl erupted again in 1994. This new activity typically comprises pulsating emissions of tephra and fumarolic gases (Love et al., 1998; Goff et al., 1998; Stremme et al., 2011), associated with subsequent episodes of rapid lava dome growth at the summit crater (Macías and Siebe, 2005; Gómez-Vázquez et al., 2016), as well as some Vulcanian-style explosions that emplace PDCs and lahar deposits (e.g., the 2001 explosion; Macías et al., 2020).

The modern edifice of Popocatepetl (**Fig. 2a**), which is mostly comprised of andesitic to dacitic lava flows (Robin, 1984), is constructed over the remnants of previous edifices (~538 ka; Conte et al., 2004; Sosa-Ceballos et al., 2015; Delgado-Granados et al., 2017). A sector collapse produced an extensive debris avalanche deposit to the south at ~27.8 cal. ka BP (~23.5 ka BP; Siebe et al., 2017). This was accompanied by the Plinian White Pumice fallout, also dispersed to the south (Robin and Boudal, 1987; Siebe et al., 1993, 1995, 2017). Since then, Popocatepetl has produced at least six Plinian eruptions, including the 16,796-18,201 cal yr BP Tutti Frutti caldera-forming eruption (2σ ; recalibrating dates of Siebe et al., 2017 and references therein using the northern hemisphere calibration curve IntCal20 (Reimer et al. 2020) and OxCal (Bronk Ramsey, 2009), which is assumed to be the largest eruption from Popocatepetl based on its widespread distribution and distal thickness (e.g., 10 cm in modern México City, Siebe et al., 1999; Sosa-Ceballos et al., 2012). Three Plinian eruptions have been identified during the Holocene: the 5,333-5,509 cal. yr BP Ochre Pumice (2σ ; recalibrating dates of Robin and Boudal 1987; Siebe et al., 1997; Arana-Salinas et al., 2010), 2,150 yr Lorenzo Pumice (Siebe and Macías, 2006), and 1,100 yr BP Pink Pumice (Siebe et al., 1996). These eruptions had dispersal axes to the NE (Panfil et al., 1999; Siebe and Macías, 2006). Siebe et al. (1996) noted

that these three Holocene eruptions began with the emplacement of dilute PDCs, followed by extensive pumice fallouts, and ended with the emplacement of dense PDCs.

2.1.4. Summary of the SNVR state-of-the-art

The eruptive history of the SNVR, and particularly the record of the middle to late Pleistocene explosive activity of the stratovolcanoes, is still poorly constrained. For Tláloc-Telapón, five late Pleistocene ignimbrites have been identified and dated (Cornwall, 1971; Huddart and González, 2004; Rueda et al., 2006; Meier et al., 2007; Macías et al., 2012), but the only radiometric ages available are radiocarbon ages, and the glass chemistry of the units have not yet been characterized. For Iztaccíhuatl, only the collapse of Los Pies Cone and its associated avalanche and ignimbrites are dated by $^{40}\text{Ar}/^{39}\text{Ar}$ (Macías et al., 2012). Other pyroclastic deposits attributed to Iztaccíhuatl have been recognised in the Nepopualco gully (Section 4.1.2; García-Tenorio et al., 2012), but no chemical, stratigraphic or chronological results have been previously published. Popocatepetl has been the subject of several geological studies in the last three decades (e.g. Siebe et al., 1995; 1996; 2017; De la Cruz-Reyna et al., 1995; Espinasa-Pereña and Martín-Del Pozzo, 2006; Arana-Salinas et al., 2010; Sosa-Ceballos et al., 2012), resulting in the stratigraphy of explosive eruptions for the last ~30 ka being fairly well-constrained. However, there is a lack of detailed tephrostratigraphic studies, including glass chemistry, for older sequences, which are likely to date back to around 540 ka when the construction of the Paleo-Popocatepetl is estimated to have commenced (e.g., Delgado-Granados et al., 2017).

3. Methods

3.1. Field work

Logging and sampling of the middle to late Pleistocene tephra from the SNVR volcanoes was carried out in March 2019. Published volcanological data was reviewed (e.g., Macías et al., 2012; Rueda et al., 2013; Sosa-Ceballos et al., 2015; Siebe et al., 2017) and the fieldwork was supported by researchers from the National Autonomous University of México (UNAM). Fieldwork was undertaken in accessible, well-exposed outcrops, near the villages of Nepopualco and Xalitlintla (**Fig. 1**). Roadcuts, deep gullies and quarries, that display multiple tephra units, bound by palaeosols often developed on top of reworked volcanoclastic materials (remobilized products of preceding eruptions that we have interpreted to have been redeposited by dilute lahars, or by other non-volcanic processes) were the focus for this study. Thickness and grain size were measured for each tephra layer, and the textures, colour and concentration

of lithics were described. Samples of all units were taken for glass chemical analysis and thick and coarse tephras were sampled for $^{40}\text{Ar}/^{39}\text{Ar}$ dating. Localities are mapped on **Figure 1c** (DEM of 15 x 20 m precision downloaded from INEGI-México: <https://www.inegi.org.mx>), and described in **Tables 1 – 3**, including locality names and GPS coordinates. All tephra samples were given a unique sample number that was prefixed with ‘MXC-’ in the field, while individual eruption units (comprising a single event) were given a name that related to the specific site once determined, counting upwards from the base of the exposure (e.g., NT-1, for the oldest exposed tephra in the Nepopualco sequence).

3.2. Glass chemistry

Representative samples of multiple pumice clasts or of bulk ash were collected, depending on the grain-size of the tephra layers, for glass chemical analysis. Tephras were sampled vertically across the deposit to provide a compositionally representative sample and include possible internal compositional variations. Samples were cleaned, crushed, sieved, dried, and mounted in epoxy resin. Mounts were polished and photographed with a petrographic microscope to assess shard morphology and mineralogy (**Tables 1, 2, and 3**). These mounts were then carbon-coated prior to measuring the major element concentrations of glass shards using a JEOL JXA-8200 electron microprobe (EMP) equipped with five wavelength-dispersive spectrometers, Research Laboratory for Archaeology and the History of the Art (RLAHA), University of Oxford (UK). A beam accelerating voltage of 15 kV was used with a 6 nA current and a beam diameter of 10 μm . A narrower beam of 5 μm was used for a few highly vesicular samples. The EMP was calibrated using a suite of mineral standards. This calibration was verified using a range of secondary glass standards (ATHO-G, StHs6/80-G and GOR128-G; see **Supplementary Material 1**; [Jochum et al., 2006](#)). Approximately 25 glass analyses, from separate glassy fragments derived from the crushed and sieved samples, were obtained for each of the 71 samples. This includes 25 previously undescribed tephra deposits from Nepopualco, 27 from Xalitziñtla, and new characterisation of 13 previously identified and named tephra deposits known to originate from Tláloc-Telapón, Popocatepetl and Iztaccíhuatl (e.g. [Macías et al., 2012](#); [Siebe et al., 2017](#)), sampled from other sites around the SNVR (**Fig. 1c**; and listed as the 13 non-Nepopualco tephras in **Table 1**). All glass compositions were normalized to 100% for comparative purposes.

3.3 Argon-Argon geochronology

Samples for $^{40}\text{Ar}/^{39}\text{Ar}$ dating were taken from the thickest and coarsest tephras with large phenocrysts (including hornblende, plagioclase and sanidine). These samples were collected from units in the Nepopualco Sequence and the various Xalitlintla outcrops. The stratigraphically oldest Tláloc ignimbrite was also sampled for dating. Clean pumice clasts were separated from bulk samples and crushed to obtain juvenile-hosted mineral concentrations. Crushed samples were sieved to 250-500 μm fractions then washed using an ultrasonic bath to remove adhering dust particles. Bulk feldspar was magnetically separated from amphiboles and pyroxenes and subsequently separated into sanidine and plagioclase fractions using lithium metatungstate (LMT) heavy liquid (density $\sim 3.7 \text{ mg/l}$). Feldspars and amphibole were acid-leached following methods of Siegburg et al. (2018) prior to being hand-picked under binocular microscope to avoid inclusion-rich or altered crystals. Samples were irradiated at the Oregon State University (OSU) Irradiation Center using the CLICIT facilities and analysis was carried out in the NEIF Argon Isotope Laboratory at SUERC. Single crystals of sanidine were fused at $\sim 7 \text{ W}$ in a single step. Plagioclase and hornblendes were analysed in multigrain aliquots of ~ 30 crystals that were heated in two-steps: a low power (0.6W) degassing step followed by a fusion step at $\sim 7 \text{ W}$. Sample aliquots with high-age uncertainties ($>100\%$) or negative ages were rejected; this resulted in $< 5\%$ of the analyses being removed from the data set. The remaining data were then filtered principally against MSWD criteria (see **Supplementary material 2**). Approximately 25 analyses of aliquots were plotted together (see **Supplementary material 3**) in order to achieve a precision of $\sim 10\%$ (2σ) for each sample.

4. Field tephrostratigraphy

4.1 Characterisation of previously identified proximal deposits of the SNVR volcanoes

Several sites around the SNVR (**Fig. 1**) were visited in order to sample deposits of large explosive eruptions from previously identified exposures. These samples were analysed to provide insights into the glass compositional range of each SNVR volcano, which could be used to interpret the origin of other previously undescribed tephras from our study sites (**Table 1**).

4.1.1. Tláloc-Telapón

The fieldwork around Tláloc-Telapón was focused on sampling the deposits of previously identified late Pleistocene ignimbrites (Rueda et al., 2007; 2013; García-Tovar and Martínez-Serrano, 2011; Macías et al., 2012) to chemically characterize their glass chemistry (outcrops 1 to 4 in **Fig. 1c**). Three separate ignimbrites (MWP, San Valentín, and Cuauhtémoc) were

sampled from several sites. The oldest of these, the San Valentín Ignimbrite, was sampled for both radiocarbon and $^{40}\text{Ar}/^{39}\text{Ar}$ dating to corroborate the previously published radiocarbon age of ~ 46 cal. ka BP (Macías et al., 2012), particularly because the age is close to the upper limit of the radiocarbon method and may thus be less reliable. Details of the Tlálloc PDCs and the physical parameters of the associated eruptions (e.g., distribution, column height, and magma volume) are documented in Macías et al. (2012) and Rueda et al. (2013).

4.1.2. Popocatepetl and Iztaccíhuatl

Four previously described pumice fall deposits (Pink, Lorenzo, White and Tutti Frutti) from < 30 ka Plinian explosive eruptions of Popocatepetl (e.g. Sosa-Ceballos et al., 2012; Siebe et al., 2017), were sampled from four separate sites around the volcano (Fig. 1). Two subunits from the Tutti Frutti and Pink Pumice deposits were analysed (Pink 1 and 3 from the Pink Pumice; and the Milky and Grey Pumice units from the Tutti Frutti eruption; Table 1). Due to limited exposures, challenging access, and the close spacing between volcanic sources, only one pyroclastic deposit has been previously described and categorically ascribed to Iztaccíhuatl, the Los Pies B&A Flow (Table 1; Macías et al., 2012; García-Tenorio et al., 2012; 2015). As multiple eruptions help to better classify the compositional range of the deposits of a volcano, we have included an additional, previously undescribed deposit towards the base of the Nepopualco sequence: the Nepopualco Ignimbrite (Table 1, Fig. 3). This deposit is comprised of dilute PDC deposits and a pumice fall (Nepopualco Fall, Table 1, Fig. 3), interpreted to have been produced in a single eruptive event (i.e. in conformable contact and not separated by a paleosol and/or reworked deposits). The following observations suggest Iztaccíhuatl was the source: (1) The geomorphology of the gully lies within a deep fan to the East of Iztaccíhuatl (see section 4.2 and Fig. 1c). Topographically, due to PDCs being gravity-driven currents, the location of this primary ignimbrite deposit implies emplacement from the west, and the local terrain of the Puebla basin does not feasibly support a transport direction from any other volcano in the SNVR (Fig. 1c); (2) Glass data from these deposits are similar to the underlying Los Pies B&A Flows (documented below; Fig. 10, Table 4); (3) $^{40}\text{Ar}/^{39}\text{Ar}$ Ages from the Nepopualco Ignimbrite, 631 ± 44 ka [2σ], are consistent with known activity from Iztaccíhuatl, and older than any dated deposits of Paleo-Popocatepetl (~538 ka; Robin and Boudal, 1987; Conte et al., 2004; Sosa-Ceballos et al., 2015; Delgado-Granados et al., 2017).

4.2 Nepopualco and Xalitzintla sites

The remainder of our fieldwork concentrated on the numerous additional well-preserved tephra units in the Nepopualco exposure, and at the additional site of Xalitzintla (outcrops 6-9 in **Fig. 1c**), ~10 km to the SSW. These two sites lie roughly at the same distance from Iztaccíhuatl and Popocatepetl (~20 km), so the tephra at Nepopualco and Xalitzintla outcrops could be from either volcano.

4.2.1 Nepopualco tephra sequence

The Nepopualco site is located ~14 km east of Iztaccíhuatl and 19 km NE of Popocatepetl (outcrop 5 in **Fig. 1c**) and preserves pyroclastic deposits of at least 25 different eruptive events within a 150-m-deep gully (**Table 2; Fig. 2b**). The Nepopualco tephra sequence overlies the LPDAD (MXC-01, **Fig. 2b**), which forms an extensive, low-gradient and elevated debris fan, onto which the thick pyroclastic deposits have accumulated. The fan is deeply incised by numerous gullies, and a recent landslide in the northern wall of the Nepopualco gully (triggered by the 2017 M 7.1 earthquake with an epicentre ~40 km south of Popocatepetl volcano; [Mirwald et al., 2019](#); **Fig. 2b**) exposes a horizontally stratified sequence of the pyroclastic deposits. The sequence was described from several exposures observable along a footpath that goes from Nepopualco town to the river that drains at the bottom of the gully. All tephra deposits are separated by palaeosols that have developed at the top of each tephra unit, or by layers of reworked volcanoclastic material that often overlie erosive surfaces at the top of the underlying tephra. These volcanoclastic layers commonly also display palaeosols developed at their tops (see stratigraphic logs in **Fig. 3b, 4b and 5c**). Apart from the stratigraphic and textural characteristics of the tephra units, the glass compositions, mineralogy and chronological information (Section 5 and 6) have been used to distinguish the tephra units. As this section is mainly focused on the hitherto undescribed Nepopualco pyroclastic deposits, we direct the reader to **Figures 3, 4 and 5** for further details regarding the reworked volcanoclastic deposits and palaeosols between tephra units. Additionally, for simplicity, primary pyroclastic deposits with angular pumice, which are well-sorted and clast-supported, are interpreted as tephra fallouts deposits, while primary pyroclastic deposits with sub-angular to sub-rounded pumice, poorly sorted in a matrix of volcanic ash, are interpreted as PDC deposits (ignimbrites). Given the large number of tephra units in the Nepopualco sequence, the stratigraphy has been divided in three subgroups: Lower, Middle and Upper Nepopualco tephra units. The limit between subgroups was defined by the presence of particularly thick (up to 3 m) reworked units with

palaeosols developed at the top (see logs in **Figs. 3, 4, and 5**), possibly indicating long hiatuses of volcanic activity.

4.2.1.1. Lower Nepopualco tephras

The lowermost pyroclastic unit in the Nepopualco sequence is the Los Pies B&A Flows deposit (ignimbrite related to the LPDAD; [Macías et al., 2012](#); [García-Tenorio et al., 2012; 2015](#)). This thick unit (up to 30 m), is labelled as NT-1 (all tephras are numerically named with increase in stratigraphic order from base to top, **Fig. 3b and c; Table 2**). The next unit (NT-2, which we have named here Nepopualco Ignimbrite as described in section 4.1.2 and attributed to Iztaccíhuatl volcano) is a 6-cm-thick unit comprised of multiple brown laminated PDCs of coarse to medium ash (MXC-03; the Nepopualco dry PDCs), followed by 15 cm of cross-stratified white PDCs (MXC-04; Nepopualco wet PDCs), and a 85-cm-thick reversely graded pumice fallout of fine to medium lapilli (MXC-05; Nepopualco Fall; **Fig. 3b and c**). NT-3 is a 35-cm-thick pumice fallout of medium lapilli that is yellowish in colour (MXC-06, **Fig. 3b**) and rich in lithics. NT-4 is a fallout unit that is 52-cm-thick and comprised of white fine to medium pumice lapilli (MXC-07, **Fig. 3b and d**), which is diffusely laminated and crystal-rich. NT-5 is a 30-cm-thick fallout unit of dark grey coarse ash, and comprised of clasts that are poorly vesicular with large phenocrysts (MXC-08). NT-6 is an 18-cm-thick fallout deposit of medium to coarse grey pumice lapilli (MXC-09). NT-7 is a 70-cm-thick bedded fallout deposit (MXC-10, **Fig. 3a, b, and e**) of grey coarse lapilli pumice and rich in lithics (especially in the upper 20 cm). NT-8 is a lens of ignimbrite up to 80 cm in thickness, with large white pumice clasts (up to 10 cm) in a brown ash matrix (MXC-11, **Fig. 3b and e**). NT-9 is a 35-cm-thick, lithic-rich fallout deposit of scoria and orange crystal-rich pumice (MXC-12, **Fig. 3b and f**). The uppermost tephra of this Lower Nepopualco sequence (NT-10) is a bedded 90-cm-thick fallout of lithic-rich, coarse pumice lapilli with darker ash layers in the uppermost part (MXC-13, **Fig. 3b and f**).

4.2.1.2. Middle Nepopualco Tephras

The first tephra unit of this subgroup (NT-11) is a 70-cm-thick fallout unit of a bedded white pumice that is normally graded, with clasts ranging from coarse to medium lapilli and rich in fine lithics (<0.5 mm), larger near the top, that grades into a 25-cm-thick ignimbrite (MXC-14, **Fig. 4a, b, and c**). NT-12 is a 55-cm-thick fallout deposit of coarse orange pumice lapilli (MXC-15, **Fig. 4a, b, and d**), rich in coarse lithics (0.5 – 2 cm, especially in the upper 20 cm). NT-13 is a 25-cm-thick orange pumice fallout consisting of a 10-cm-thick sub-unit of medium lapilli with fine lithics at the base (MXC-35) and a 15-cm-thick sub-unit of fine lapilli in a dark

matrix at the top. NT-14 is an 8-cm-thick medium lapilli pumice fallout (MXC-36, **Fig. 4e**). NT-15 is a 15-cm-thick lithic-rich fallout comprised of fine to medium lapilli pumice (MXC-37, **Fig. 4g**). The NT-16 tephra layer is a 27-cm-thick reverse graded fallout unit of white coarse ash to fine lapilli pumice (MXC-38). NT-17 is a 51-cm-thick fallout sequence that starts with 4 cm of dark ash followed by 20 cm of medium to fine pumice lapilli (normally graded) rich in lithics (MXC-39), with another 3-cm-thick layer of dark ash, followed by 24 cm of coarse orange pumice with few coarse lithics (0.5 – 2 cm) at the top (MXC-40; **Fig. 4 b**). NT-18 is a 90-cm-thick pumice fallout with a couple of fine ash layers in the middle (**Fig. 4f**): the first 30 cm are a coarse orange fallout deposit (rich in lithics towards the top), followed by a thin layer (3 cm) of fine and hardened white ash, 39 cm of bedded pumice (MXC-41), another fine ash layer (2 cm), and a 16-cm-thick unit of medium to fine pumice lapilli.

4.2.1.3. Upper Nepopualco tephras

The first tephra of this subgroup (NT-19) is a 30-cm-thick white pumice fallout with medium lapilli and small lithics (MXC-42, **Fig. 5a and c**). NT-20 is an 8-cm-thick dark fallout unit comprised of lithics (> 70%) and a few fine lapilli pumices and coarse ash (MXC-43, **Fig. 5a and c**). NT-21 is a 35-cm-thick fallout of weathered orange pumice, comprised of coarse lapilli rich in lithics (MXC-44, **Fig. 5a and c**). NT-22 is a 77-cm-thick fallout unit of coarse orange lapilli rich in lithics (MXC-45, **Fig. 5b and c**). NT-23 is a 160-cm-thick, medium to coarse white lapilli fallout unit (MXC-46, **Fig. 5b and c**). At the top of the Nepopualco outcrop are two zones of white ash pods within 2 m of soil developed in reworked deposits: the first pod (NT-24) is a fallout unit up to 10 cm thick and comprised of very fine ash (MXC-47, **Fig. 5d and e**), and the second fallout (NT-25) is comprised of medium ash that is rich in biotite (MXC-48, **Fig. 5d and f**). Overlying NT-25 is the present-day soil.

4.2.2. Xalitzintla

Tephra layers deposited in the Xalitzintla region are exposed in roadcuts and quarries along the Paso de Cortés road (outcrops 6-9, **Fig. 1c and 6a**) and within Xalitzintla town. The town is located in a wide valley between the southern margin of the LPDAD and the NE limits of Popocatepetl's flank (**Fig. 1c and 6a**). The Xalitzintla exposures are located on the northern side of this valley. The sequences described here are from four separate exposures (**Table 3**): 1) East of the Restaurant, 2) West of the Restaurant, 3) Fork in the road, and 4) Xalitzintla Quarry. The chronostratigraphic order of these sites will be discussed later in section 7, and cannot be determined from field characteristics or topographic relationships, due to discontinuous exposures and an absence of visually correlatable horizons. The Xalitzintla

tephras are all fallouts and commonly bound by reworked volcanoclastic materials with palaeosols at the top (see stratigraphic logs in **Figs. 6c, 7c, 8c, and 9b**).

4.2.2.1 East of the Restaurant

At least seven different pyroclastic deposits are preserved in this outcrop (ERT-1 to 7, numerically named in stratigraphic order from base to top, as in Nepopualco; **Fig. 6b and c**), which is located east of the Montaña Fresca Burger restaurant (point 6 in **Fig. 6a**). The lowermost tephra (ERT-1) is a 43-cm-thick, normal graded, orange weathered pumice fallout (sample MXC-16; **Fig. 6c and d**) displaying coarse to medium lapilli. Two types of pumice comprise this deposit: one is grey exhibiting felsic phenocrystals and the other is pink with occasional mm-sized mafic crystals. ERT-2 is a 37-cm-thick, lithic-rich fallout unit, which consists of two normally graded subunits of coarse pinkish pumice lapilli to coarse ash at the top (MXC-17 and 18, **Fig. 6e**), that are separated by a thin layer of lithics. ERT-3 is a distinctive 78-cm-thick fallout sequence made up of several horizontally bedded sub-units separated by lithic-rich horizons (MXC-19 and 20, **Fig. 6c and f**). The base of this sequence is a 7-cm-thick coarse ash fall with a 0.5-cm-thick lithic-rich layer at the top, followed by eight ~10-cm-thick (each) layers of white medium lapilli pumice. ERT-4 is a grey 5-cm-thick ash fallout layer (MXC-21) and ERT-5 a 20-cm-thick medium to coarse pumice lapilli fallout layer (MXC-22). ERT-6 is a 35-cm-thick fallout unit of medium pumice lapilli (MXC-23). The uppermost tephra of this outcrop (ERT-7) is a 30-cm-thick pumice fallout of coarse lapilli (MXC-24). Lying above ERT-7 are 2 m of reworked volcanoclastic material with the present-day soil developed above.

4.2.2.2. West of the Restaurant

On the western side of the restaurant (point 7 in **Fig. 6a**) is a small quarry where at least eight pyroclastic units are preserved (WRT-1 to 8; **Fig. 7**). This sequence sits on a topographic high and dips ~20° towards the road, from where there is a panoramic view of Popocatepetl volcano (**Fig. 7a**). The lowermost tephra layer of this sequence (WRT-1) is a 3-cm-thick fallout unit of dark pumice (sample MXC-25, **Fig. 7b and c**). WRT-2 is a 25-cm-thick pinkish fallout of reversely graded medium to coarse pumice lapilli (MXC-26), which is rich in mafic crystals (orthopyroxene and hornblende) and interbedded in its upper portion with a layer of hydrothermally altered lithics. Above is a 5 cm more of pumice lapilli fall at the top (MXC-27), which is laterally discontinuous and eroded in some parts of the outcrop. It is discordantly overlain by WRT-3, a 40-cm-thick dark fallout unit composed of grey fine-to-medium lapilli pumice with abundant lithics (MXC-28), which grades into a 10-cm-thick fallout unit of

reddish coarse ash (MXC-29). WRT-4 is a 35-cm-thick lithic-rich fallout of coarse grey pumice (MXC-30, **Fig. 7 d**). WRT-5 is a 35-cm-thick white medium to coarse lapilli pumice fallout (MXC-31), which is slightly finer at the top. WRT-6 is a light-grey, laminated pumice fallout that is 120 cm thick (MXC-32). The basal sub-unit of this deposit is a bedded, 30-cm-thick, coarse ash to fine lapilli fall that is topped brown, lithic-rich horizons. The next sub-unit structureless 40-cm-thick, comprising fine to medium pumice lapilli fall, with a higher concentration of lithics towards the top. The top sub-unit comprises 40 cm of pumice fall interbedded with brown lithic-rich horizons. WRT-7 is a 110-cm-thick fallout unit, which is massive with white to yellowish medium lapilli and pink coarse pumice clasts that are up to 4 cm in diameter (MXC-33). The uppermost tephra of this sequence (WRT-8) starts with 10 cm of medium dark grey ash followed by 45 cm of a medium to coarse lapilli pumice fallout, which is rich in lithics (MXC-34, **Fig. 7e**) and grades into ~2 m of reworked volcanoclastic material with the present-day soil at the top.

4.2.2.3. Fork in the road:

Six more tephra layers are exposed in another small quarry along the Paso de Cortés road (FRT-1 to 6; **Fig. 8**; point 8 in **Fig. 6a**). The lowermost unit (FRT-1) is a 100-cm-thick, normal graded, white pumice fallout, with clasts ranging from coarse to medium lapilli, and a lithic-rich layer at the top comprising up to 70% lithics (MXC-102, **Fig. 8a, b, and c**). FRT-2 is a 15-cm-thick pumice fallout of medium to coarse sub-angular lapilli (MXC-103, **Fig. 8c**). FRT-3 is a distinctive 120-cm-thick, dark grey, normal graded and thinly bedded pumice fallout, with clasts ranging from medium to fine lapilli to coarse ash, that transitions into a lithic-rich (>45%) layer with medium lapilli pumice at the top (MXC-104, **Fig. 8d and e**). FRT-4 is a 10-cm-thick lithic-rich fallout of brown pumice comprised of coarse lapilli (MXC-105; **Fig. 8d and e**). FRT-5 is a 23-cm-thick yellowish pumice fallout inversely graded with clasts ranging from medium to coarse lapilli, with a lithic-rich layer in the middle (MXC-106, **Fig. 8f**). FRT-6 is a 12-cm-thick coarse grey ash fallout layer with sub-rounded and embedded orange coarse pumice clasts (mostly at the base of the unit; MXC-107, **Fig. 8f**). At the top of the sequence there are 100 cm of reworked volcanoclastic material that grades into the present-day soil.

4.2.2.4. Xalitlintla Quarry

At least eleven tephra layers are preserved in a large quarry located NW of Xalitintla (point 9 in **Fig. 6a**). Unfortunately, the upper 4 pyroclastic units were out of reach and could not be sampled or described in detail (**Fig. 9a and b**). The lowermost pyroclastic deposit of this sequence (XQT-1) is a lithic-poor dark-grey scoria fallout that is 22-cm-thick and comprised

of medium lapilli clasts (sample MXC-97, **Fig. 9c**). XQT-2 is a 26-cm-thick fallout unit comprised of dark coarse ash (MXC-98, **Fig. 9 d**). XQT-3 is a 39-cm-thick white pumice fallout that is lithic-poor (<5%) and slightly inversely graded, with clasts ranging from fine to medium lapilli and the occasional clast that is up to 3 cm in diameter (MXC-99, **Fig. 9e**). The next four tephra layers are within a 78-cm-thick sequence interbedded by thin layers of reworked material (**Fig. 9f**). XQT-4 is a normally graded 8-cm-thick dark pumice fallout, with fine to medium lapilli to coarse ash, and rich in fine-to-medium lava lithics (MXC-100, **Fig. 9g**). XQT-5 is a 10-cm-thick yellowish fallout unit of medium lapilli pumice with few coarse clasts up to 2 cm in diameter. XQT-6 is a dark 12-cm-thick normally graded fallout unit, from coarse to medium pumice lapilli and rich in fine-to-medium lithics. XQT-7 is a dark brown 19-cm-thick coarse pumice fallout rich in medium to coarse lava lithics (MXC-101, **Fig. 9h**). The tephra layers of the uppermost part of the outcrop could not be reached and were not sampled and include: XQT-8, a ~50-cm-thick dark pumice fallout unit with a lithic-rich layer; XQT-9, a ~80-cm-thick light-grey layered pumice fallout of fine to medium lapilli interbedded with thin layers of coarse ash (**Fig. 9a and b**); XQT-10, a ~50-cm-thick brown pumice fallout unit; and XQT-11, the uppermost tephra recorded in this outcrop, is a ~ 2-m-thick orange coarse pumice lapilli deposit (**Fig. 9a and b**) into which the present-day soil has been developed.

5. Glass chemistry and tephra correlation

The glass compositions of all the tephra layers identified in the outcrops described above were analysed in order to build a tephrostratigraphy that could be used to correlate sites around the SNVR volcanoes, to identify the source of the tephra exposed at Nepopualco and Xalitlintla, and to develop the longer-term explosive eruption history of the SNVR. Given that some of the units have been dated here and in other studies (e.g. [Macías et al., 2012](#)), this tephrostratigraphy can be used to constrain the chronology at other sites and help evaluate the explosive eruptive history of the volcanoes (e.g., as marker horizons in other regional stratigraphic records; [Brown et al., 2019](#)).

5.1. Glass compositional fields of Tláloc-Telapón, Iztaccíhuatl and Popocatepetl

As explained in Section 4.1, we analysed glass from pyroclastic deposits that had been previously attributed to Tláloc-Telapón, Iztaccíhuatl, or Popocatepetl (**Table 4**; secondary standards in **Supplementary Material 1**) in order to establish the compositional fields of the potential source volcanoes of the newly described tephra in the Nepopualco and Xalitlintla sequences.

Major element abundances displayed in a total alkali vs. silica diagram (TAS, **Fig. 10a**) and bivariate plots (**Fig. 10b-e**) show that the glass compositions of the late Pleistocene ignimbrites erupted from Tláloc-Telapón are relatively K-rich and rhyolitic. The deposits are compositionally homogenous and plot within a narrow cluster (green area in **Fig. 10**). They have 74.93-77.66 wt% SiO₂, 0.27 - 1.60 wt% CaO, 3.68-4.96 wt% K₂O, 12.86-14.20 wt% Al₂O₃, and up to 0.31 wt% MgO. The products of known eruptions from Iztaccíhuatl and Popocatepetl are quite variable in composition, and two slightly different evolutionary trends can be discerned (red and blue areas in **Fig. 10**). The middle Pleistocene Iztaccíhuatl deposits have lower K and Mg (red area in **Fig. 10**) and higher Ca and Al at given SiO₂ content than deposits from Popocatepetl (blue area in **Fig. 10**). Glass compositions of the Iztaccíhuatl deposits are rhyolitic with 71.30-78.92 wt% SiO₂, up to 0.56 wt% MgO, 0.46-2.65 wt% CaO, 2.15-4.41 wt% K₂O, and 11.68-16.61 wt% Al₂O₃. In contrast, the late Pleistocene - Holocene Popocatepetl eruption deposits have glass compositions that extend from andesite to rhyolite, with ranges of 58.82-71.84 wt% SiO₂, 0.58-2.61 wt% MgO, 1.78-8.13 wt% CaO, 0.85-3.76 wt% K₂O, and 14.05-22.73 wt% Al₂O₃.

Although Popocatepetl's products fall within a consistent linear trend, which implies that the melts have evolved along the same fractionation trend in the past 24 ka, we cannot be certain that all melts erupted from this volcano followed the same fractionation trend during the earlier stages of its history. Our studied tephra deposits span an older time interval (Section 6), but it is notable that many of these deposits overlap compositionally with our defined post-24 ka Popocatepetl field. This suggests that magmas of a similar composition have been erupted over a long-time interval from the SNVR, and in the absence of conflicting information, we attribute all magmas that plot along the higher-K fractionation trend to the Popocatepetl source. Temporally, our known Iztaccíhuatl samples are much closer in age to the stratigraphic interval that is being studied, but as discussed in section 4.1.2, the limitation of these is that our compositional field is only based on two closely spaced eruptions. Nevertheless, these Iztaccíhuatl samples define a distinct linear compositional trend from the post-24 ka Popocatepetl field, with lower K₂O at given SiO₂ contents, and we use this to define an Iztaccíhuatl compositional field. Although it is possible that the melt compositions erupted by both Popocatepetl and Iztaccíhuatl varied between these low-K and high-K trends over time, we do not consider this likely, given that fractionation trends at other closely-spaced volcanoes are observed to be stable over prolonged periods of time (e.g. Daisen and Sambe volcanoes in Japan; [Albert et al., 2019](#)). In the absence of further source compositional constraints, we adopt

the simplest interpretation and attribute the two low-K and high-K compositional types that occur within our dataset, to Iztaccíhuatl and Popocatepetl respectively.

5.2 Composition of Nepopualco tephtras and correlation to their volcanic source

The tephra layers in the Nepopualco site have a wide range of sub-alkaline glass compositions, from andesites to rhyolites (**Fig. 11 and Table 5**; secondary standards in **Supplementary Material 1**). These major element glass compositions of the Nepopualco tephtras (**Fig. 11 b-e**) partially plot within the two defined compositional fields of Iztaccíhuatl and Popocatepetl. For example, the andesitic to dacitic glass compositions of NT-6, 9, 12, and NT-16 to 23 (concentrations of 61.40-69.61 wt% SiO₂, 0.92-2.54 wt% MgO, 2.93-6.07 wt% CaO, 1.62-2.48 wt% K₂O, and 18.72-14.91 wt% Al₂O₃) plot within the high-K Popocatepetl compositional field (blue area in **Fig. 11**), and most likely were sourced from Popocatepetl. The rhyolitic glasses of NT-2 to 4, and NT-8, 11 and 13 (concentrations of 70.52-78.91 wt% SiO₂, 0.12-0.75 wt% MgO, 0.46-2.85 wt% CaO, 2.28-4.46 wt% K₂O, and 11.67-16.43 wt% Al₂O₃) plot within the low-K Iztaccíhuatl compositional field (red area in **Fig. 11**). NT-24, which is a K-rich rhyolitic white fine-ash fallout (75.65-77.04 wt% SiO₂, 0.36-0.47 wt% CaO, 4.63-5.43 wt% K₂O, 12.39-13.40 wt% Al₂O₃, and up to 0.09 wt% MgO), plots partially within the compositional field defined by the known Tláloc-Telapón pyroclastic deposits, and is distinct from all other tephtras in the Nepopualco sequence (orange dots and green area in **Fig. 11**).

Three tephtras in Nepopualco do not plot clearly into any of our defined compositional fields. The NT-5, 7, and 10 units (grey and blue diamonds, and yellow square in **Fig. 11**) have a bimodal glass composition, which overlap with both the Popocatepetl and Iztaccíhuatl fields.

5.3 Composition of Xalitzintla tephtras and correlation to their volcanic source

Major element glass compositions of the tephtras around Xalitzintla also span a wide range of sub-alkaline compositions (**Table 6**; secondary standards in **Supplementary Material 1**), but mostly plot within the Popocatepetl compositional field (andesite-dacite units within and close to the blue area in **Fig. 12**; 59.61-68.47 wt% SiO₂, 0.84-2.83 wt% MgO, 2.86-6.03 wt% CaO, 1.42-3.28 wt% K₂O, and 15.42-18.28 wt% Al₂O₃), with only two units within the Iztaccíhuatl field (XQT-3 and FRT-1 within the red area of **Fig. 12**; 71.38-75.34 wt% SiO₂, 0.13-0.67 wt% Mg, 1.23-2.48 wt% CaO, 2.50-3.16 wt% K₂O, and 13.92-15.61 wt% Al₂O₃). None of the Xalitzintla tephtras plot into the Tláloc-Telapón compositional field (no plots within green area, **Fig. 12**), but several tephtras plot outside our defined Popocatepetl field (yellow diamonds, **Fig. 12a**). Other tephtra layers outside the fields include XQT-4 (blue diamonds in **Fig. 12**) and

WRT-1 (red square in **Fig. 12**), which are andesites with slightly lower CaO and Al₂O₃ glass compositions relative to the Popocatepetl trend.

6. New Argon-Argon dates

Various deposits from the studied outcrops were ⁴⁰Ar/³⁹Ar dated in this study. These new ⁴⁰Ar/³⁹Ar age ranges are reported at 2σ. From these, two analyses related to the San Valentín Ignimbrite (samples MXC-50 and MXC-88 from sites 2 and 3 respectively in **Fig. 1c**), that erupted from Tláloc-Telapón volcano, were previously dated by radiocarbon to ~46 cal. ka BP (around the limit of the technique; [Rueda et al., 2007](#); [García-Tovar and Martínez-Serrano, 2011](#); [Macías et al., 2012](#)). Analyses on single sanidine crystals yielded ages of 101 ± 2 ka (MXC-50; 2σ) and 103 ± 3 ka (MXC-88; 2σ), indicating that this ignimbrite is substantially older than previously inferred from radiocarbon dating (**Table 7**). Moreover, new radiocarbon dates obtained from large charcoal pieces found within this deposit were beyond the upper limit of this method (>50 ka; **Supplementary material 2**).

Three ⁴⁰Ar/³⁹Ar ages were obtained from the Nepopualco sequence. Unfortunately, no sanidines were found in the tephras so the resulting ages were determined from plagioclase and hornblende concentrates, producing ages with larger errors. Analyses on hornblendes (sample MXC-05) from NT-2 (the Nepopualco Ignimbrite), which is the lowermost tephra of this sequence, yielded an eruption age of 631 ± 44 ka (2σ). This new date is consistent with the underlying LPDAD age range but suggests that the DAD is older than the median age previously reported (440 ± 190 ka; [Macías et al., 2012](#); **Fig. 3**). Analyses on plagioclase from the NT-12 fallout unit (sample MXC-15), located in the Middle Nepopualco Tephras (**Fig. 4**), yielded an eruption age of 620 ± 52 ka (2σ). This age is very similar to that of NT-2, but based on their error averages, a time interval of up to ~100 ka could have elapsed between the NT-2 and NT-12 eruptions. At least nine additional explosive eruptions occurred during this period based on the Nepopualco stratigraphy (**Table 2**). Analyses on plagioclase from the NT-23 (sample MXC-46), located in the Upper Nepopualco Tephras (**Fig. 5**), yielded an eruption age of 369 ± 22 ka (2σ). Several eruption deposits occur between the two dated horizons (NT-12 and NT-23).

Three additional reliable ages were obtained from the Xalitlintla Restaurant sites: one from a tephra exposed in the easternmost outcrop (ERT-3 unit) and two from tephras in the westernmost outcrop (WRT-6 and 7). Unfortunately, tephras from the other two Xalitlintla sites (Quarry and Fork in the road) did not yield suitable results due to the absence of

appropriate minerals (e.g., sanidines or hornblendes, and inclusion-free plagioclases). All $^{40}\text{Ar}/^{39}\text{Ar}$ dates for these Xalitzintla tephras were from aliquots of plagioclase crystals. ERT-2 yielded a 2σ eruption age of 236 ± 24 ka (Fig. 6), WRT-6 an age of 431 ± 40 ka (Fig. 7) and WRT-7 an age of 354 ± 58 ka (Table 7). A summary of the $^{40}\text{Ar}/^{39}\text{Ar}$ dates is reported in Table 7 (raw data and age plots in Supplementary materials 3 and 4).

7. Tephra correlations

7.1 Tephra correlations between the Xalitzintla and Nepopualco sequences

In order to complement the chemical characterization and the correlation of the studied tephras, we plotted the abundance of TiO_2 vs SiO_2 for the Xalitzintla and Nepopualco tephras (Fig. 13). The data are distributed into two well-defined fields, which largely coincide with the defined compositional fields of Popocatepetl and Iztaccíhuatl volcanoes (blue and red areas in Fig. 13a). Because these plots do not follow a narrow trend (as generally is the case in the other bivariate plots of MgO , CaO , K_2O , and Al_2O_3 ; Figs. 11 and 12), but are more spatially separated, it is possible to infer some tephra correlations between these two sites. For example, the rhyolitic FRT-1 tephra (yellow triangles in Fig. 13e) recorded in Xalitzintla is very similar to the NT-11 (solid green diamonds in Fig. 13e) in its glass composition (rhyolitic), both forming tight clusters with limited overlap with any other units. Both deposits share a similar mineralogy (e.g. both contain hornblende; Tables 2 and 3) and physical characteristics, being ~1 m-thick, normal graded, white pumice fallout deposits that are lithic-rich at the top (see section 4 for more details and Fig. 14). We infer that these pyroclastic deposits (FRT-1 and NT-11) are associated to the same explosive eruption and were most likely produced by Iztaccíhuatl volcano. Another rhyolitic tephra recorded in Xalitzintla, XQT-3 (empty red diamonds in Fig. 13e), partially overlaps the compositional field of NT-3, NT-4, and NT-8 (empty green triangles and diamonds, and green dashes in Fig. 13e), but based on its overall physical and sedimentological characteristics, it could only be potentially correlative with NT-4. Both XQT-3 and NT-4 are white pumice fallouts that are 39 and 52-cm-thick respectively (see section 4 and Fig. 14), while NT-8 is an ignimbrite without any associated fallout, and NT-3 is a 35-cm-thick, lithic-rich, coarse lapilli fallout. NT-04 is compositionally diverse and although most of the glass chemical analyses are scattered, there are some analyses that plot within the XQT-3 field, which suggests they could correlate.

Some andesite-dacite tephras at Xalitzintla, which plot within the Popocatepetl compositional field (blue area in Fig. 13), are chemically similar to some Nepopualco units. WRT-7 (yellow

646 plus sign in **Fig. 13b**) appears to correlate with NT-23 (solid blue diamonds in **Fig. 13c**), as the
 647 glass chemistry is similar. They are both thick white pumice fallout units (1.6 and 1.1 m
 648 respectively, **Fig. 14**) comprising medium to coarse lapilli, and the same mineralogy
 649 (plagioclase, orthopyroxene, and oxides; **Tables 2 and 3**). Moreover, their $^{40}\text{Ar}/^{39}\text{Ar}$ ages also
 650 support this correlation - NT-23 is dated to 369 ± 11 ka and WRT-7 is 354 ± 29 ka. These data
 651 suggest that WRT-7 correlates to NT-23 and both stem from the same Popocatepetl eruption.
 652 Although less clear, there is some compositional overlap between WRT-6 (solid orange dots,
 653 **Fig. 13b**) and NT-19 (solid sky-blue squares, **Fig. 13b**) as well as NT-22 (solid marine-blue
 654 triangles, **Fig. 13b**). Differences in the deposit characteristics and stratigraphy of the deposits
 655 do not support a correlation between WRT-6 and NT-19, but a correlation with NT-22 is
 656 supported: NT-22 is a 78-cm-thick pumice fallout of medium to coarse lapilli, rich in lithics
 657 and similar to the medial part of the WRT-6 deposit (**Fig. 14**). The mineralogy (hornblende,
 658 plagioclase, orthopyroxene, and oxides; **Tables 2 and 3**) and stratigraphy order further support
 659 that WRT-6 and NT-22 could have been produced by the same explosive eruption. The similar
 660 glass compositions, deposit characteristics, mineralogy, and stratigraphic positions of NT-21
 661 (blue crosses in **Fig. 13c**) and WRT-4 (yellow crosses in **Fig. 13c**) also suggest that they
 662 correlate. Both are 35-cm-thick lithic-rich, coarse lapilli pumice fallout units (see section 3 and
 663 **Fig. 14**). Finally, NT-20 (blue dashes in **Fig. 13c**) shows similarities to WRT-3 (solid orange
 664 triangles in **Fig. 13c**) based on the glass chemistry (**Figs. 11 and 12**), mineralogy (plagioclase,
 665 orthopyroxene, and oxides; **Tables 2 and 3**) and chronostratigraphy (**Fig. 14**). However, the
 666 WRT-3 deposit is a 50-cm-thick dark unit composed of grey fine-to-medium lapilli pumice
 667 with abundant lithics, and is lithologically different from NT-20, which is an 8-cm-thick dark
 668 unit of lithics (> 70%) with a few fine lapilli pumices and coarse ash. This correlation is thus
 669 less certain, although both deposits could stem from the same eruption if the Nepopualco site
 670 was located at the fallout margin with respect to the dispersal axis of the deposit. There are
 671 other units with similar glass geochemistry (**Fig. 13d**) but their mineralogy (see **Tables 2 and**
 672 **3**) and chronostratigraphy (**Fig. 14**) do not feasible correlations.

673 Despite both sequences spanning comparable age ranges, several other tephra units recorded
 674 in Xalitizintla cannot be correlated to any of the Nepopualco tephras based on glass
 675 compositions (**Fig. 13a**). These include: XQT-2 (solid yellow squares), XQT-4 (solid yellow
 676 diamonds), WRT-2 (solid orange diamonds), FRT-4 (brown plus signs), ERT-5 (red dashes),
 677 FRT-6 (brown dashes), and ERT-7 (red plus sign). Thus, these deposits appear to represent
 678 additional explosive eruptions to the 25 units already recorded at Nepopualco. Their absence

in Nepopualco may either be related to the dispersal axis not overlapping with Nepopualco, due to the primary deposits being too thin to be preserved as discrete, visible horizons. Nevertheless, the matching characteristics of multiple tephras within a continuous stratigraphic section at both Nepopualco and Xalitlintla (particularly WRT), supported by $^{40}\text{Ar}/^{39}\text{Ar}$ ages, allow for a robust correlation between these two sites.

7.2 Chronological order of the Xalitlintla outcrops

The Xalitlintla outcrops had not been previously studied and given the limited lateral continuity of the field exposures, it was not possible to correlate any single tephra unit across all of the four sites. However, the new $^{40}\text{Ar}/^{39}\text{Ar}$ dates and glass chemical analyses provide preliminary chronostratigraphic constraints. ERT-3 preserved in the sequence exposed at the East of the Restaurant site (**Fig. 6**) has been dated to 236 ± 12 ka, and the WRT-7 tephra exposed at the West of the Restaurant (**Fig. 7**) has an age of 339 ± 16 ka, suggesting that the western outcrop comprises an older segment of the stratigraphy. In addition, we infer that tephras exposed at the Xalitlintla Quarry and Fork in the Road (**Figs. 8 and 9**) are older than those at the restaurant sites (**Fig. 14**) because the lowermost units include rhyolitic tephras (FRT-1 and XQT-3, **Fig. 12 and 13**) that correlate to the Nepopualco Lower Tephras erupted from Iztaccíhuatl volcano (NT-4 and NT-11, **Fig. 14**). Iztaccíhuatl is thought to have been largely active before activity commenced at Popocatepetl ~ 540 ka (e.g. [Cadoux et al., 2011](#); [Delgado-Granados et al., 2017](#); see also **section 2.1**). These observations suggest the Xalitlintla exposures are separate stratigraphic sections and do not overlap (**Fig 14**).

8. Chemical variations through the Nepopualco tephra sequence and its implications for the volcanic histories of Popocatepetl and Iztaccíhuatl

Considering the geochemical compositions of the tephra layers in the Nepopualco sequence, and the possible correlation of tephras to their volcanic sources using glass chemistry (see **Fig. 11**), we propose that Iztaccíhuatl is the source of the rhyolitic tephras recorded near the base of the gully since at least 631 ± 44 ka ($^{40}\text{Ar}/^{39}\text{Ar}$ age of Nepopualco Ignimbrite or NT-2; **Fig. 3 and Table 1**), while Popocatepetl started its eruptive activity later, erupting generally andesite-dacite tephras (**Table 2**). It appears that there was a period of coeval activity between Iztaccíhuatl and Popocatepetl volcanoes, when rhyolitic and andesite-dacite tephras were deposited contemporaneously. The oldest Popocatepetl unit that we recognise is NT-6. Although this is not directly dated, it lies well below NT-12 (also attributed to Popocatepetl; dated at 620 ± 52 ka). This suggests that Popocatepetl was active prior to 600 ka. Between the

NT-6 and NT-14 eruptions (both attributed to Popocatepetl, and representing ~100 ka considering the new $^{40}\text{Ar}/^{39}\text{Ar}$ ages of NT-2 and NT-12; **Table 2**), we identify several explosive eruptions from Iztaccíhuatl, but no more after this point. This is inferred from the absence of younger pumice fallouts with glass compositions that plot along the Iztaccíhuatl fractionation trend in the younger stratigraphy. Meanwhile, most of the deposits recorded in the Middle and Upper Nepopualco Tephra plot along the Popocatepetl fractionation trend, indicating that it has continued to periodically erupt and distribute tephra over the region up until the present day (**Figs. 4, 5, and 11; Table 2**).

The fine ash layer (NT-24) deposited at the top of the sequence (**Fig. 5**) may have been produced by Tláloc-Telapón (for example, from a co-ignimbritic ash plume of one of the late-Pleistocene Tláloc-Telapón ignimbrites; **Fig. 11**).

The Nepopualco tephra sequence contains evidence for at least 25 explosive eruptions produced during the last ~650 ka: at least 13 are from Popocatepetl and 6 are from Iztaccíhuatl. But explosive eruptions from other sources are also recorded in Nepopualco, including one from the Tláloc-Telapón and one from an unknown mafic source (possibly a nearby monogenetic cone). There are two units near the base of the Nepopualco sequence with an uncertain source, and at least three in the older Xalitlintla sequences (XQT and FRT) that we are unable to attribute. It is possible that these events, which would overlap with both the earliest stages of Popocatepetl's explosive eruption history, or the final stages of Iztaccíhuatl's explosive eruption history (based on the inferences we make above), represent more compositionally diverse magmatism during this transitional phase of SNVR development.

9. Insight into the general volcanic history, magnitudes, and tephra distribution in the México basin

The chronological, chemical, and stratigraphic correlation between Xalitlintla and Nepopualco tephras (including NT-23 to WRT-7 and WRT-8 to ERT-1, **Fig. 14**) allows us to establish that at least 7 explosive eruptions from Popocatepetl are recorded at Xalitlintla in addition to the 13 eruptions registered in Nepopualco. These are associated with the 7 tephras recorded in the East of the Restaurant site (ERT-1 to ERT-7, including the 236 ± 12 ka ERT-3), which is the youngest unit from Popocatepetl that we document. The late Pleistocene – Holocene Plinian deposits studied previously by other authors (e.g. the Grey, White or Tutti Frutti pumices) have not been observed in these Xalitlintla tephra sequences we have studied, and fall within a younger stratigraphic interval than is exposed in our study area.

743 During the middle to late Pleistocene, our new observations imply that the SNVR produced
744 widespread tephra deposits from at least 20 medium-to-large explosive eruptions from
745 Popocatepetl volcano, 6 from Iztaccíhuatl, 1 from Tláloc-Telapón, and 2 eruptions from nearby
746 unknown mafic sources. At least 5 further eruptions, based on their location, physico-chemical
747 characteristics and stratigraphic position, are also likely to have been erupted from either by
748 Popocatepetl or Iztaccíhuatl. The results of this tephrostratigraphic work considerably extend
749 the longer-term understanding of the explosive volcanic history of the Popocatepetl,
750 Iztaccíhuatl and Tláloc-Telapón volcanoes (**Fig. 15**).

751 Comparing the recorded thicknesses in these tephra sequences with those of the most recent
752 Popocatepetl eruptions (e.g. the ~27.8 cal. ka BP White Pumice, [Siebe et al., 2017](#); or the
753 16,796-18,201 cal. yr Tutti Frutti Pumice, [Sosa-Ceballos et al., 2012](#)) and considering the
754 prevailing winds of the region ([Bonasia et al., 2014](#)), most of the middle to late Pleistocene
755 explosive eruptions identified in the Nepopualco and Xalitlintla outcrops are likely to have
756 distributed tephra over the México and/or Puebla basins. For example, previous studies on the
757 Tutti Frutti eruption estimated that the México City area was covered with at least 10 cm of
758 tephra ([Siebe et al., 1999](#); [Sosa-Ceballos et al., 2012](#)), with thicknesses of ~150 cm in the
759 Xalitlintla region ([Siebe et al., 2017](#)). If we assume at least some of the eruptions, especially
760 those with thicknesses of ~1m, documented above had a similar NW dispersal axis, these
761 eruptions could have also deposited tephra across the México Basin and the area occupied
762 today by México City. The eruption related to the WRT-7/NT-23 tephra (354 ± 29 ka old),
763 deposited 1.1 m of pyroclastic material in Xalitlintla and 1.6 m in Nepopualco (**Fig. 14**). It
764 could have deposited several cm of tephra across the México Basin and the area occupied today
765 by México City. If the dispersal axis for the WRT-7/NT-23 eruption was the same as that for
766 the Tutti Frutti event, its thickness at our study sites suggests an eruption of similar magnitude
767 (VEI ~ 6; involving 5 km^3 of tephra and an estimated 44 km high eruption column; [Sosa-](#)
768 [Ceballos et al., 2012](#)).

769 Recent studies on lacustrine sediments in Lake Chalco, which lies in the southern part of
770 México Basin, east of SNVR (e.g., [Ortega-Guerrero et al., 2018](#)) have correlated several tephra
771 layers to eruptions of nearby stratovolcanoes, including the Tutti Frutti Pumice from
772 Popocatepetl ([Siebe et al., 1999](#); [Sosa-Ceballos et al., 2012](#)), the MWP tephra from Tláloc
773 ([Rueda et al., 2013](#)) and the Upper and Lower Toluca Pumice deposits from Nevado de Toluca
774 volcano ([Arce et al., 2003, 2013](#)). However, these studies have only considered sediments from
775 the uppermost 122 m of the Chalco sequence that spans ~140 ka ([Lozano-García et al., 1994](#),

2015; Caballero and Ortega-Guerrero, 1998; Ortega-Guerrero et al., 2017). Older tephras recorded in deeper sections of Lake Chalco sediments cores (520 m) drilled in 2016 by the International Continental Scientific Drilling Program (ICDP) MexiDrill project (Brown et al., 2019; Valero-Garcés et al., 2021). These will provide a more complete and long-term record of the explosive volcanism around the México Basin, from which eruption frequencies, styles, and magnitudes can be ascertained. The tephrostratigraphy, ages, and glass compositions presented here will be of significance in reliably correlating newly identified tephras to their volcanic sources.

10. Conclusions

This chronostratigraphic and geochemical study of the Xalitlintla and Nepopualco tephra sequences in the Sierra Nevada Volcanic Range (SNVR) provides new insights into the middle to late Pleistocene explosive history of volcanoes surrounding the México basin.

Major element glass compositions determined by electron microprobe analysis have defined glass compositional fields for Popocatepetl, Iztaccíhuatl, and Tláloc-Telapón volcanoes, and permitted the correlations of tephra layers exposed in the Nepopualco and Xalitlintla sequences to their volcanic source. The Neopopualco and Xalitintla sequences contain deposits representing 20 Popocatepetl and 6 Iztaccíhuatl explosive eruptions, 5 deposits of uncertain source but likely originating from these two volcanoes, and five deposits from more distal vents. These include at least 2 mafic deposits from unidentified sources (possibly from nearby monogenetic cones) and 1 tephra from Tláloc-Telapón volcano related to one of their 5 late Pleistocene ignimbrite eruptions (including the San Vicente Ignimbrite, recently $^{40}\text{Ar}/^{39}\text{Ar}$ dated in this study at ~102 ka).

Since the lateral collapse of the Iztaccíhuatl's Los Pies Cone (LPDAD event), dated in this study to $\sim 631 \pm 44$ ka (2σ), Iztaccíhuatl has produced at least 6 explosive eruptions that have deposited ~1-m-thick pyroclastic deposits, pumice fallout units and/or ignimbrites that are rhyolitic in composition (e.g., Nepopualco ignimbrite or FRT-1/NT-11 fall). After a period of coeval activity with Popocatepetl volcano, explosive activity at Iztaccíhuatl ceased (probably between 500 and 400 ka ago) while Popocatepetl continued its explosive activity until today. In addition to the 7 known Plinian eruptions in the last ~24 ka, Popocatepetl has produced at least 20 additional explosive eruptions during the Late Pleistocene. The Popocatepetl eruption deposits identified in Nepopualco and Xalitlintla sites are consistent with Plinian to sub-Plinian eruptive columns, which deposited pumice fallout units with thicknesses of up to 1.6 m. These

Popocatepetl deposits are predominantly andesitic to dacitic in composition with a few extending to more evolved rhyolitic compositions, and plot along a fractionation trend that is displaced to higher K₂O relative to the deposits of Iztaccíhuatl. Some of these eruptions (e.g. NT-23/WRT-7) are likely to have deposited centimetres of ash on the area that is now México City. This work provides a deeper insight into the explosive volcanic histories of Popocatepetl and Iztaccíhuatl volcanoes and characterizes many previously unidentified Late Pleistocene pyroclastic deposits in the SNVR.

The glass compositions of the well-known Popocatepetl, Iztaccíhuatl and Tláloc-Telapón deposits, together with the classification of Nepopualco and Xalitzintla tephtras, provides a chemical database for future correlations between the Chalco tephtras and their volcanic sources, and other eruption deposits.

In summary, the chemical, stratigraphic and geochronologic investigations made on the Xalitzintla and Nepopualco tephtras, provide valuable information on the long-term volcanic history of the volcanoes of the SNVR, including Popocatepetl, one of the most active volcanoes in the country. These data are crucial in densely populated regions located in very active tectonic and volcanic settings, such as México City, and provide a basis to assess potential risk and design strategies to adequately address the hazard to urban infrastructure and human lives.

11. Acknowledgements

ISP and this study were funded by the Natural Environment Research Council (NERC), UK (NE/S009035; awarded to VCS, SFLW, MB and DFM). AGEH was funded by a NERC PhD studentship awarded through the Central England NERC Training Alliance (CENTA; grant reference NE/L002493/1). We acknowledge fieldwork logistic support from the National Autonomous University of Mexico (UNAM) and the field assistance of undergraduate students from the Institute of Geology, UNAM, including Miguel Meza, Jesús Morales and Kai Melo. Field support was also provided by Ainhoa Lorenzo. CS acknowledges funding from various CONACyT-México and UNAM-DGAPA grants. We thank two anonymous reviewers for their detailed and constructive comments, and Prof. Heidy Mader for editorial handling.

12. References

Albert, P.G., Smith, V.C., Suzuki, T., McLean, D., Tomlinson, E.L., Miyabuchi, Y., Kitaba, I., Mark, D.F., Moriwaki, H., Nakagawa, T., Members, S.P., 2019. Geochemical characterisation of the Late Quaternary widespread Japanese tephrostratigraphic markers and correlations to the Lake Suigetsu sedimentary archive (SG06 core). *Quaternary Geochronology* 1–75. <https://doi.org/10.1016/j.quageo.2019.01.005>

841 Arana-Salinas, L., Siebe, C., Macías, J.L., (2010). Dynamics of the ca. 4,965 yr. B.P. “Ochre Pumice”
842 Plinian eruption of Popocatepetl Volcano, México. *J. Volcanol. Geotherm. Res.* 192:212–231.
843 <http://dx.doi.org/10.1016/j.jvolgeores.2010.02.022>.

844 Arce, J.L., Macías, J.L., Vázquez-Selem, L., (2003). The 10.5 ka Plinian eruption of Nevado de Toluca
845 volcano, Mexico: stratigraphy and hazard implications. *Geol. Soc. Am. Bull.* 115 (2), 230–248.

846 Arce, J. L., Layer, P. W., Morales-Casique, E., Benowitz, J. A., Rangel, E., & Escolero, O. (2013). New
847 constraints on the subsurface geology of the Mexico City Basin: The San Lorenzo Tezonco deep
848 well, on the basis of ⁴⁰Ar/³⁹Ar geochronology and whole-rock chemistry. *Journal of*
849 *Volcanology and Geothermal Research*, 266, 34–49. doi:10.1016/j.jvolgeores.2013.09.004

850 Arce, J. L., Cruz-Fuentes, D., Ramírez-Luna, A., Herrera-Huerta, I. A., & Girón-García, P. (2017).
851 Pómez Bosque de Tlalpan, producto de una erupción de gran magnitud en el margen suroeste de
852 la cuenca de México. *Revista Mexicana de Ciencias Geológicas*, 34(3). DOI:
853 <http://dx.doi.org/10.22201/cgeo.20072902e.2017.3.485>

854 Bonasia, R., Scaini, C., Capra, L., Nathenson, M., Siebe, C., Arana-Salinas, L., & Folch, A., (2014).
855 Long-range hazard assessment of volcanic ash dispersal for a Plinian eruptive scenario at
856 Popocatepetl volcano (Mexico): implications for civil aviation safety. doi:10.1007/s00445-013-
857 0789-z

858 Branney, M.J., Kokelaar, P., (2002). Pyroclastic density currents and the sedimentation of ignimbrites.
859 *Geol. Soc. Lond. Mem.* 27 (152 pp.).

860 Bronk Ramsey, C. (2009). Bayesian analysis of radiocarbon dates. *Radiocarbon*, 51(1), 337–360.

861 Bronk Ramsey, C., Housley, R.A., Lane, C.S., Smith, V.C., Pollard, A.M., (2015). The RESET tephra
862 database and associated analytical tools. *Quat. Sci. Rev.* 118, 33–47.
863 doi:<https://doi.org/10.1016/j.quascirev.2014.11.008>

864 Brown ET, Caballero M, Cabral Cano E, Fawcett PJ, Lozano-García S, Ortega B et al (2019). Scientific
865 drilling of Lake Chalco, Basin of Mexico (MexiDrill). *Scient Drill*. [https://doi.org/10.5194/sd-7-](https://doi.org/10.5194/sd-7-1-2019)
866 1-2019

867 Caballero, M., Guerrero, B., (1998). Lake Levels since about 40,000 Years Ago at Lake Chalco, near
868 Mexico City. *Quatern Res* 50(1):69–79. <https://doi.org/10.1006/qres.1998.1969>

869 Cadoux, A., Missenard, Y., Martinez-Serrano, R.G., Guillou, H., (2011). Trenchward Plio-Quaternary
870 volcanism migration in the Trans-Mexican Volcanic Belt: the case of the Sierra Nevada range.
871 *Geol. Mag.* 148, 492–506. doi:DOI: 10.1017/S0016756810000993

872 Conte, G., Urrutia-Fucugauchi, J., Goguitchaichvili, A., Soler-Arechalde, A. M. & Morton-Bermea, O.
873 (2004). Paleomagnetic study of lavas from the Popocatepetl volcanic region, Central Mexico.
874 *International Geology Review* 46, 210–25.

875 Cornwall, I.W., (1971). Geology and Early Man in Central Mexico. The Henry Stopes Lecture,
876 *Proceedings Geologist's Association* 82 (3), 379–391. 6/S0016-7878(71)80016-0

877 De la Cruz-Reyna, S., Quezada, J.L., Peña, C., Zepeda, O., and Sánchez, T., (1995). Historia de la
878 actividad del Popocatepetl (1354–1995), Volcán Popocatepetl: Estudios Realizados durante la
879 crisis de 1994–1995: Centro Nacional de Prevención de Desastres, Universidad Nacional
880 Autónoma de México, p. 3–22.

881 Delgado Granados, H., Cassatta, W., Gisbert Pinto, G. and Renee, P., (2017). Los edificios volcánicos
882 antiguos. In: Martin Del Pozzo, A.L., Alatorre Ibargüengoitia, M., Arana Salinas, L., Bonasia, R.,
883 Capra Pedol, L., Cassata, W., Cordoba, G., Cortés Ramos, J., Delgado Granados, H., Ferrés López,
884 M.D., Fonseca Álvarez, R., García Reynoso, J.A., Gisbert, G., Guerrero López, D.A., Jaimes
885 Viera, M.C., Macías Vázquez, J.L., Nieto Obregon, J., Nieto Torres, A., Paredes Ruiz, P.A.,
886 Portocarrero Martínez, J., Renne, P., Rodríguez Espinosa, D.M., Salinas Sánchez, S., Siebe
887 Grabach, C., and Tellez Ugalde, E. Estudios geológicos y actualización del mapa de peligros del
888 volcán Popocatepetl. Memoria técnica del mapa de peligros del volcán Popocatepetl. Monografías

889 del Instituto de 846 Geofísica - UNAM, 22. Universidad Nacional Autónoma de México, México.
890 166 p. ISBN 978-607-02-9782-3.

891 Espinasa-Pereña, R., and Martín-Del Pozzo, A.L., (2006). Morphostratigraphic evolution of
892 Popocatepetl volcano, México, in Siebe, C., Macías, J.L., Aguirre-Díaz, G., eds., Neogene-
893 Quaternary continental margin volcanism: A perspective from Mexico, Geological Society of
894 America Special Paper 402, Penrose Conference Series, p. 115–137. doi:10.1130/2006.2402(05).

895 Ferrari, L., Orozco-Esquivel, T., Manea, V., Manea, M., (2012). Tectonophysics The dynamic history
896 of the Trans-Mexican Volcanic Belt and the Mexico subduction zone. Tectonophysics 522–523,
897 122–149. doi:10.1016/j.tecto.2011.09.018

898 García-Palomo, A., Macías, J.L., Tolson, G., Valdez, G., Mora, J.C., (2002). Volcanic stratigraphy and
899 geologic evolution of the Apan region, east-central sector of the Trans-Mexican Volcanic Belt.
900 Geofísica Internacional 41, 133–150.

901 García-Tenorio, F., (2008). Avalancha de Escombros del Pleistoceno Tardío Del Cono Los Pies,
902 Complejo Volcánico Iztaccíhuatl [M.S. thesis]: Posgrado en Geología, ESIA- IPN, p 147.

903 García-Tenorio F., Macías J.L. and Layer P.W., 2012, Eruptive History of the Iztaccíhuatl Volcanic
904 Complex during the past 450,000 years, Cities on Volcanoes 7, 19-23 November 2012, Colima
905 Mexico.

906 García-Tenorio F., Sosa-Ceballos G., and Macías J.L., 2015. Las erupciones piroclásticas del volcán
907 Iztaccíhuatl de los últimos 300,000 Años . Resumen de la Reunión Anual de la Unión Geofísica
908 Mexicana, Puerto Vallarta, 2-7 Noviembre 2015.

909 García-Tovar, G.P., and Martínez-Serrano, R.G., (2011). Geología y geoquímica de las lavas
910 pleistocénicas del estratovolcán Telapón, Sierra Nevada: México Revista Mexicana de Ciencias
911 Geológicas, v. 28, p. 301–322.

912 Goff, F., Janik, C.J., Delgado, H., Werner, C., Counce, D., Stimac, J.A., Siebe, C., Love, S.P., Williams,
913 S.N., Fischer, T., Johnson, L., (1998). Geochemical surveillance of magmatic volatiles at
914 Popocatepetl volcano, México. Geol. Soc. Am. Bull. 110-6:695–710.
915 [http://dx.doi.org/10.1130/0016-7606\(1998\)110b0695:GSOMVAN2.3.CO;2](http://dx.doi.org/10.1130/0016-7606(1998)110b0695:GSOMVAN2.3.CO;2).

916 Gómez-Vázquez, A., De la Cruz-Reyna, S., Mendoza-Rosas, A.T., (2016). The ongoing dome
917 emplacement and destruction cyclic process at Popocatepetl volcano, Central México. Bull.
918 Volcanol. 78:58. <http://dx.doi.org/10.1007/s00445-016-1054-z>.

919 Gómez-Tuena, A., Orozco-Esquivel, T., Ferrari, L., (2007). Igneous petrogenesis of the Trans-Mexican
920 Volcanic Belt. In: Alaniz-Álvarez, S.A., Nieto-Samaniego, Á.F. (Eds.), Geology of México:
921 celebrating the Centenary of the Geological Society of México: Geological Society of America
922 Special Paper, 422, pp. 1–53. doi:10.1130/2007.2422(05).

923 Huddart, D., González, S., (2004). Pyroclastic flows and associated sediments, Tláloc–Telapón,
924 piedmont fringe of the eastern basin of Mexico. In: Aguirre-Díaz, G.J., Macías, J.L., Siebe, C.
925 (Eds.), Penrose Conference, Metepec, Puebla, Mexico, p. 35.

926 Jaimes-Viera, M.C., Martín Del Pozzo, A.L., Layer, P.W., Benowitz, J.A., Nieto-Torres, A., (2018).
927 Timing the evolution of a monogenetic volcanic field: Sierra Chichinautzin, Central Mexico. J.
928 Volcanol. Geotherm. Res. 356, 225–242. doi:<https://doi.org/10.1016/j.jvolgeores.2018.03.013>

929 Jochum, K.P., Stoll, B., Herwig, K., Willbold, M., Hofmann, A.W., Amini, M., Aarburg, S.,
930 Abouchami, W., Hellebrand, E., Mocek, B., Raczek, I., Stracke, A., Alard, O., Bouman, C.,
931 Becker, S., Dücking, M., Brätz, H., Klemm, R., de Bruin, D., Canil, D., Cornell, D., de Hoog, C.,
932 Dalpé, C., Danyushevsky, L., Eisenhauer, A., Gao, Y., Snow, J.E., Groschopf, N., Günther, D.,
933 Latkoczy, C., Guillong, M., Hauri, E., Höfer, H.E., Lahaye, Y., Horz, K., Jacob, D.E., Kasemann,
934 S.A., Kent, A.J.R., Ludwig, T., Zack, T., Mason, P.R.D., Meixner, A., Rosner, M., Misawa, K.,
935 Nash, B.P., Pfänder, J., Premo, W.R., Sun, W.D., Tiepolo, M., Vannucci, R., Vennemann, T.,
936 Wayne, D., Woodhead, J.D., (2006). MPI- DING reference glasses for in situ microanalysis: New
937 reference values for element concentrations and isotope ratios. Geochem. Geophys. Geosyst. 7

938 (Q02008). [http://dx.doi.org/ 10.1029/2005GC001060](http://dx.doi.org/10.1029/2005GC001060).

939 Lozano-García, M.S., Ortega-Guerrero, B., (1994). Palynological and magnetic susceptibility records
 940 of Lake Chalco, central Mexico. *Palaeogeography, Palaeoclimatology, Palaeoecology* 109, 177–
 941 191.

942 Lozano-García, S., Ortega, B., Roy, P., Beramendi-Orosco, L., Caballero, M. (2015) Climatic
 943 variability in the northern sector of the American tropics since the latest MIS 3. *Quatern Res*
 944 84(2):262–271. <https://doi.org/10.1016/j.yqres.2015.07.002>

945 Love, S.P., Goff, F., Counce, D., Siebe, C., Delgado, H., (1998). Passive infrared spectroscopy of the
 946 eruption plume at Popocatepetl volcano, México. *Nature* 396, 563–567.

947 Macías, J.L., Siebe, C., (2005). Popocatepetl's crater filled to the brim: significance for hazard
 948 evaluation. *J. Volcanol. Geotherm. Res.* 141:327–330. <http://dx.doi.org/10.1016/j.jvolgeores.2004.10.005>.

950 Macías, J.L., Arce, J.L., García-Tenorio, F., Layer, P.W., Rueda, H., Reyes-Agustín, G., López-Pizaña,
 951 F., Avellán, D., (2012). Geology and geochronology of Tlaloc, Telapón, Iztaccíhuatl, and
 952 Popocatepetl volcanoes, Sierra Nevada, central Mexico. *Geol. Soc. Am. Field Guide* 25:163–193.
 953 [http://dx.doi.org/10.1130/2012.0025\(08\)](http://dx.doi.org/10.1130/2012.0025(08)).

954 Macías, J.L., Arce, J.L., García-tenorio, F., Sosa-ceballos, G., Gardner, J.E., (2020). Source and
 955 behavior of pyroclastic density currents generated by Vulcanian-style explosions of Popocatepetl
 956 volcano (Mexico) on 22 January 2001. *J. Volcanol. Geotherm. Res.* 406, 107071.
 957 doi:10.1016/j.jvolgeores.2020.107071

958 Martínez-Serrano, G.P.G.R.G., (2011). Geología y geoquímica de las lavas pleistocénicas del
 959 estratovolcán Telapón , Sierra Nevada , México 301–322.

960 Martínez-Abarca, R., Ortega-Guerrero, B., Lozano-García, S., Caballero, M., Valero-Garcés, B.,
 961 McGee, D., Brown, E.T., Stockhecke, M., Hodgetts, A.G.E., (2021). Sedimentary stratigraphy of
 962 Lake Chalco (Central Mexico) during its formative stages. *Int. J. Earth Sci.* doi:10.1007/s00531-
 963 020-01964-z

964 McLean, D., Albert, P.G., Nakagawa, T., Suzuki, T., Staff, R.A., Yamada, K., Kitaba, I., Haraguchi,
 965 T., Kitagawa, J., Smith, V.C., (2018). Integrating the Holocene tephrostratigraphy for East Asia
 966 using a high-resolution cryptotephra study from Lake Suigetsu (SG14 core), central Japan. *Quat.*
 967 *Sci. Rev.* 183, 36–58. doi:<https://doi.org/10.1016/j.quascirev.2017.12.013>

968 Meier, M., Grobéty, B., Arce, J.L., Rueda, H., (2007). Origin and Age of the Volcanic Rocks of Tlaloc
 969 Volcano, Sierra Nevada, Central Mexico. AGU, Joint Assembly. (#V23A-01).

970 Mirwald, A., Cruz- Atienza, V. M., Díaz- Mojica, J., Iglesias, A., Singh, S. K., Villafuerte, C.,
 971 & Tago, J. (2019). The 19 September 2017 (M_w 7.1) intermediate- depth Mexican earthquake: A
 972 slow and energetically inefficient deadly shock. *Geophysical Research*
 973 *Letters*, 46, 2054– 2064. <https://doi.org/10.1029/2018GL080904>

974 Mooser F (1963). Historia tectónica de la Cuenca de México. *Boletín de la Asociación Mexicana de*
 975 *Geólogos Petroleros* 15:239–245.

976 Mora-Alvarez, G., Caballero, C., Urrutia-Fucugauchi, J., Uchiumi, S., (1991). Southward migration of
 977 volcanic activity in the Sierra de Las Cruces, Basin of Mexico. A preliminary K-Ar dating and
 978 paleomagnetic study: *Geofísica Internacional*, 30, 61-70.

979 Niespolo EM, Rutte D, Deino AL, Renne PR (2017). Intercalibration and age of the Alder Creek
 980 sanidine Ar-40/Ar-39 standard. *Quaternary Geochronology* 39, 205-213.
 981 [10.1016/j.quageo.2016.09.004](https://doi.org/10.1016/j.quageo.2016.09.004)

982 Nixon, G. T. (1988). Petrology of the younger andesites and dacites of Iztaccíhuatl volcano, Mexico:
 983 II. Chemical stratigraphy, magma mixing, and the composition of basaltic magma influx. *Journal*
 984 *of Petrology* 29, 265–303.

985 Nixon, G. T. (1989). The Geology of Iztaccíhuatl Volcano and Adjacent Areas of the Sierra Nevada
986 and Valley of Mexico. Geological Society of America, Special Paper no. 219, 58 pp.

987 Ortega-Guerrero, B., Caballero García, L., Linares-López, C., (2018). Tephrostratigraphy of the late
988 Quaternary record from Lake Chalco, central México. J. South Am. Earth Sci. 81, 122–140.
989 doi:<https://doi.org/10.1016/j.jsames.2017.11.009>

990 Ortega-Guerrero, B., Lozano-García, S., Herrera-Hern, D., (2017). Lithostratigraphy and physical
991 properties of lacustrine sediments of the last ca. 150 kyr from Chalco basin, central México Journal
992 of South American Earth Sciences doi:10.1016/j.jsames.2017.09.003

993 Panfil, M.S., Gardner, T.W., Hirth, K.G., (1999). Late Holocene stratigraphy of the Tetimpa
994 archaeological sites, northeast flank of Popocatepetl volcano, central Mexico. Geological Society
995 of America Bulletin, 111(2), 204–218.

996 Reimer, P.J., Austin, WEN., Bard, E., Bayliss. A., Blackwell, P.G., Bronk Ramsey, C., Butzin, M.,
997 Cheng, H., Edwards, R.L., Friedrich, M., Grootes, P.M., Guilderson, T.P., Hajdas, I., Heaton, T.J.,
998 Hogg, A.G., Hughen, K.A., Kromer, B., Manning, S.W., Muscheler, R., Palmer, J.G., Pearson, C.,
999 van der Plicht, J., Reimer, R.W., Richards, D.A., Scott, E.M., Southon, J.R., Turney, C.S.M.,
1000 Wacker, L., Adolphi, F., Büntgen, U., Capano, M., Fahrni, S., Fogtmann-Schulz, A., Friedrich,
1001 R., Köhler, P., Kudsk, S., Miyake, F., Olsen, J., Reinig, F., Sakamoto, M., Sookdeo, A., Talamo,
1002 S., 2020. The IntCal20 Northern Hemisphere radiocarbon age calibration curve (0-55 cal kBP).
1003 Radiocarbon 62 (4), 725–757. doi: 10.1017/RDC.2020.41.

1004 Renne, P.R., Balco, G., Ludwig, K.R., Mundil, R., Min, K., (2011). Response to the comment by W.H.
1005 Schwarz et al. on “Joint determination of K-40 decay constants and Ar-40*/K-40 for the Fish
1006 Canyon sanidine standard, and improved accuracy for Ar-40/Ar-39 geochronology” by PR Renne,
1007 et al. (2010). Geochimica et Cosmochimica Acta 75 (17), 5097e5100. [http://dx.doi.org/](http://dx.doi.org/10.1016/j.gca.2011.06.021)
1008 10.1016/j.gca.2011.06.021.

1009 Robin, C., (1984). Le volcan Popocatepetl (Mexique): structure, evolution pétrologique et risques. Bull.
1010 Volcanol. 47, 1–23.

1011 Robin, C., Boudal, C., (1987). A gigantic Bezymianny-type event at the beginning of modern
1012 Popocatepetl. J. Volcanol. Geotherm. Res. 31, 115–130.

1013 Rueda, H., Arce, J.L., Macías, J.L., García-Palomo, A., (2006). ~31 ka Plinian–Subplinian eruption at
1014 Tláloc Volcano, Sierra Nevada, México. AGU Fall Meeting, San Francisco (CA, US).

1015 Rueda, H., Macías, J.L., Arce, J.L., Gardner, J.E., Layer, P.W., (2013). The ~ 31 ka rhyolitic Plinian to
1016 sub-Plinian eruption of Tlaloc Volcano , Sierra Nevada , central Mexico. J. Volcanol. Geotherm.
1017 Res. 252, 73–91. doi:10.1016/j.jvolgeores.2012.12.001

1018 Siebe, C., Delgado, H., Abrams, M., (1993). Recurrent cone collapse of Volcán Popocatepetl, Central
1019 Mexico: implications for risk evaluation. Eos. Trans. AGU 74-43, 640.

1020 Siebe, C., Abrams, M. and Macías, J. L. (1995). Derrumbes Gigantes, Depósitos de Avalancha de
1021 Escombros y Edad del Actual Cono del Volcán Popocatepetl. Volcán Popocatepetl: Estudios
1022 Realizados Durante la Crisis de 1994–1995. pp. 195–220. México D.F.: SINAPROC –
1023 CENAPRED – UNAM.

1024 Siebe, C., Abrams, M., Macías, J.L., Obenholzner, J., (1996). Repeated volcanic disasters in Prehispanic
1025 time at Popocatepetl, Central Mexico: past key to the future? Geology 24 (5):399–402.
1026 [http://dx.doi.org/10.1130/0091-7613\(1996\)024b0399:RVDIPTN2.3.CO;2](http://dx.doi.org/10.1130/0091-7613(1996)024b0399:RVDIPTN2.3.CO;2).

1027 Siebe, C., Schaaf, P., Urrutia-Fucugauchi, F., (1999). Mammoth bones embedded in a late Pleistocene
1028 lahar from Popocatepetl volcano, near Tocuila, central Mexico. Geological Society of America
1029 Bulletin 111, 1550–1562.

1030 Siebe, C., Macías, J.L., (2004). Volcanic hazards in the Mexico City metropolitan area from eruptions
1031 at Popocatepetl, Nevado de Toluca, and Jocotitlán stratovolcanoes and monogenetic scoria cones
1032 in the Sierra Chichinautzin volcanic field. Field Guide, Penrose Conference. Neogene-Quaternary

- Continental Margin Volcanism, January 2004. Geological Society of America, State of Puebla, México: Boulder, Colorado, p. 77.
- Siebe, C., and Macías, J.L., (2006). Volcanic hazards in the Mexico City metropolitan area from eruptions at Popocatepetl, Nevado de Toluca, and Jocotitlán stratovolcanoes and monogenetic scoria cones in the Sierra Chichinautzin Volcanic Field, in Siebe, C., Macías, J.L., and Aguirre, G., eds., Neogene-Quaternary Continental Margin Volcanism: A perspective from Mexico: Geological Society of America Special Paper 402, p. 253– 329, doi:10.1130/2004.VHITMC.SP402.
- Siebe, C., Salinas, S., Arana-Salinas, L., Macías, J.L., Gardner, J., Bonasia, R., (2017). The ~ 23, 500 y 14 C BP White Pumice Plinian eruption and associated debris avalanche and Tochimilco lava flow of Popocatepetl volcano, México Journal of Volcanology and Geothermal Research, Volumes 333–334, 2017, Pages 66-95, ISSN 0377-0273, <https://doi.org/10.1016/j.jvolgeores.2017.01.011>.
- Siegburg, M., Gernon T.M., Bull J. M., Kier, D., Barfod D. N., Taylor R.N., Abebe, B., Ayele, A., (2018) Geological evolution of the Boset-Bericha Volcanic Complex, Main Ethiopian Rift: $^{40}\text{Ar}/^{39}\text{Ar}$ evidence for episodic Pleistocene to Holocene volcanism. Journal of Volcanology and Geothermal Research 351(1) 115-133. 10.1016/j.jvolgeores.2017.12.014
- Smith, R.E Smith, V.C., Fontijn, K., Gebhardt, A.C., (2019). Refining the Late Quaternary tephrochronology for southern South America using the Laguna Potrok Aike sedimentary record Quat. Sci. Rev. 218, 137–156. doi:10.1016/j.quascirev.2019.06.001
- Sosa-Ceballos, G., Gardner, J.E., Siebe, C., Macías, J.L., (2012). A caldera-forming eruption ~ 14,100 14 C yr BP at Popocatepetl volcano , México: Insights from eruption dynamics and magma mixing 214, 27–40. doi:10.1016/j.jvolgeores.2011.11.001
- Sosa-Ceballos, G., Macías, J.L., García-Tenorio, F., Layer, P., Schaaf, P., Solís-Pichardo, G., Arce, J.L., (2015). El Ventorrillo, a paleostructure of Popocatepetl volcano: insights from geochronology and geochemistry. Bull. Volcanol. 77 (10):1–20. <http://dx.doi.org/10.1007/s00445-015-0975-2>.
- Stremme, W., Ortega, I., Siebe, C., Grutter, M., (2011). Gas composition of Popocatepetl volcano between 2007 and 2008: FTIR spectroscopic measurements of an explosive event and during quiescent degassing. Earth Planet. Sci. Lett. 301:502–510. <http://dx.doi.org/10.1016/j.epsl.2010.11.032>.
- Valero-Garcés, B., Stockhecke, M., Lozano-García, S., Ortega, B., Caballero, M., Fawcett, P., Werne, J.P., Brown, E., Najera, S.S., Pearthree, K., McGee, D., Hodgetts, A.G.E., Martínez, R., (2021). Stratigraphy and Sedimentology of the Upper Pleistocene to Holocene Lake Chalco Drill Cores (Mexico Basin), in: Rosen, M.R., Finkelstein, D.B., Park Boush, L., Pla-Pueyo, S. (Eds.), Limnogeology: Progress, Challenges and Opportunities : A Tribute to Elizabeth Gierlowski-Kordesch. Springer International Publishing, Cham, pp. 415–443. doi:10.1007/978-3-030-66576-0_14

Figure captions

Fig.1: a) Map of the Trans-Mexican Volcanic Belt (TMVB, area within white dashed line) showing main Quaternary stratovolcanoes (yellow triangles) and calderas (yellow dots), as well as México City (white dot); b) map of the metropolitan region of México City (yellow area) in the central TMVB, with the principal volcanic centres marked, including Popocatepetl, Iztaccíhuatl, and Tláloc-Telapón volcanoes along the Sierra Nevada Volcanic Range (SNVR). SCVF = Sierra Chichinautzin Volcanic Field, SLCVR = Sierra Las Cruces Volcanic Range,

1078 ATVF = Apan-Tezontepec Volcanic Field; and c) Digital elevation model (DEM) of the
1079 SNVR, showing the location of the studied outcrops (yellow stars; see Table 1 for outcrop
1080 locality details), including Nepopualco (n.5) and Xalitizintla sites (n.6-9). The white dashed line
1081 shows the limit of Los Pies Debris Avalanche Deposit (LPDAD; [Macías et al., 2012](#)).

1082 **Fig. 2:** a) Panoramic view of Popocatepetl and Iztaccíhuatl volcanoes (1 = Los Pies; 2 = Las
1083 Rodillas; 3 = El Pecho; and 4 = La Cabeza craters), located in the southern portion of the Sierra
1084 Nevada Volcanic Range (SNVR); b) tephra layers exposed by a landslide in the Nepopualco
1085 gully (outcrop 5 in Fig. 1c). This tephra sequence is interbedded by several remobilized
1086 volcanoclastic units and overlies the Los Pies Debris Avalanche Deposit (LPDAD) from
1087 Iztaccíhuatl volcano.

1088 **Fig. 3:** a) Outcrop displaying several units of the lowermost part of the Nepopualco gully
1089 sequence. b) Stratigraphic log of the Lower Nepopualco Tephra (Legend: mLT = massive
1090 Lapilli Tuff, llsT = parallel-stratified tuff, xsT = cross-stratified tuff, mpL = massive pumice
1091 Lapilli, V.clast = volcanoclastic, mpLlr = mpL lithic-rich, llpL = parallel stratified pumice
1092 lapilli, mA = massive Ash and llpLlr = llpL lithic-rich; nomenclature based on [Branney and
1093 Kokelaar, 2002](#)). V.clast in the photographs/logs indicates a reworked (non-primary)
1094 volcanoclastic unit, bounding the units that are interpreted as primary eruption deposits. Details
1095 of: c) the first pyroclastic layers (MXC-3 to 5 of NT-2) above the Los Pies PDCs (NT-1), d)
1096 the NT-4 white fallout, e) the NT-8 above reworked volcanoclastic materials deposited on top
1097 of NT-7, and f) the layered NT-10 fallout above the mafic NT-9 fall with reworked materials
1098 in-between.

1099 **Fig. 4:** a) Outcrop and b) stratigraphic log of the Middle Nepopualco Tephra (see caption of
1100 Fig. 3 for the legend). Details of: c) the thick pumice fallout at the base of NT-11 and the
1101 overlying PDCs, d) the coarse pumice from NT-12, e) the thin NT-14 fallout interbedded
1102 within reworked volcanoclastic materials, f) the stratified NT-18 fallout with two interbedded
1103 dilute PDCs deposits, and g) the lithic-rich NT-15.

1104 **Fig. 5:** Detail of: a) the mafic NT-20 and the coarse orange pumice from NT-21 above the
1105 palaeosol on top of the white NT-19 pumice fallout, and b) the 1.6-m-thick NT-23 white fallout
1106 above the orange NT-22. c) Stratigraphic log of the Upper Nepopualco Tephra (see caption of
1107 Fig. 4 for the legend). d) Uppermost part of the Nepopualco sequence with two zones of fine
1108 ash pods: e) the NT-24 and f) the NT-25.

1109 **Fig. 6: a)** Map of the Xalitzintla region with the location of the four study sites (yellow stars).
1110 **b)** East of Restaurant (ER) outcrop exposed along the Paso de Cortés road (site number 6 in **a**);
1111 **c)** stratigraphic log displaying the seven pyroclastic units interbedded with reworked material
1112 and palaeosols (see caption of Fig. 4 for the legend); **d**), **e**) and **f**) field photos showing textural
1113 characteristics of tephra layers described in the text (ERT-1 to 5).

1114 **Fig. 7: a)** Panoramic view of Popocatepetl volcano from the West of the Restaurant (WR) site
1115 near Xalitzintla (outcrop 7 in Fig. 6a) during a small explosive eruption (~2-km-high plume on
1116 the 5th of April, 2019) with an ash cloud moving towards the SE. Note the geologist in the
1117 bottom-right of the photo (within yellow ellipsoid) for scale of the outcrop; **b)** tephra sequence
1118 exposed in a quarry of this WR-site; **c)** stratigraphic log showing the eight pyroclastic units
1119 interbedded with reworked material and palaeosols (see caption of Fig. 4 for the legend); **d**)
1120 and **e)** field photos showing textural characteristics of the tephra layers described in the text.

1121 **Fig. 8: a)** Small quarry at the Fork in the Road (FR) site near Xalitzintla (outcrop 8 in Fig. 6a),
1122 **b)** stratigraphic log displaying six identified fall layers recorded in this site, **c – f**) field photos
1123 showing textural characteristics of the tephra layers described in the text.

1124 **Fig. 9: b)** Xalitzintla Quarry, **b)** stratigraphic log displaying eleven pyroclastic units recorded
1125 in this site and interbedded with thick reworked volcanoclastic material units and palaeosols, **c**
1126 – **h)** field photos showing textural characteristics of the tephra layers described in the text.

1127 **Fig. 10:** Glass chemistry of previously described pyroclastic deposits erupted by Popocatepetl,
1128 Iztaccíhuatl, and Tláloc-Telapón volcanoes, with the addition of an ascribed Iztaccíhuatl
1129 deposit (see Section 4.1.2) plotted in: **a)** Total alkalis vs silica (TAS diagram) of the tephra
1130 units; and bi-variate plots of **b)** SiO₂ vs MgO, **c)** SiO₂ vs CaO, **d)** SiO₂ vs K₂O and **e)** SiO₂ vs
1131 Al₂O₃ (selected bivariate plots). Compositional fields of Popocatepetl (blue area) Iztaccíhuatl
1132 (red area), and Tláloc (green area) volcanoes estimated with OxCal/RESET software ([Bronk](#)
1133 [Ramsey et al., 2015](#)).

1134 **Fig. 11: a)** Total alkalis vs silica (TAS) of 24 analysed pyroclastic deposits through the
1135 Nepopualco gully; and bivariate plots of **b)** SiO₂ vs MgO, **c)** SiO₂ vs CaO, **d)** SiO₂ vs K₂O and
1136 **e)** SiO₂ vs Al₂O₃, displayed together with the compositional field of Popocatepetl (blue area),
1137 Iztaccíhuatl (red area), and Tláloc-Telapón (green area) volcanoes.

1138 **Fig. 12: a)** Total alkalis vs silica (TAS) of 26 tephras identified in the Xalitzintla region (shown
1139 in **Fig. 6a**); and bivariate plots of **b)** SiO₂ vs MgO, **c)** SiO₂ vs CaO, **d)** SiO₂ vs K₂O and **e)** SiO₂

1140 vs Al_2O_3 , displayed together with the compositional field of Popocatepetl (blue area),
1141 Iztaccíhuatl (red area), and Tláloc-Telapón (green area) volcanoes.

1142 **Fig. 13:** TiO_2 vs SiO_2 plots of: **a)** tephras from East of the Restaurant (ERT, blue colours) in
1143 front of the West of the Restaurant tephras (WRT, red colours) of Xalitlintla; **b)** tephras from
1144 WR in front of tephras from Xalitlintla Quarry (XQ, yellow colours) and Fork in the Road
1145 tephras (green colours); **c)** tephras recorded in Nepopualco region (NT, green and blue colours)
1146 in front of Xalitlintla tephras (ERT, WRT, XQT and FRT, red and yellow colours), displayed
1147 together with the compositional fields of Popocatepetl (blue area), Iztaccíhuatl (red area), and
1148 Tláloc (green area) volcanoes; **d)** and **e)** details of two extended areas of the graph in **c)**.

1149 **Fig. 14:** Stratigraphic correlation of **a)** Nepopualco and **b) – c)** Xalitlintla tephra layers (East
1150 and West of the Restaurant, Fork in the road and Xalitlintla Quarry). The blue stars indicate
1151 the SiO_2 (wt%) composition and the orange stars the K_2O (wt%). V.S = volcanic source, P =
1152 Popocatepetl (in blue), I = Iztaccíhuatl (in red), T-T = Tláloc-Telapón (in green), MU = mafic
1153 unknown (in yellow), UC = uncertain (in grey), and US = unsampled pyroclastic deposits
1154 (white).

1155 **Fig. 15:** Topographic profile of the Sierra Nevada Volcanic Range (SNVR), which illustrates
1156 chronologically the new identified explosive eruptions from Popocatepetl and Iztaccíhuatl, as
1157 well as the new $^{40}\text{Ar}/^{39}\text{Ar}$ age for the San Valentín Ignimbrite from Tláloc-Telapón together
1158 with other relevant eruptive episodes during the formation of the range (after [García-Tovar and](#)
1159 [Martínez-Serrano, 2011](#)). The dashed lines indicate the inferred time of activity for each
1160 volcano. The black rectangles are lavas with published $^{40}\text{Ar}/^{39}\text{Ar}$ or $^{40}\text{K}/^{40}\text{Ar}$ ages, the black
1161 hexagon is the debris avalanche deposit related to Los Pies collapse (LPDAD), the red and
1162 yellow hexagons are relative and absolute ages of the pyroclastic deposits characterized for the
1163 first time in this study, and the empty symbols are published C14 ages (rectangles for lavas and
1164 hexagons for tephras). 1 = [Cadoux et al., \(2011; 2σ\)](#); 2 = This study ($^{40}\text{Ar}/^{39}\text{Ar}$; 2σ); 3 = [Macías](#)
1165 [et al. \(2012; 1σ\)](#); 4 = [García-Tovar and Martínez-Serrano \(2011; 2σ\)](#); 5 = [Nixon \(1989;](#)
1166 [assuming 2σ\)](#); 6 = [Conte et al. \(2004; assuming 2σ\)](#); 7 = [Sosa-Ceballos et al. \(2015; 1σ\)](#); 8 =
1167 [Siebe et al. \(1996; assuming 2σ\)](#).

1168 **Table 1:** Proximal deposits of Tláloc-Telapón, Popocatepetl, and Iztaccíhuatl volcanoes.

1169 **Table 2:** Tephra layers of the Nepopualco sequence.

1170 **Table 3:** Tephra layers of Xalitlintla sites.

- 1171 **Table 4:** Major element composition from the proximal deposits of Tlálloc, Popocatepetl, and
1172 Iztaccíhuatl volcanoes.
- 1173 **Table 5:** Major element compositions of tephras recorded in Nepopualco.
- 1174 **Table 6:** Major element compositions of tephras recorded in Xalitzintla.
- 1175 **Table 7:** Summary of $^{40}\text{Ar}/^{39}\text{Ar}$ dates reported in this study.

Table 1

a) Description of some of the previous identified late Pleistocene pyroclastic deposits of Tláloc volcano

Unit		Description				Location				Age (ka)
Name	Sample	Deposit type	T (m)	Shard morphology	APCS (cm)	North	West	Locality	Outcrop	C14* and Ar/Ar**
Chuahtemoc Ign. MWP Ign.	MXC-91	Poorly sorted pumice and lithics in a fine-medium ash matrix	24 33	PU, poor but large V	7.5	19.387378°	98.574229°	San Juan C.	4	25.6 ka BP *
	MXC-68	Large pumice and lithics-rich in a fine-medium ash matrix	4	PU, elongate V, MI	8	19.497127°	98.715072°	G. Amanalco	1	31.5 ka BP *
	MXC-67	Poorly sorted pumice and lithics in a fine-medium ash matrix	25	PU, BW, elongate V	3	19.497127°	98.715072°	G. Amanalco	1	
	MXC-66	Stratified pumice fall-out/base	2.3 29.5	PU, rich in large V	2	19.497127°	98.715072°	G. Amanalco	1	
San Valentin Ign.	MXC-50	Stratified pumice fall-out	2	PU, large V, BW,	1.5	19.477587°	98.575406°	Nanacamilpa	2	44.2 ka BP *
	MXC-90	Pumice fall-out at the top of the sequence	28	PU, V, BW, CU	2	19.395989°	98.624235°	San Juan C.	3	101 ± 2 ka **
	MXC-88	Poorly sorted pumice and lithics in a fine-medium ash matrix	1.5	PU, large rounded V	4.5	19.396556°	98.624861°	San Juan C.	3	103 ± 3 ka **

T = Thickness, PU = Pumicious, PL = Platy, CU = Cuspate, BW = Bubble-Walled, F= Fluted, V = Vesicular, MV = Microvesicular, MI = Microlite Inclusions (McLean et al., 2018; and Smith et al., 2019)

APCS = Average Pumice Clast Size (approximative, as a guidance); MWP = Multilayered White Pumice (Rueda et al., 2013); * C14 ages from Macias et al., 2012; ** Ar/Ar ages from this study

The mineralogy content of Tlaloc deposits is quartz + sanidine + plagioclase + biotite, with some hornblende and Ti-Fe oxides

b) Description of some of the previous identified late Pleistocene - Holocene pyroclastic deposits of Popocatepetl volcano

Unit		Description				Location				Age (ka)
Name	Sample	Deposit type	T (m)	Shard morphology	APCS (cm)	North	West	Locality	Outcrop	C14
Pink-3 Pumice	MXC-118	Sub-unit of coarse non-graded pumice fallout with large lithics	45	SC, BW, large V, CU	2.2	18.987954°	98.453027°	Tianguismanalco	11	1.1 ka BP α
Pink-1 Pumice	MXC-114	Sub-unit of coarse angular, non-graded pumice fallout	18	SC, BW, V, CU	1.5	18.987954°	98.453027°	Tianguismanalco	11	1.1 ka BP α
Lorenzo Pumice	MXC-115	Yellowish pumice fallout of medium lapilli	80	SC, CU, V, BW, MI	1.1	19.040076°	98.563864°	Xalpilcayatl	10	2.1 ka BP β
Milky Pumice	MXC-120	Reversely graded, well-sorted, milky pumice fallout	55	PL, CU, rounded V, MI	2.1	19.075599°	98.731117°	S.P. Nexapa	13	14.3 ka BP γ
White Pumice	MXC-116	Massive whitish pumice fallout, bedded toward the top	110	SC, BW, large V, MI	1.6	18.962417°	98.663488°	Apatlahuaya	12	23.5 ka BP δ
Grey Pumice	MXC-121	Finely laminated beds of grayish pumice fallout rich in lithics	62	SC, BW, CU, large V, MI	2.4	19.075599°	98.731117°	S.P. Nexapa	13	14.3 ka BP γ

α= Siebe et al., 1996; **β**= Siebe and Macias, 2006; **γ**= Sosa-Ceballos et al., 2012; **δ**= Siebe et al., 2017

The mineralogy content of Popocatepetl deposits is plagioclase + pyroxene + Ti-Fe oxides

c) Description of the previous identified late Pleistocene pyroclastic deposits of Iztaccihuatl volcano

Unit		Description				Location				Age (ka)
Name	Sample	Deposit type	T (m)	Shard morphology	APCS (cm)	North	West	Locality	Outcrop	Ar/Ar ages (2σ)
Los Pies B&A flow	MXC-02	Reverse grading pumice fall deposit	0.85	SC, rich large/rounded V	2.5	19.149749°	98.508040°	Nepopualco	5	631 ± 44 ka *
Nepopualco dry PDCs	MXC-03	Cross-Stratification ash flows (wet surges)	0.15	2 types? 1 PL and 1 SC	1.5	19.149749°	98.508040°	Nepopualco	5	
Nepopualco wet PDCs	MXC-04	Interbedded medium to coarse ash flows	0.06	2 types? 1 PL and 1 SC	0.1	19.149749°	98.508040°	Nepopualco	5	
Nepopualco fall	MXC-05	Block and ash flow deposit (PDC sequence)	>30	SC, PL, CU, BW, MV	5	19.149749°	98.508040°	Nepopualco	5	440 ± 190 ka **

* Ar/Ar ages of this study; ** Ar/Ar ages from Macias et al., 2012

The mineralogy content of Popocatepetl deposits is plagioclase + hornblende + pyroxene + Ti-Fe oxides and some biotites

Table 2

Description of tephras recorded in Nepopualco sequence (outcrop 5 in Fig. 1c), located 14 km East of Iztaccíhuatl and 19 NE of Popocatepl (19.149749° N, 98.508040° W)

Tephra unit	Sample	Deposit type	T (m)	Shard morphology	Mineralogy	APCS (cm)	Volcanic Source	⁴⁰ Ar/ ³⁹ Ar ages (2σ)
NT-25	MXC-48	Well-sorted medium ash fall rich in biotite	0.15	PU, BW, rich elongate V, F,	plag, hbl, px, ox, bi, qz	0.05	Uncertain	
NT-24	MXC-47	Well-sorted fine coignimbritic ash	0.1	PU, large V, BW,	qz, san, bi, hbl, ox	0.01	Tláloc-Telapón	
NT-23	MXC-46	White fallout unit of fine to medium lapilli pumice	1.6	PL, BW, CU, large V,	plag, px and ox	1.6	Popocatepetl	369 ± 22 ka
NT-22	MXC-45	Well-sorted orange pumice fall rich in lithics	0.77	SC, PL, CU, BW, MI	plag, hbl, px, ox	3.7	Popocatepetl	
NT-21	MXC-44	Lithics-rich orange pumice fallout of coarse lapilli	0.35	PL, CU, large V, BW, MI	plag, px and ox	3.5	Popocatepetl	
NT-20	MXC-43	Dark fallout unit of fine lapilli rich in lithics (70%)	0.08	PL, large/rounded V, MV, CU	plag, px and ox	0.5	Popocatepetl	
NT-19	MXC-42	Well-sorted white pumice fall poor in lithics	0.3	SC, BW, large V, MI	plag, hbl, px, ox	1.8	Popocatepetl	
NT-18	MXC-41	Normal graded and layered pumice and ash fall	0.9	SC, high V, CU, BW,	plag, px and ox	2.9	Popocatepetl	
NT-17	MXC-39/40	Pumice fall with two ash layers in the middle	0.51	SC, PL, elongate V, CU, rich MI	plag, px and ox	2.8	Popocatepetl	
NT-16	MXC-38	Reverse graded of white ash to fine lapilli	0.27	PU with MV, and SC, large V	plag, px and ox	0.8	Popocatepetl	
NT-15	MXC-37	Lithich-rich massive pumice fallout	0.15	PL, MV, CU, BW, MI	plag, hbl, px, ox	1.4	Popocatepetl	620 ± 52 ka
NT-14	MXC-36	Reverse grading pumice fall deposit	0.08	2 types: 1 PL and 1 SC	plag, hbl, px, ox	1.5	Popocatepetl	
NT-13	MXC-35	Normal graded pumice fall with ash fall at top	0.25	PL, BW, CU, V, MI	plag, hbl, px, ox, qz	1.2	Iztaccíhuatl	
NT-12	MXC-15	Coarse pumice fallout lithic-rich	0.55	SC, BW, rich V, MI	plag, hbl, px, ox	3	Popocatepetl	
NT-11	MXC-14	Normal graded white pumice with PDC at top	0.7	BW, CU, rich V	plag, hbl, px, ox	2.5	Iztaccíhuatl	
NT-10	MXC-13	Bedded pumice fall lithic-rich	0.9	SC, large V, CU, BW, MI	plag, px and ox	2.8	Uncertain	
NT-9	MXC-12	Mafic scoria and ochre pumice fallout	0.35	SC, PL, CU, BW, MI	plag, px and ox	2.7	Popocatepetl	
NT-8	MXC-11	Lense of PDC deposit	0.8	SC, CU, elongated V, MV	plag, hbl, px, ox, qz	3.2	Iztaccíhuatl	
NT-7	MXC-10	Bedded pumice fall rich in lithics	0.7	SC, BW, CU, rich V, MI	plag, hbl, px, ox, bi	2.8	Uncertain	
NT-6	MXC-09	Grey pumice fallout	0.18	PL, SC, large/elongated V, BW	plag, hbl, px, ox	2.4	Popocatepetl	
NT-5	MXC-08	Well-sorted dark coarse ash	0.3	PL, large/poor V, MI	plag, px and ox	0.2	Mono. Cone	
NT-4	MXC-07	Well-sorted white pumice fall	0.52	SC, PL, BW, elongated V, MI	plag, hbl, px, ox, bi, qz	1.6	Iztaccíhuatl	
NT-3	MXC-06	Well-sorted lithic-rich yellow pumice fall	0.35	SC, PL, CU, BW, high V, MI,	plag, hbl, px, ox	1.3	Iztaccíhuatl	
NT-2/ Nepopualco	MXC-05	Reverse grading pumice fall deposit	0.85	SC, rich large/rounded V,	plag, hbl, px, ox	2.5	Iztaccíhuatl	631 ± 44 ka
Ignimbrite (dry/wet	MXC-04	Cross-Stratification ash flows (wet surges)	0.15	2 types? 1 PL and 1 SC	plag, hbl, px, ox, qz	1.5	Iztaccíhuatl	
PDe's and fallout)	MXC-03	Interbedded medium to coarse ash flows	0.06	2 types? 1 PL and 1 SC	plag, hbl, px, ox	0.1	Iztaccíhuatl	
NT-1 / Los Pies B&A	MXC-02	Block and ash flow deposit (PDC sequence)	>30	SC, PL, CU, BW, MV	plag, hbl, px, ox, bi	5	Iztaccíhuatl	*440 ± 190 ka
LPDAD	MXC-01	Debris Avalanche with large blocks	>10	PL, big/poor V, MI	plag, hbl, px, ox, qz	20	Iztaccíhuatl	

PU = Pumicious, PL = Platy, CU = Cusate, BW = Bubble-Walled, F= Fluted, V = Vesicular, MV = Microvesicular, MI = Microlite Inclusions (McLean et al., 2018; and Smith et al., 2019)

APCS = Average Pumice Clast Size (approximative, as a guidance), LPDAD = Los Pies Debris Avalanche deposit (Macias et al., 2012), T = Thickness, * Age from [Macias et al. \(2012\)](#)

Table 3

Description of Xalitizintla tephtras by outcrops (6 to 9 in Fig. 1c and 6a): East of the Restaurant (19.078794° N, 98.506966° W), West of the Restaurant (19.080099° N, 98.507531° W), Fork in the Road (19.084910° N, 98.514919° W) and Xalitizintla Quarry (19.084671° N, 98.520788° W). Tephtras and outcrops are in stratigraphic order, from oldest at the base to youngest at top.

Outcrop	Unit	Sample	Deposit type	T (m)	Shard morphology	Mineralogy	APCS (cm)	Volcanic source	⁴⁰ Ar/ ³⁹ Ar ages (2σ)
East of Restaurant									
	ERT-7	MXC-24	Well-sorted pumice fallout of coarse lapilli	0.30	SC, BW, large V, CU	plag, px, ox	2.2	Popocatepetl	
	ERT-6	MXC-23	Fallout of medium pumice lapilli	0.35	SC, CU, rich V, BW, rich MI	plag, hbl, px, ox	1.5	Popocatepetl	
	ERT-5	MXC-22	Medium to coarse pumice fallout	0.20	BW, CU, elongate V, MI	plag, px, ox	2	Popocatepetl	
	ERT-4	MXC-21	Grey layer of coarse ash	0.05	PL, CU, rounded V, MI	plag, px, ox	0.5	Popocatepetl	
	ERT-3	MXC-20	Laminated pumice fallout sequence with nine sub-units	0.78	SC, BW, large V, MI	plag, px, ox	1.6	Popocatepetl	
		MXC-19	Coarsest sub-unit at the base of the fallout sequence		SC, BW, CU, large V, MI	plag, px, ox	2.4	Popocatepetl	236 ± 24 ka
	ERT-2	MXC-18	Uppermost sub-unit of a normal-graded pumice fallout	0.22	SC, BW, CU, large V, MI	plag, px, ox	1	Popocatepetl	
		MXC-17	Lowermost sub-unit, normal graded with a lithic-rich top	0.15	SC, large V, MI, MV	plag, px, ox	2.3	Popocatepetl	
	ERT-1	MXC-16	Normal graded orange fallout with two types of pumice	0.43	PL, CU, BW, elongate V,	plag, px, ox	1.8	Popocatepetl	
West of Restaurant									
	WRT-8	MXC-34	Medium to coarse fallout with a basal grey ash layer	0.55	SC, BW, rich V, large MI	plag, px, ox	2.4	Popocatepetl	
	WRT-7	MXC-33	Massive white yellowish medium lapilli	1.10	BW, CU, V, MI	plag, px, ox	1.2	Popocatepetl	354 ± 58 ka
	WRT-6	MXC-32	Light-grey laminated sequence of pumice fallouts	1.20	SC, BW, large V, MI	plag, hbl, px, ox	1.3	Popocatepetl	431 ± 40 ka
	WRT-5	MXC-31	white medium lapilli pumice fallout finer at top	0.35	BW, CU, rich V, rich MI	plag, px, ox	1.9	Popocatepetl	
	WRT-4	MXC-30	Lithic-rich fallout unit of coarse grey pumice	0.35	PL, large rounded V, MV	plag, px, ox	2.8	Popocatepetl	
	WRT-3	MXC-29	Well-sorted reddish coarse ash fall	0.10	SC, BW, large V, MI, few MV	plag, px, ox	0.3	Popocatepetl	
		MXC-28	Dark-grey medium pumice lapilli fallout	0.40	SC, PU, BW, CU, large V, MI	plag, hbl, px, ox	1.4	Popocatepetl	
	WRT-2	MXC-27	Medium pumice lapilli fall with a lithic-rich basal layer	0.05	SC, BW, V, rich in MI	plag, px, ox	1.5	Popocatepetl	
		MXC-26	Reverse graded pumice medium-to-coarse lapilli	0.25	SC, BW, V, MV, MI	plag, px, hbl, ox	2	Popocatepetl	
	WRT-1	MXC-25	Scoria fallout layer	0.03	SC, BW, CU, V, rich MI	plag, px, ox	1.5	Popocatepetl	
Fork in the Road									
	FRT-6	MXC-107	Coarse grey ash layer with coarse sub-rounded pumices	0.12	PL, elongate V, MI	plag, px, ox, qz	0.4	Popocatepetl	
	FRT-5	MXC-106	Reverse graded yellowish pumice fallout lithic-rich	0.23	PL, PU, large V, MV, MI	plag, px, ox	2.2	Uncertain	
	FRT-4	MXC-105	Brown pumice fallout of coarse lapilli and lithic-rich	0.10	SC, BW, V, MV, rich MI	plag, px, ox	2.7	Popocatepetl	
	FRT-3	MXC-104	Grey bedded pumice fallout sequence with granoclass.	1.20	PU, rich V, rich MI	plag, px, ox	1.2	Popocatepetl	
	FRT-2	MXC-103	Pumice fallout of medium to coarse sub-angular lapilli	0.15	SC, BW, C, large/rounded V	plag, px, ox, qz	2.1	Uncertain	
	FRT-1	MXC-102	Normal graded pumice fallout with lithic layer at top	1.00	SC, large/rounded V, rich MI	plag, px, ox, hbl	1.5	Iztaccíhuatl	
Xalitizintla Quarry									
	XQT-7	MXC-101	Dark brown coarse pumice fallout rich in lithics	0.19	PU, rounded V, MI	plag, px, ox	2.4	Popocatepetl	
	XQT-4	MXC-100	Dark pumice fallout, granoclassified, rich in fine lithics	0.08	SC, PL, BW, larg V, rich MI	plag, px, ox	1.1	Mono. Cone	
	XQT-3	MXC-99	White pumice fallout, lithic-poor and inverse gradation	0.39	BW, large V, some MV, MI	plag, px, ox	1.8	Iztaccíhuatl	
	XQT-2	MXC-98	Dark Coarse ash fall	0.26	PL, CU, large V, MI	plag, px, ox	0.3	Uncertain	
	XQT-1	MXC-97	Dark-grey scoria of medium lapilli size	0.22	PL, CU, poor/large V, rich iMI	plag, px, ox	1.5	Mono. Cone	

PU = Pumicious, SC = Scoriaceous, PL = Platy, CU = Cusplate, BW = Bubble-Walled, F= Fluted, V = Vesicular, MV = Microvesicular, MI = Microlite Inclusions (McLean et al., 2018; and Smith et al., 2019); APCS = Average Pumice Clast Size (aproximative, as a guidance), T = Thickness,

Table 4**a) Major element composition (average and standard deviation) of the matrix glass (anhydrous) from the Tlaloc volcano proximal deposits**

Major element composition (average and standard deviation) of the matrix glass (amorphous) from the three volcanic proximal deposits														
Sample	MXC-91	MXC-68	MXC-67	MXC-66	MXC-50	MXC-90	MXC-88							
Eruption	Cuahtemoc Ignimbrite	MWP Ignimbrite	MWP Ignimbrite	MWP Ignimbrite	MWP Ignimbrite	San Valentin Ignimbrite	San Valentin Ignimbrite	San Valentin Ignimbrite						
N	24	21	22	23	28	27	22							
SiO ₂	77.14	0.18	77.07	0.22	77.05	0.35	77.09	0.21	77.06	0.28	77.16	0.22	77.21	0.31
TiO ₂	0.03	0.02	0.03	0.02	0.03	0.02	0.03	0.03	0.03	0.03	0.02	0.02	0.03	0.03
Al ₂ O ₃	13.45	0.08	13.49	0.14	13.47	0.25	13.27	0.17	13.55	0.16	13.43	0.19	13.42	0.18
FeO*	0.56	0.05	0.58	0.03	0.58	0.05	0.59	0.04	0.57	0.04	0.58	0.04	0.56	0.04
MnO	0.09	0.02	0.09	0.02	0.09	0.01	0.09	0.02	0.10	0.02	0.08	0.02	0.08	0.02
MgO	0.03	0.02	0.02	0.02	0.02	0.02	0.04	0.02	0.03	0.02	0.04	0.03	0.04	0.02
CaO	0.32	0.02	0.31	0.02	0.34	0.05	0.36	0.03	0.31	0.02	0.36	0.03	0.34	0.02
Na ₂ O	3.77	0.12	3.90	0.13	4.07	0.19	4.04	0.14	4.02	0.13	3.80	0.25	3.77	0.17
K ₂ O	4.56	0.10	4.45	0.08	4.31	0.11	4.44	0.12	4.26	0.11	4.47	0.25	4.49	0.15
P ₂ O ₃	0.03	0.02	0.01	0.01	0.02	0.01	0.02	0.02	0.03	0.02	0.02	0.02	0.02	0.02
Cl	0.03	0.01	0.03	0.01	0.03	0.01	0.03	0.01	0.03	0.02	0.03	0.02	0.03	0.02

Average and standard deviations (italics) for tephra deposits recorded through the Nepopualco sequence. Compositions in weight percent (wt%) were determined using a wavelength-dispersive EMP (see Section 5). N = number of analyses. See Supplementary material for the raw data and secondary standards. ** For bimodal samples it is showed a representative composition of each group of plots instead than the general average and standard deviation.

b) Major element composition (average and standard deviation) of the matrix glass (anhydrous) from the Popocateptl volcano proximal deposits

Sample	MXC-118		MXC-114**		MXC-115		MXC-120		MXC-116		MXC-121	
Eruption	Pink-3 Pumice		Pink-1 Pumice		Lorenzo Pumice		Milky pumice		White Pumice		Grey Pumice	
N												
SiO ₂	68.45	0.57	68.10	71.52	66.58	0.31	63.11	0.54	69.64	0.49	62.15	1.92
TiO ₂	0.79	0.03	0.86	0.72	1.08	0.04	0.67	0.04	0.48	0.01	0.61	0.17
Al ₂ O ₃	15.47	0.22	15.15	14.29	15.77	0.11	18.00	0.49	15.99	0.55	19.38	2.15
FeO*	3.26	0.13	3.38	2.62	3.82	0.12	4.23	0.23	2.52	0.18	3.44	0.81
MnO	0.07	0.03	0.05	0.06	0.05	0.04	0.09	0.03	0.06	0.01	0.06	0.04
MgO	1.00	0.08	1.12	0.60	1.38	0.07	2.01	0.09	0.68	0.04	1.58	0.57
CaO	3.01	0.20	3.07	1.90	3.70	0.16	5.19	0.46	2.66	0.43	5.79	1.31
Na ₂ O	4.58	0.15	4.87	4.35	4.74	0.14	4.39	0.20	4.47	0.24	4.80	0.37
K ₂ O	3.09	0.09	3.14	3.80	2.58	0.05	1.91	0.11	3.24	0.21	1.81	0.51
P ₂ O ₃	0.17	0.05	0.15	0.05	0.21	0.03	0.26	0.02	0.12	0.01	0.26	0.08
Cl	0.10	0.02	0.11	0.09	0.07	0.03	0.16	0.06	0.14	0.02	0.13	0.04

c) Major element composition (average and standard deviation) of the matrix glass (anhydrous) from Iztaccihuatl proximal deposits.

Sample	MXC-02		MXC-03		MXC-04		MXC-05	
Eruption	Los Pies B&A flow		Nepopualco dry PDC's		Nepopualco wet PDC's		Nepopualco fall	
N	21		15		13		21	
SiO ₂	76.71	0.20	74.80	2.08	75.36	2.44	71.65	0.20
TiO ₂	0.21	0.03	0.17	0.03	0.18	0.04	0.28	0.04
Al ₂ O ₃	13.09	0.14	14.49	1.38	14.26	1.76	16.22	0.14
FeO*	0.95	0.10	1.14	0.30	0.80	0.18	1.69	0.06
MnO	0.03	0.02	0.05	0.02	0.04	0.02	0.05	0.03
MgO	0.20	0.02	0.32	0.13	0.22	0.09	0.51	0.03
CaO	1.08	0.05	1.67	0.65	1.58	0.76	2.54	0.04
Na ₂ O	3.58	0.16	4.39	0.53	4.24	0.79	4.59	0.16
K ₂ O	4.06	0.17	2.82	0.54	3.19	0.63	2.22	0.04
P ₂ O ₃	0.02	0.02	0.06	0.03	0.06	0.03	0.08	0.03

Table 5Major element composition (average and *standard deviation*) of the matrix glass (anhydrous) from the Nepopualco tephra sequence.

Sample	MXC-02		MXC-03		MXC-04		MXC-05		MXC-06		MXC-07		MXC-08		MXC-09		MXC-10**	
Eruption	NT-1 (L. Pies B&A)		NT-2 (Nepopualco Ign: Dry and wet PDC's and fallout)															
N	21		15		13		21		24		27		22		23		24	
SiO ₂	76.71	<i>0.20</i>	74.80	<i>2.08</i>	75.36	<i>2.44</i>	71.65	<i>0.20</i>	73.26	<i>1.04</i>	72.13	<i>1.17</i>	69.26	<i>1.51</i>	67.94	<i>0.40</i>	73.95	66.27
TiO ₂	0.21	<i>0.03</i>	0.17	<i>0.03</i>	0.18	<i>0.04</i>	0.28	<i>0.04</i>	0.31	<i>0.07</i>	0.29	<i>0.06</i>	1.04	<i>0.20</i>	0.90	<i>0.05</i>	0.18	0.50
Al ₂ O ₃	13.09	<i>0.14</i>	14.49	<i>1.38</i>	14.26	<i>1.76</i>	16.22	<i>0.14</i>	14.65	<i>0.49</i>	15.44	<i>0.57</i>	14.51	<i>1.23</i>	15.52	<i>0.27</i>	14.56	17.95
FeO*	0.95	<i>0.10</i>	1.14	<i>0.30</i>	0.80	<i>0.18</i>	1.69	<i>0.06</i>	1.86	<i>0.26</i>	1.96	<i>0.28</i>	3.79	<i>0.71</i>	3.68	<i>0.19</i>	1.34	2.80
MnO	0.03	<i>0.02</i>	0.05	<i>0.02</i>	0.04	<i>0.02</i>	0.05	<i>0.03</i>	0.04	<i>0.02</i>	0.06	<i>0.02</i>	0.06	<i>0.02</i>	0.07	<i>0.02</i>	0.07	0.06
MgO	0.20	<i>0.02</i>	0.32	<i>0.13</i>	0.22	<i>0.09</i>	0.51	<i>0.03</i>	0.45	<i>0.12</i>	0.56	<i>0.11</i>	0.74	<i>0.30</i>	1.19	<i>0.09</i>	0.48	0.91
CaO	1.08	<i>0.05</i>	1.67	<i>0.65</i>	1.58	<i>0.76</i>	2.54	<i>0.04</i>	1.96	<i>0.31</i>	2.11	<i>0.31</i>	3.05	<i>0.72</i>	3.47	<i>0.22</i>	1.57	4.62
Na ₂ O	3.58	<i>0.16</i>	4.39	<i>0.53</i>	4.24	<i>0.79</i>	4.59	<i>0.16</i>	4.77	<i>0.22</i>	4.61	<i>0.11</i>	4.52	<i>0.24</i>	4.68	<i>0.20</i>	4.90	4.79
K ₂ O	4.06	<i>0.17</i>	2.82	<i>0.54</i>	3.19	<i>0.63</i>	2.22	<i>0.04</i>	2.56	<i>0.17</i>	2.63	<i>0.14</i>	2.75	<i>0.36</i>	2.20	<i>0.13</i>	2.80	1.85
P ₂ O ₃	0.02	<i>0.02</i>	0.06	<i>0.03</i>	0.06	<i>0.03</i>	0.08	<i>0.03</i>	0.07	<i>0.03</i>	0.10	<i>0.04</i>	0.19	<i>0.07</i>	0.19	<i>0.02</i>	0.06	0.19
Cl	0.08	<i>0.02</i>	0.09	<i>0.02</i>	0.07	<i>0.05</i>	0.17	<i>0.09</i>	0.08	<i>0.04</i>	0.11	<i>0.02</i>	0.09	<i>0.07</i>	0.16	<i>0.19</i>	0.10	0.07

Average and standard deviations (italics) for tephra deposits recorded through the Nepopualco sequence. Compositions in weight percent (wt%) were determined using a wavelength-dispersive EMP (see Section 5). N = number of analyses. See Supplementary material for the raw data and secondary standards. ** Bimodal samples are shown as selected representative compositions for each sub-component instead of by the average and standard deviation.

Table 5 (continued)

Sample	MXC-11**		MXC-12		MXC-13*		MXC-14		MXC-15		MXC-35		MXC-36		MXC-37		MXC-38	
Eruption	NT-08		NT-09		NT-10		NT-11		NT-12		NT-13		NT-14		NT-15		NT-16	
N	16		5		21		16		10		25		25		23		17	
SiO ₂	74.25	70.66	62.47	<i>0.31</i>	73.15	68.22	71.86	<i>0.34</i>	64.34	<i>0.31</i>	76.30	<i>1.39</i>	64.93	<i>0.33</i>	62.36	<i>0.34</i>	68.34	<i>0.99</i>
TiO ₂	0.28	0.65	1.27	<i>0.09</i>	0.53	0.83	0.41	<i>0.03</i>	0.88	<i>0.05</i>	0.30	<i>0.07</i>	1.00	<i>0.12</i>	1.08	<i>0.03</i>	0.77	<i>0.07</i>
Al ₂ O ₃	14.39	15.35	16.80	<i>0.26</i>	13.99	15.55	15.07	<i>0.21</i>	17.32	<i>0.38</i>	13.12	<i>0.75</i>	16.57	<i>0.34</i>	17.07	<i>0.14</i>	15.82	<i>0.36</i>
FeO*	1.67	2.75	5.52	<i>0.11</i>	2.39	3.61	2.29	<i>0.11</i>	3.99	<i>0.26</i>	1.33	<i>0.26</i>	4.08	<i>0.23</i>	5.12	<i>0.18</i>	3.27	<i>0.17</i>
MnO	0.03	0.03	0.11	<i>0.01</i>	0.02	0.06	0.04	<i>0.02</i>	0.06	<i>0.02</i>	0.03	<i>0.02</i>	0.07	<i>0.02</i>	0.09	<i>0.02</i>	0.07	<i>0.02</i>
MgO	0.26	0.71	2.13	<i>0.29</i>	0.59	1.17	0.60	<i>0.04</i>	1.80	<i>0.24</i>	0.21	<i>0.06</i>	1.87	<i>0.16</i>	2.34	<i>0.07</i>	1.14	<i>0.25</i>
CaO	2.05	2.65	4.71	<i>0.18</i>	2.11	3.38	2.29	<i>0.09</i>	4.52	<i>0.23</i>	1.18	<i>0.31</i>	4.55	<i>0.16</i>	5.27	<i>0.19</i>	3.41	<i>0.34</i>
Na ₂ O	4.14	4.06	4.70	<i>0.12</i>	4.39	4.69	4.62	<i>0.13</i>	4.86	<i>0.18</i>	3.79	<i>0.18</i>	4.63	<i>0.16</i>	4.61	<i>0.13</i>	4.46	<i>0.23</i>
K ₂ O	2.88	2.94	1.94	<i>0.11</i>	2.72	2.22	2.63	<i>0.06</i>	1.93	<i>0.15</i>	3.62	<i>0.18</i>	2.02	<i>0.09</i>	1.79	<i>0.08</i>	2.42	<i>0.12</i>
P ₂ O ₃	0.00	0.12	0.28	<i>0.08</i>	0.05	0.18	0.08	<i>0.03</i>	0.22	<i>0.03</i>	0.05	<i>0.03</i>	0.20	<i>0.04</i>	0.20	<i>0.04</i>	0.21	<i>0.06</i>
Cl	0.04	0.08	0.07	<i>0.03</i>	0.06	0.09	0.13	<i>0.09</i>	0.08	<i>0.01</i>	0.07	<i>0.02</i>	0.07	<i>0.03</i>	0.08	<i>0.02</i>	0.15	<i>0.08</i>

Table 5 (continued)

Sample	MXC-39		MXC-41**		MXC-42		MXC-43		MXC-44		MXC-45		MXC-46		MXC-47		MXC-48	
Eruption	NT-17		NT-18		NT-19		NT-20		NT-21		NT-22		NT-23		NT-24		NT-25	
N	20		21		22		25		20		16		23		27		15	
SiO ₂	63.83	<i>0.93</i>	66.54	63.58	66.09	<i>0.84</i>	61.40	<i>0.30</i>	61.88	<i>0.30</i>	66.56	<i>0.59</i>	69.14	<i>0.31</i>	76.79	<i>0.25</i>	77.03	<i>0.78</i>
TiO ₂	1.04	<i>0.09</i>	0.87	0.95	0.72	<i>0.04</i>	1.02	<i>0.05</i>	1.04	<i>0.04</i>	0.69	<i>0.04</i>	0.61	<i>0.04</i>	0.09	<i>0.02</i>	0.17	<i>0.03</i>
Al ₂ O ₃	16.84	<i>0.46</i>	15.63	17.09	17.42	<i>0.62</i>	17.80	<i>0.16</i>	17.58	<i>0.12</i>	16.97	<i>0.47</i>	15.89	<i>0.18</i>	12.59	<i>0.18</i>	13.19	<i>0.45</i>
FeO*	4.82	<i>0.38</i>	3.97	4.36	3.33	<i>0.20</i>	5.00	<i>0.18</i>	5.04	<i>0.13</i>	3.58	<i>0.21</i>	2.93	<i>0.09</i>	1.04	<i>0.04</i>	0.87	<i>0.14</i>
MnO	0.09	<i>0.02</i>	0.05	0.06	0.05	<i>0.02</i>	0.09	<i>0.02</i>	0.08	<i>0.02</i>	0.07	<i>0.02</i>	0.06	<i>0.02</i>	0.03	<i>0.02</i>	0.04	<i>0.02</i>
MgO	1.70	<i>0.19</i>	1.51	1.99	1.20	<i>0.18</i>	2.50	<i>0.09</i>	2.43	<i>0.10</i>	1.16	<i>0.14</i>	0.97	<i>0.12</i>	0.04	<i>0.02</i>	0.22	<i>0.06</i>
CaO	4.73	<i>0.33</i>	4.01	4.82	4.16	<i>0.43</i>	5.43	<i>0.20</i>	5.37	<i>0.16</i>	3.73	<i>0.30</i>	3.07	<i>0.18</i>	0.41	<i>0.02</i>	1.16	<i>0.20</i>
Na ₂ O	4.83	<i>0.28</i>	4.31	4.60	4.79	<i>0.22</i>	4.79	<i>0.16</i>	4.53	<i>0.11</i>	4.90	<i>0.19</i>	4.68	<i>0.18</i>	4.01	<i>0.18</i>	4.06	<i>0.19</i>
K ₂ O	1.81	<i>0.14</i>	2.29	2.20	1.97	<i>0.22</i>	1.71	<i>0.11</i>	1.79	<i>0.05</i>	2.06	<i>0.15</i>	2.39	<i>0.04</i>	4.85	<i>0.20</i>	3.12	<i>0.23</i>
P ₂ O ₃	0.22	<i>0.04</i>	0.17	0.27	0.16	<i>0.04</i>	0.20	<i>0.04</i>	0.19	<i>0.03</i>	0.21	<i>0.04</i>	0.14	<i>0.02</i>	0.01	<i>0.01</i>	0.04	<i>0.03</i>

Table 6
Major element composition (average and *standard deviation*) of the matrix glass (anhydrous) from the tephra recorded in Xalitintla region by outcrops
a) East of the Restaurant site

Sample	MXC-16****		MXC-17		MXC-18		MXC-19		MXC-20		MXC-21**		MXC-22		MXC-23		MXC-24		
Eruption	ERT-1		ERT-2		ERT-2		ERT-3		ERT-3		ERT-4		ERT-5		ERT-6		ERT-7		
N	29		23		14		13		13		10		21		25		26		
SiO ₂	68.12	65.72	62.37	67.53	0.26	67.10	0.23	67.93	0.28	67.43	0.42	70.05	67.77	66.05	0.27	64.92	0.38	66.64	0.32
TiO ₂	1.00	0.92	0.84	0.92	0.05	0.97	0.04	0.87	0.03	0.90	0.04	0.88	1.08	1.04	0.03	1.09	0.05	0.94	0.03
Al ₂ O ₃	14.66	16.16	17.20	15.85	0.22	15.99	0.13	15.74	0.18	15.90	0.13	14.69	15.20	16.02	0.13	16.05	0.13	15.81	0.11
FeO*	3.75	3.81	4.66	3.35	0.09	3.50	0.12	3.30	0.09	3.46	0.14	3.22	3.94	4.01	0.15	4.31	0.16	3.73	0.12
MnO	0.08	0.07	0.05	0.05	0.02	0.05	0.01	0.04	0.01	0.05	0.02	0.06	0.03	0.06	0.02	0.08	0.02	0.07	0.02
MgO	1.11	1.52	2.53	1.21	0.05	1.30	0.06	1.08	0.07	1.22	0.09	0.92	1.21	1.44	0.04	1.77	0.05	1.54	0.06
CaO	2.95	4.13	5.75	3.26	0.12	3.42	0.14	3.08	0.14	3.29	0.20	2.62	3.20	3.65	0.14	4.23	0.15	3.89	0.20
Na ₂ O	4.93	4.67	4.49	4.48	0.20	4.45	0.13	4.65	0.11	4.55	0.14	4.38	4.47	4.78	0.15	4.93	0.27	4.82	0.21
K ₂ O	3.11	2.62	1.91	3.02	0.08	2.94	0.07	3.04	0.09	2.94	0.07	3.02	2.76	2.60	0.05	2.31	0.04	2.32	0.06
P ₂ O ₃	0.22	0.29	0.14	0.18	0.04	0.18	0.04	0.17	0.03	0.17	0.02	0.13	0.21	0.26	0.02	0.23	0.03	0.20	0.03
Cl	0.07	0.09	0.06	0.16	0.16	0.09	0.02	0.09	0.04	0.08	0.01	0.03	0.11	0.09	0.05	0.07	0.02	0.05	0.01

Average and standard deviations (italics) for tephra deposits recorded through the Nepopualco sequence. Compositions in weight percent (wt%) were determined using a wavelength-dispersive EMP (see Section 5). N = number of analyses. See Supplementary material for the raw data and secondary standards. Bimodal** and trimodal*** samples are shown as selected representative compositions for each sub-component instead of by the average and standard deviation.”

Table 6 (continued)
b) West of the Restaurant site

Sample	MXC-25***		MXC-26		MXC-27		MXC-28		MXC-29		MXC-30		MXC-31		MXC-32		MXC-33		MXC-34		
Eruption	WRT-1		WRT-2		WRT-2		WRT-3		WRT-3		WRT-4		WRT-5		WRT-6		WRT-7		WRT-8		
N	23		14		11		26		15		21		22		12		23		12		
SiO ₂	71.80	66.79	60.19	67.56	0.36	66.60	0.52	61.35	0.34	60.81	0.21	61.70	0.23	68.49	0.62	66.92	0.41	68.95	0.46	65.02	0.59
TiO ₂	0.76	1.00	1.05	0.51	0.04	0.81	0.07	1.03	0.04	1.04	0.03	1.04	0.03	0.75	0.06	0.67	0.04	0.61	0.04	0.96	0.11
Al ₂ O ₃	14.07	15.29	17.56	16.87	0.27	16.73	0.49	17.83	0.21	18.04	0.16	17.53	0.15	15.96	0.31	16.63	0.28	15.92	0.34	16.72	0.80
FeO*	2.86	4.85	5.95	3.13	0.18	3.61	0.18	5.00	0.23	5.26	0.16	5.19	0.12	3.16	0.19	3.65	0.15	2.97	0.08	4.02	0.45
MnO	0.04	0.06	0.12	0.05	0.02	0.06	0.02	0.09	0.02	0.08	0.02	0.09	0.02	0.05	0.02	0.07	0.02	0.05	0.02	0.08	0.02
MgO	0.55	1.65	3.62	1.06	0.10	1.22	0.11	2.54	0.11	2.69	0.10	2.46	0.08	1.04	0.07	1.19	0.09	0.95	0.05	1.53	0.27
CaO	2.01	3.87	6.50	3.64	0.22	3.66	0.22	5.52	0.18	5.55	0.16	5.25	0.10	3.20	0.20	3.49	0.18	3.11	0.25	4.34	0.48
Na ₂ O	4.72	3.04	3.27	4.65	0.31	4.86	0.17	4.67	0.11	4.59	0.09	4.69	0.09	4.55	0.32	4.95	0.15	4.78	0.17	4.71	0.28
K ₂ O	3.05	3.18	1.57	2.01	0.17	2.18	0.20	1.71	0.11	1.65	0.06	1.79	0.06	2.49	0.11	2.14	0.16	2.36	0.09	2.24	0.19
P ₂ O ₃	0.09	0.25	0.11	0.16	0.03	0.17	0.04	0.19	0.04	0.21	0.02	0.20	0.03	0.16	0.04	0.20	0.04	0.14	0.04	0.26	0.03

Average and standard deviations (italics) for tephra deposits recorded through the Nepopualco sequence. Compositions in weight percent (wt%) were determined using a wavelength-dispersive EMP (see Section 5). N = number of analyses. See Supplementary material for the raw data and secondary standards. Bimodal** and trimodal*** samples are shown as selected representative compositions for each sub-component instead of by the average and standard deviation.”

Table 6 (continued)
c) Fork in the Road site

Sample	MXC-102		MXC-103		MXC-104		MXC-105		MXC-106**		MXC-107	
Eruption	FRT-1		FRT-2		FRT-3		FRT-4		FRT-5		FRT-6	
N	25		14		13		19		28		19	
SiO ₂	72.09	<i>0.21</i>	70.80	<i>0.62</i>	63.80	0.76	63.21	<i>0.35</i>	73.21	68.09	<i>66.02</i>	<i>0.62</i>
TiO ₂	0.42	<i>0.03</i>	0.78	<i>0.04</i>	0.79	0.08	0.66	<i>0.04</i>	0.49	0.91	<i>0.98</i>	<i>0.06</i>
Al ₂ O ₃	15.14	<i>0.15</i>	14.47	<i>0.30</i>	17.51	1.08	17.96	<i>0.22</i>	14.39	15.49	15.92	0.20
FeO*	2.19	<i>0.09</i>	2.99	<i>0.22</i>	4.23	0.54	4.31	<i>0.18</i>	1.92	3.47	3.96	<i>0.13</i>
MnO	0.04	<i>0.02</i>	0.06	<i>0.02</i>	0.07	0.02	0.08	<i>0.02</i>	0.02	0.07	0.06	<i>0.02</i>
MgO	0.57	<i>0.03</i>	0.75	<i>0.07</i>	1.65	0.46	2.02	<i>0.08</i>	0.47	1.11	1.59	<i>0.13</i>
CaO	2.28	<i>0.06</i>	2.37	<i>0.18</i>	4.39	0.63	5.04	<i>0.22</i>	1.79	3.01	3.93	<i>0.21</i>
Na ₂ O	4.45	<i>0.16</i>	4.77	<i>0.12</i>	4.75	0.48	4.37	<i>0.19</i>	3.82	4.65	4.80	<i>0.28</i>
K ₂ O	2.63	<i>0.05</i>	2.74	<i>0.09</i>	2.38	0.37	1.91	<i>0.07</i>	3.72	2.98	2.47	<i>0.07</i>
P ₂ O ₃	0.08	<i>0.02</i>	0.16	<i>0.11</i>	0.27	0.06	0.22	<i>0.04</i>	0.10	0.16	0.20	<i>0.04</i>
Cl	0.11	<i>0.07</i>	0.13	<i>0.01</i>	0.17	0.19	0.24	<i>0.25</i>	0.06	0.07	<i>0.06</i>	<i>0.02</i>

Average and standard deviations (italics) for tephra deposits recorded through the Nepopualco sequence. Compositions in weight percent (wt%) were determined using a wavelength-dispersive EMP (see Section 5). N = number of analyses. See Supplementary material for the raw data and secondary standards. Bimodal** and trimodal*** samples are shown as selected representative compositions for each sub-component instead of by the average and standard deviation.”

Table 7

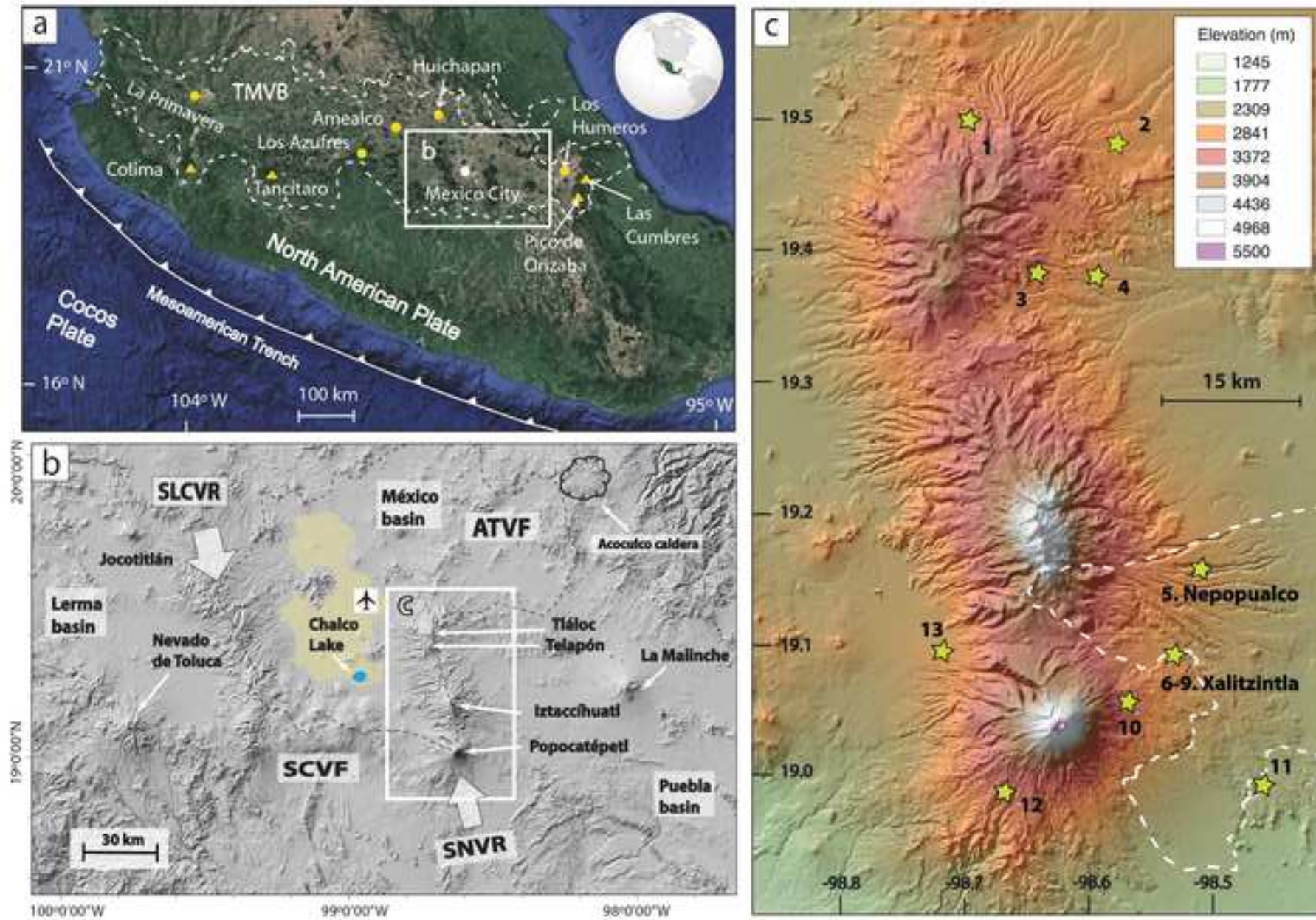
Summary of $^{40}\text{Ar}/^{39}\text{Ar}$ dates reported in this study

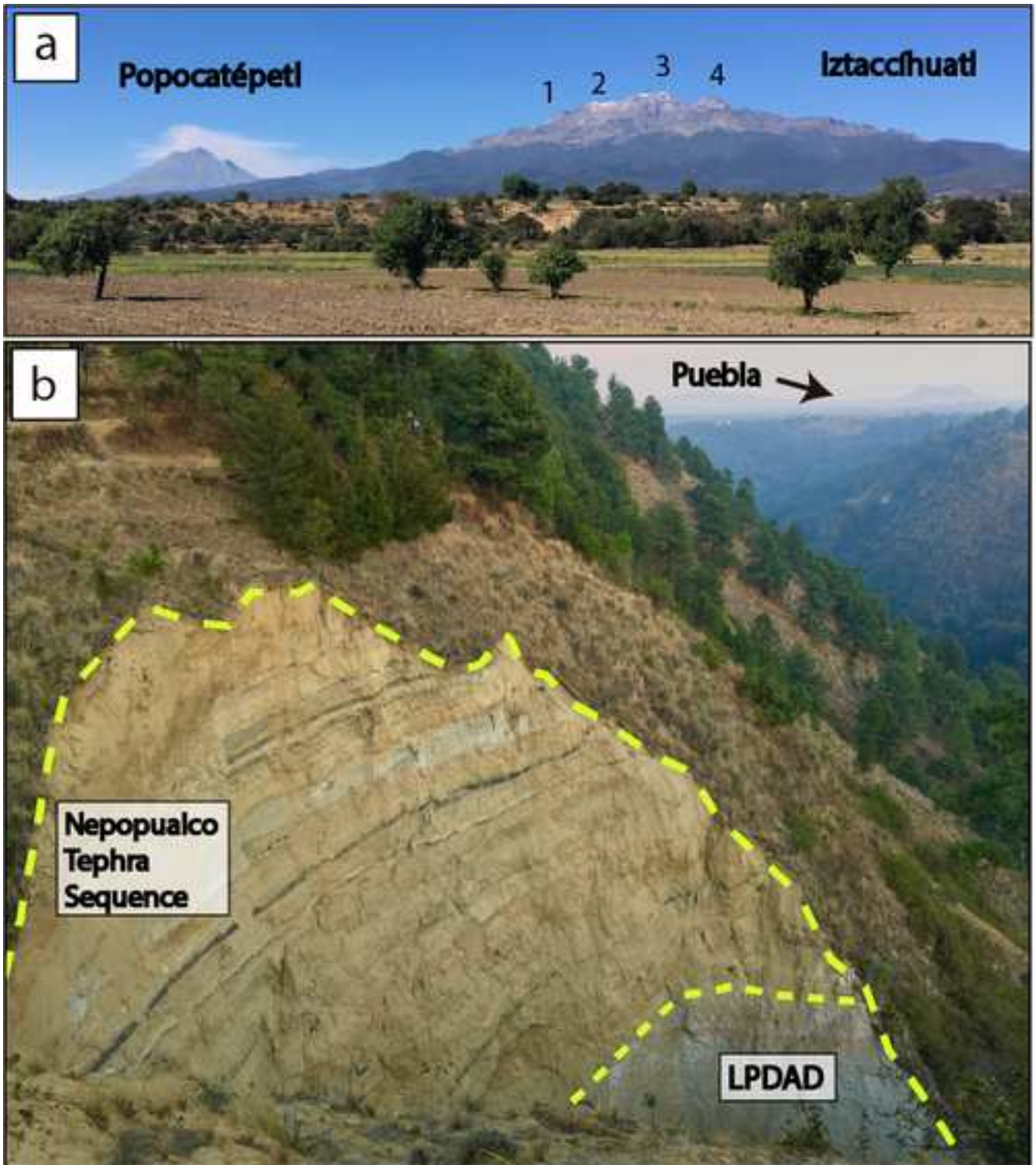
Unit	Sample	Mineral	Location		Locality	Outcrop	Age (ka;2 σ)	MSWD
			North	West				
NT-2	MXC-05	Hornblende	19.149749°	98.508040°	Nepopualco	5	630 \pm 44	1.49
NT-12	MXC-15	Plagioclase	19.149749°	98.508040°	Nepopualco	5	619 \pm 52	1.19
ERT-3	MXC-19	Plagioclase	19.078794°	98.506966°	Xalitzintla	6	236 \pm 24	1.08
WRT-6	MXC-32	Plagioclase	19.080099°	98.507531°	Xalitzintla	7	431 \pm 40	1.50
WRT-7	MXC-33	Plagioclase	19.080099°	98.507531°	Xalitzintla	7	353 \pm 58	1.54
NT-23	MXC-46	Plagioclase	19.149749°	98.508040°	Nepopualco	5	368 \pm 22	1.35
SVI	MXC-50	Sanidine*	19.477587°	98.575406°	Nanacamilpa	2	101 \pm 2	1.20
SVI	MXC-88	Sanidine*	19.396556°	98.624861°	San Juan C.	3	103 \pm 3	1.30

SVI = San Valentin Ignimbrite; NT = Nepopualco Tephra; ERT = East of the Restaurant Tephra; WRT = West of the Restaurant Tephra; ka = thousand years; 2 σ = two sigma; MSWD = Mean Squared Weighted Deviation

Fig 1

[Click here to access/download;Figure;Fig. 1. Map of TMVB, Mexico Basin and SNVR.jpg](#)





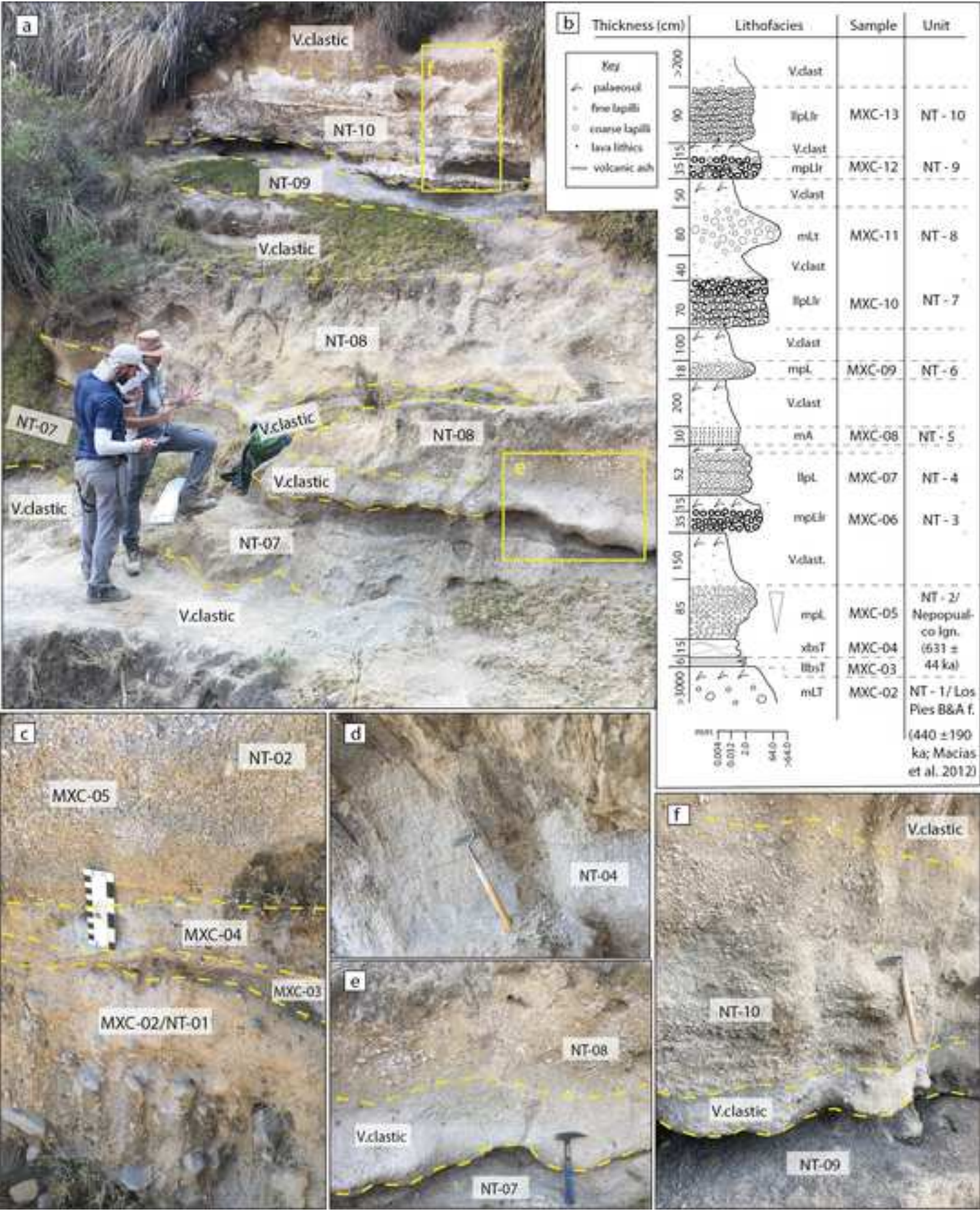


Fig 4

[Click here to access/download;Figure;Fig. 4. Nepopualco middle tephras.png](#)

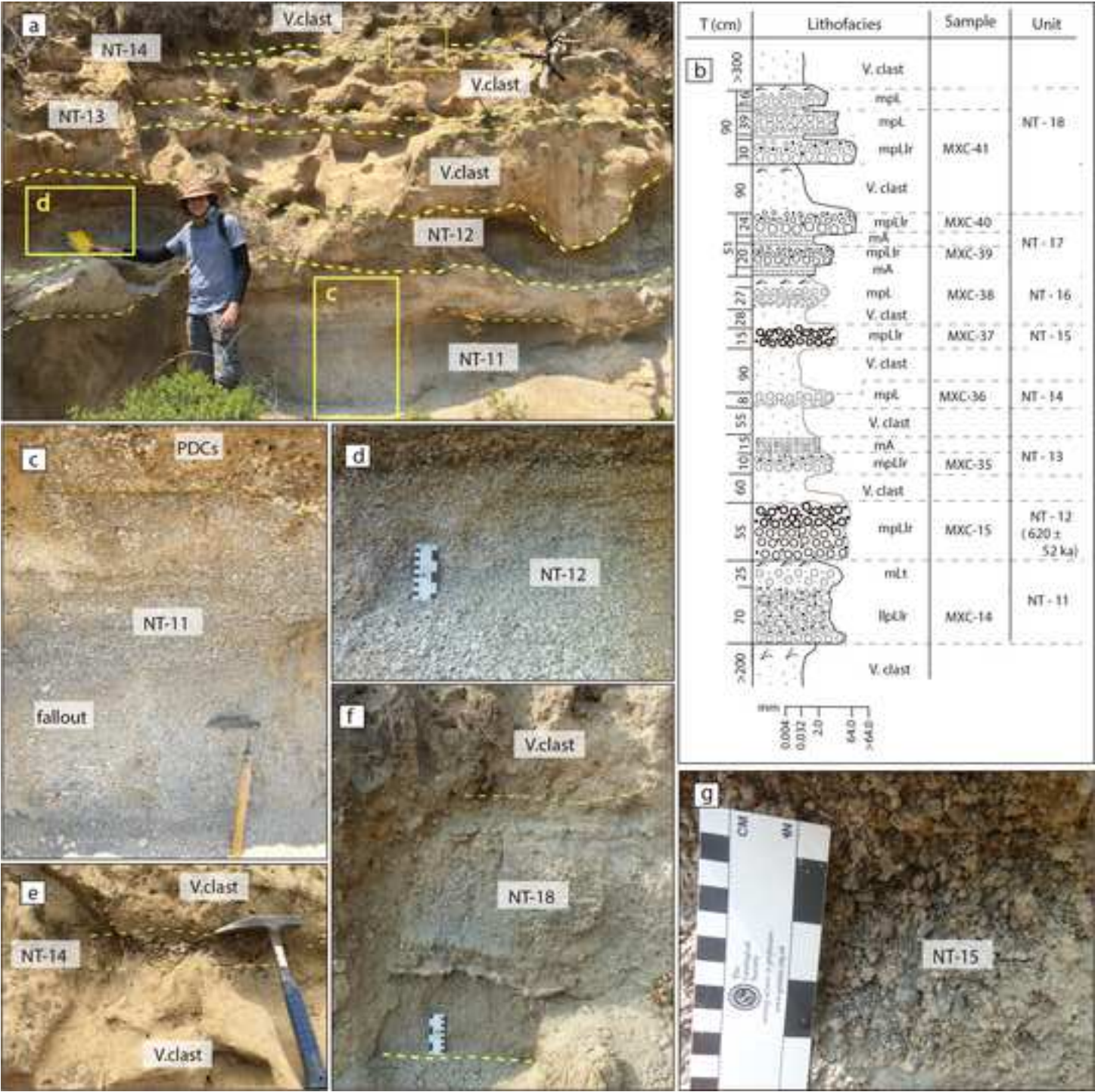
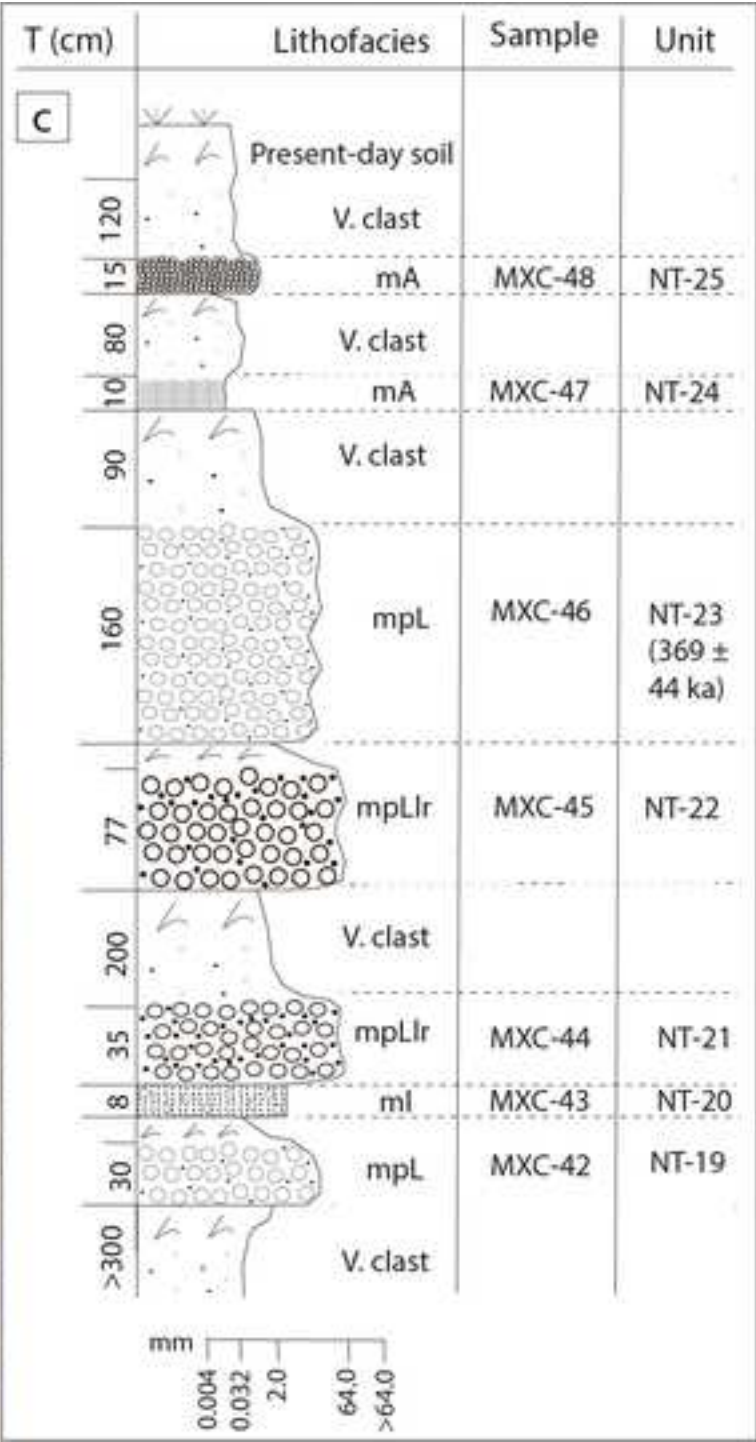
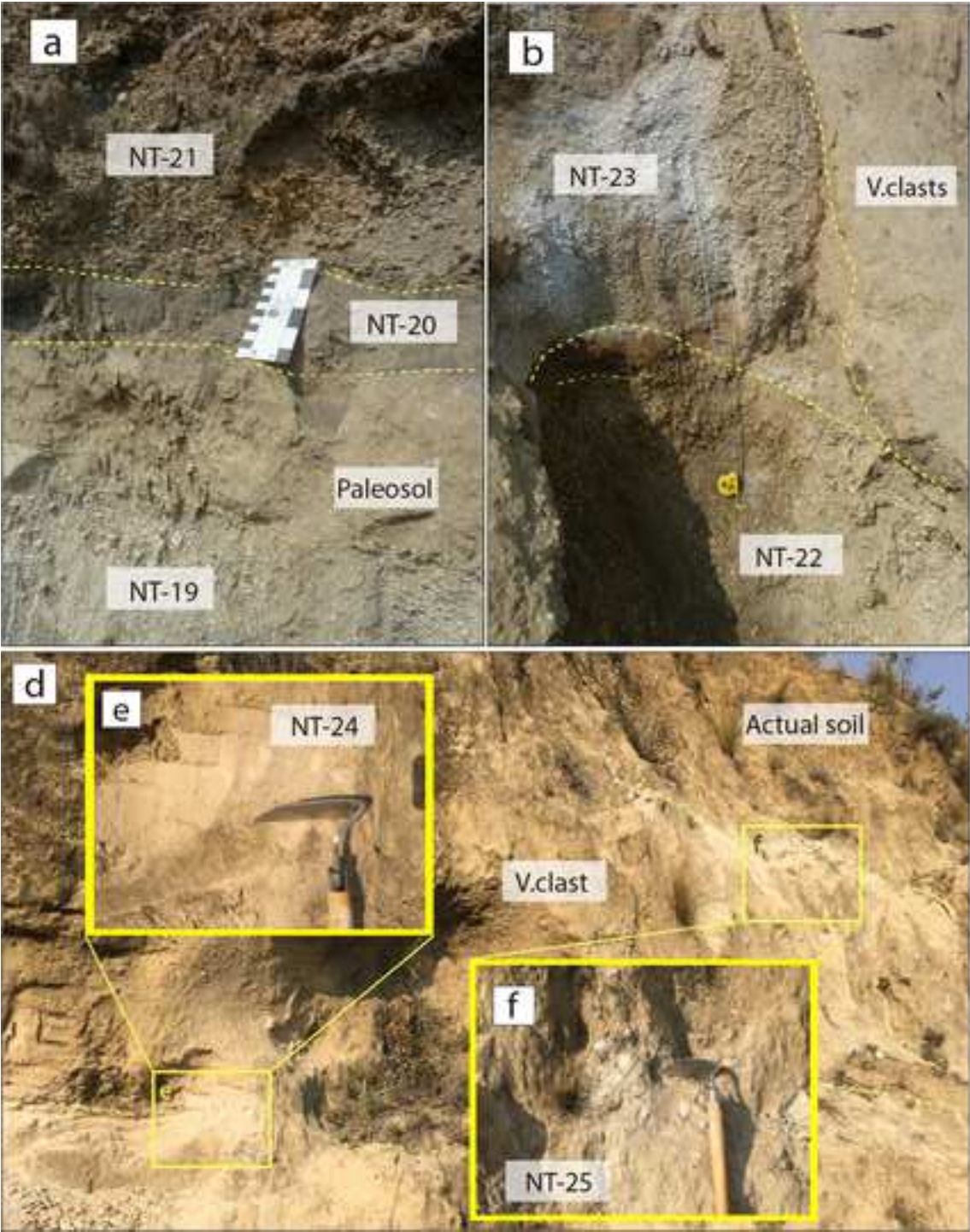
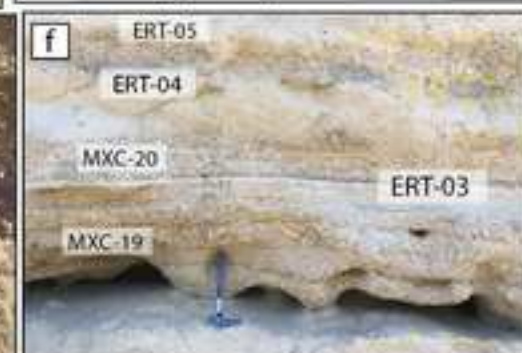
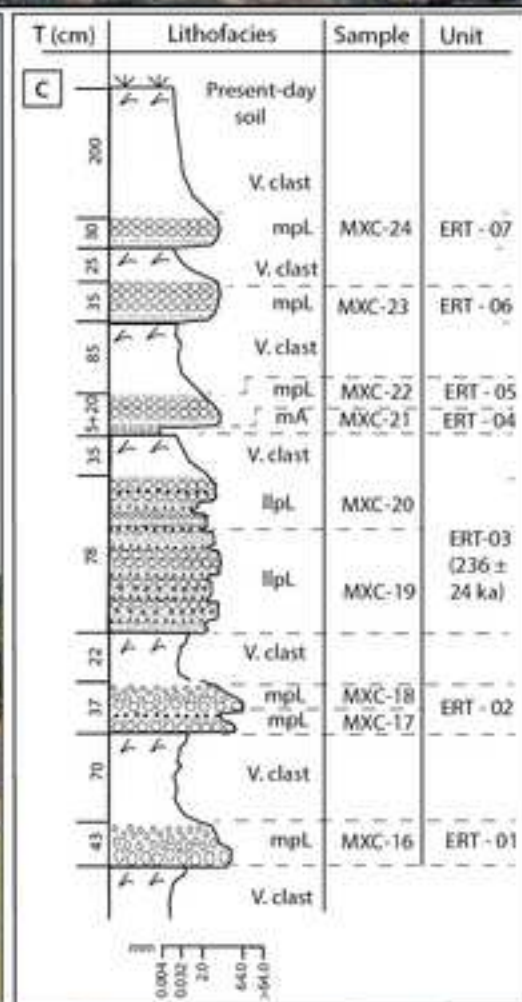
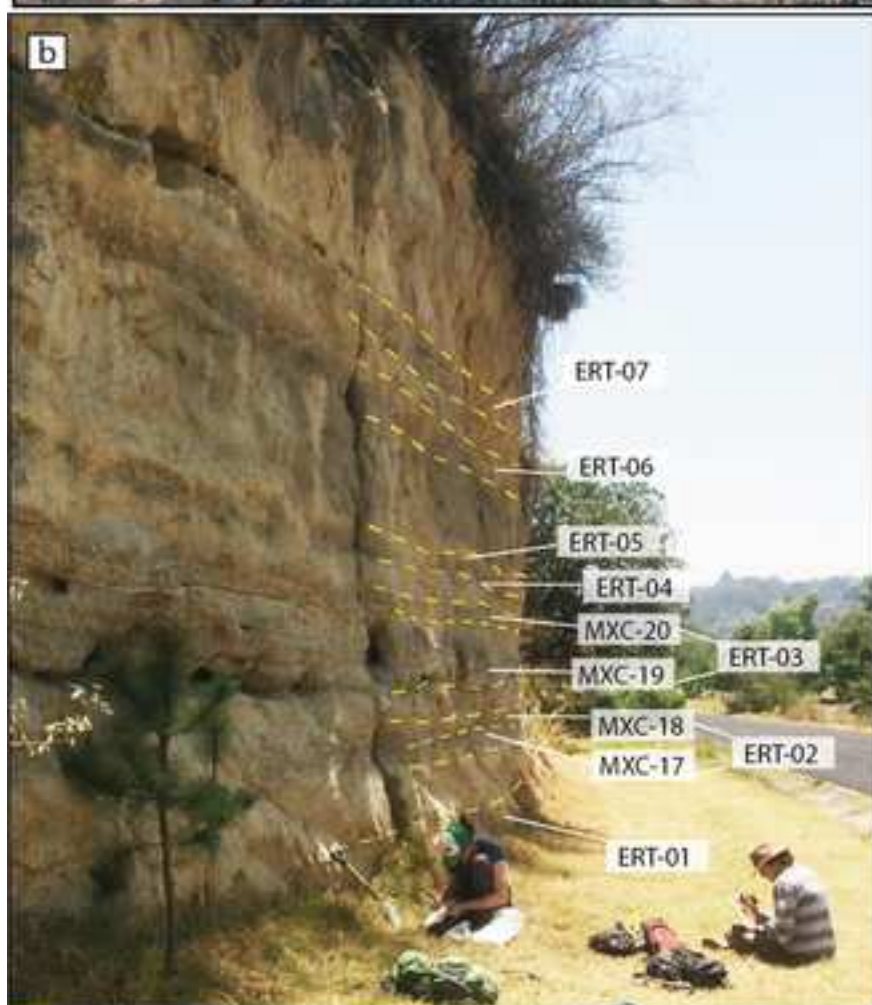


Fig 5





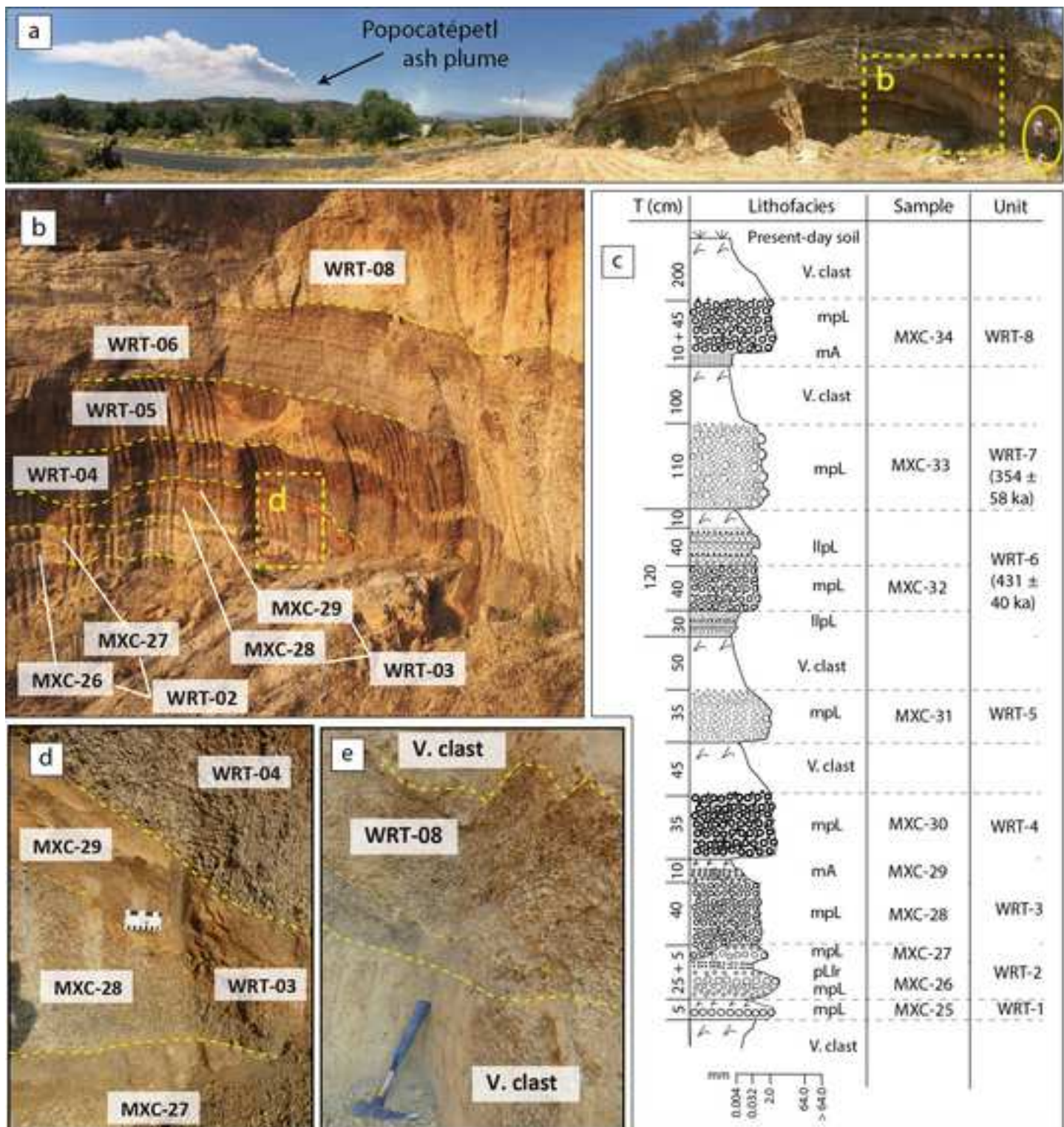
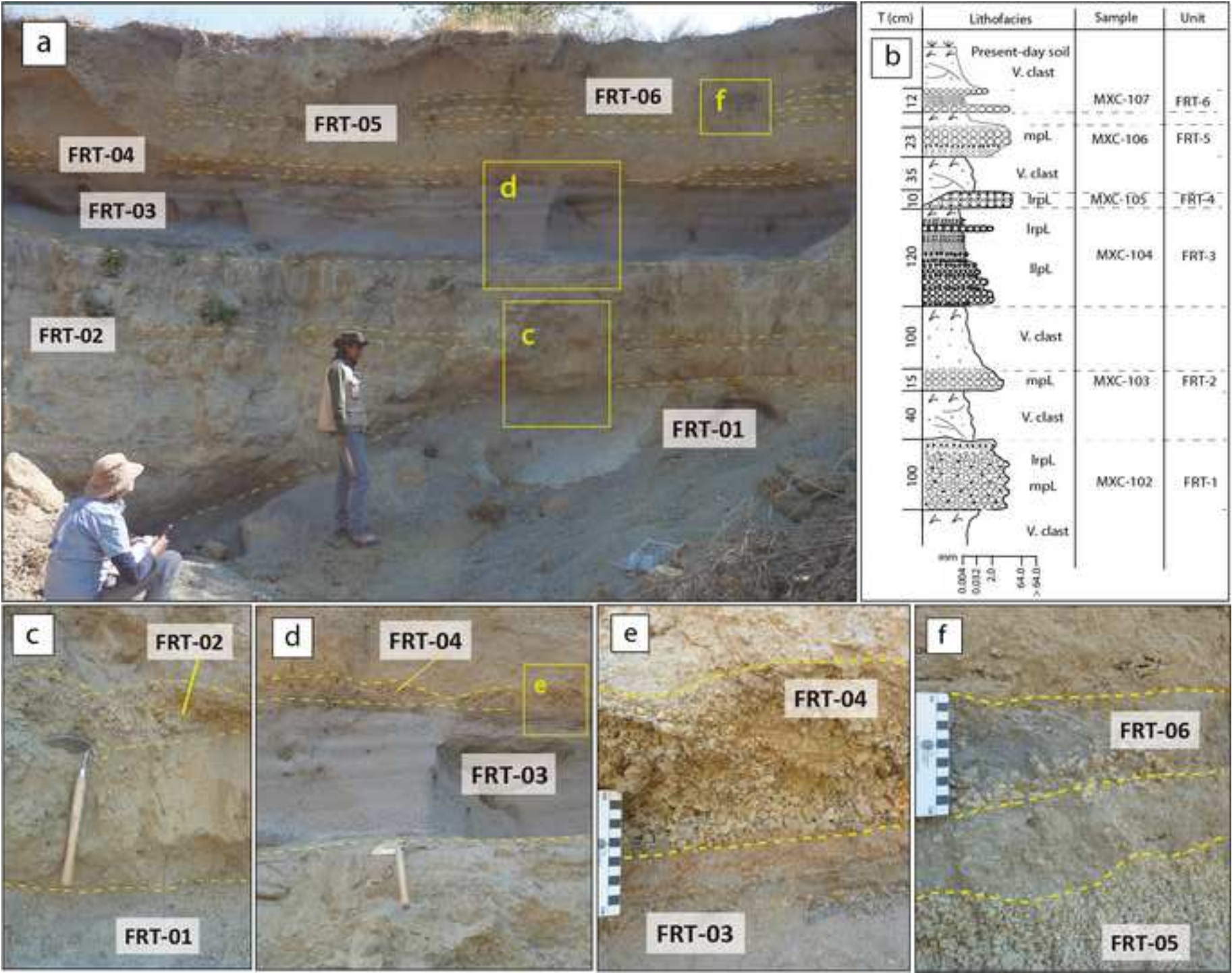


Fig 8



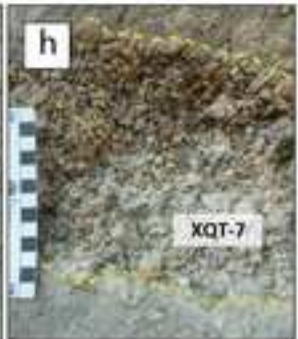
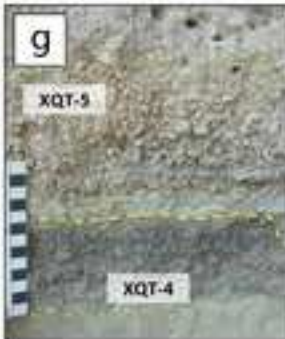
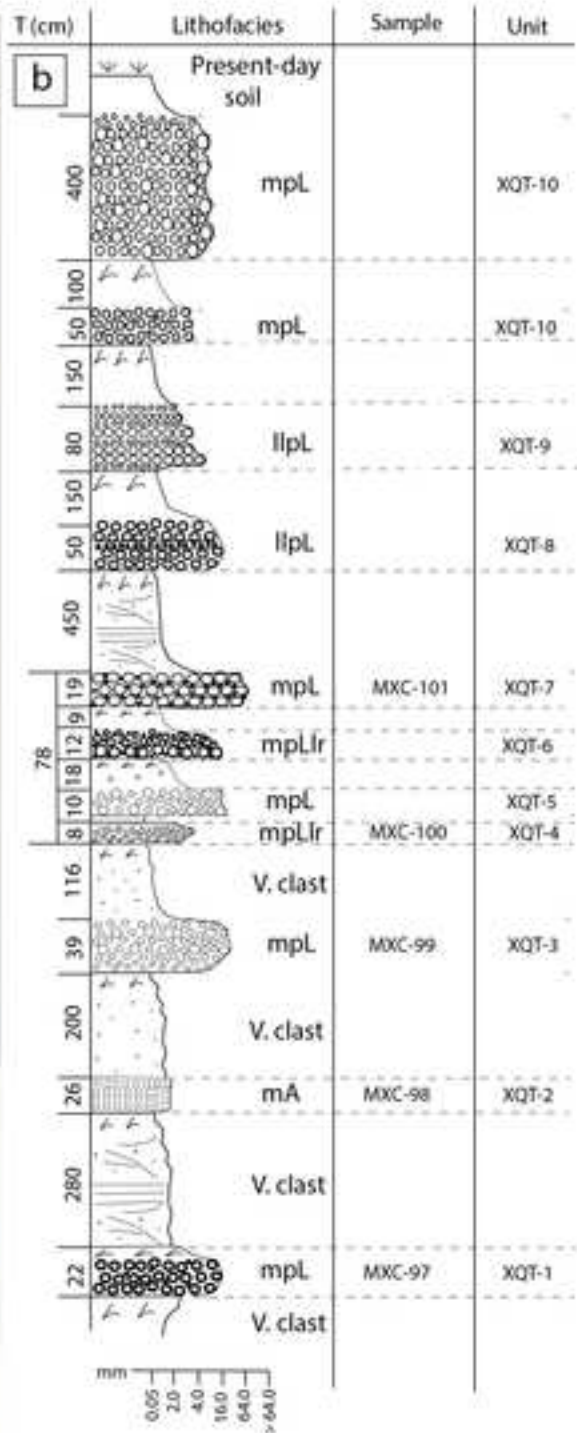
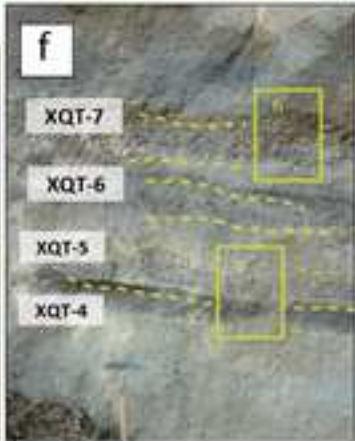
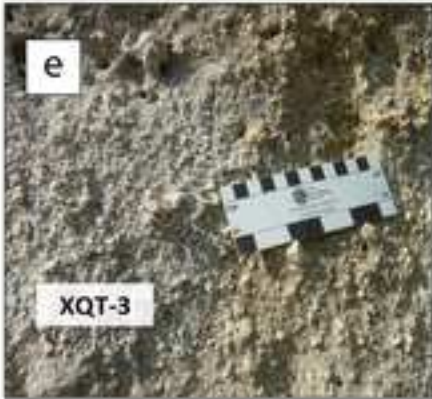
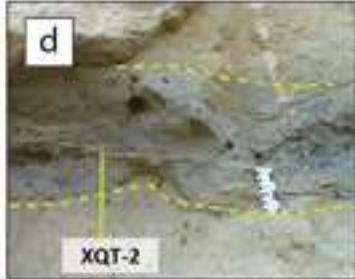
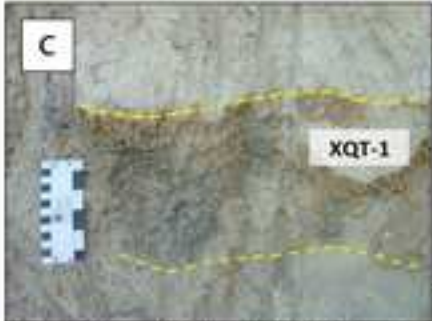
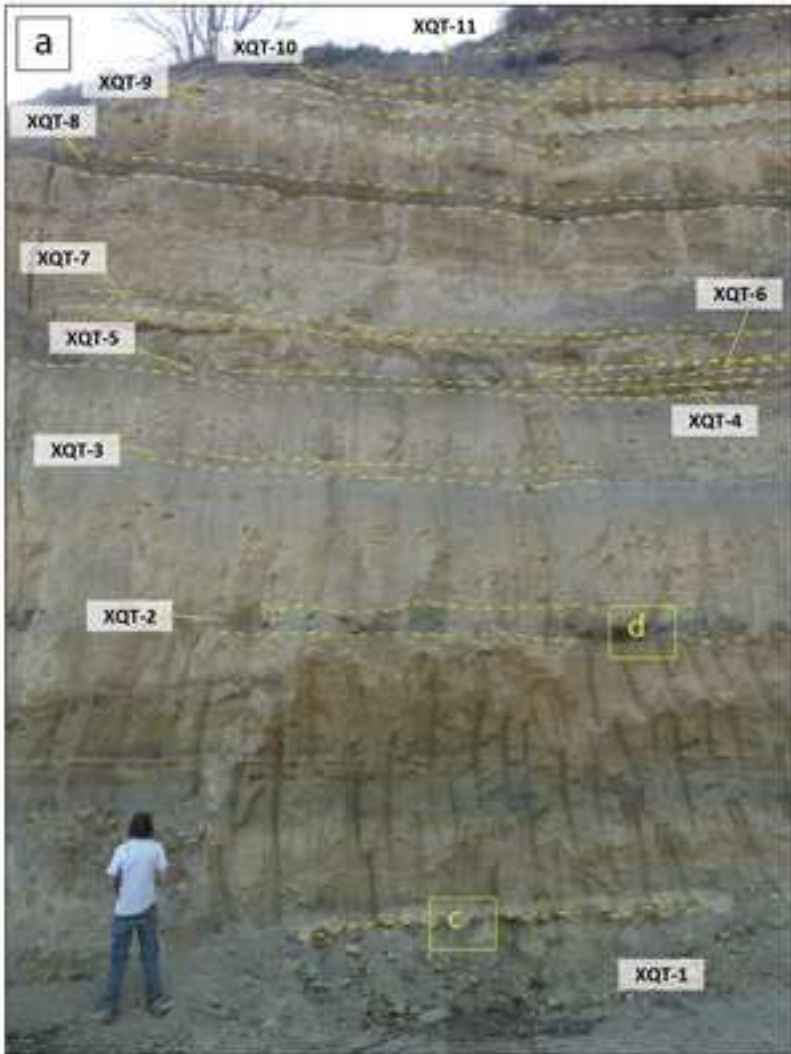
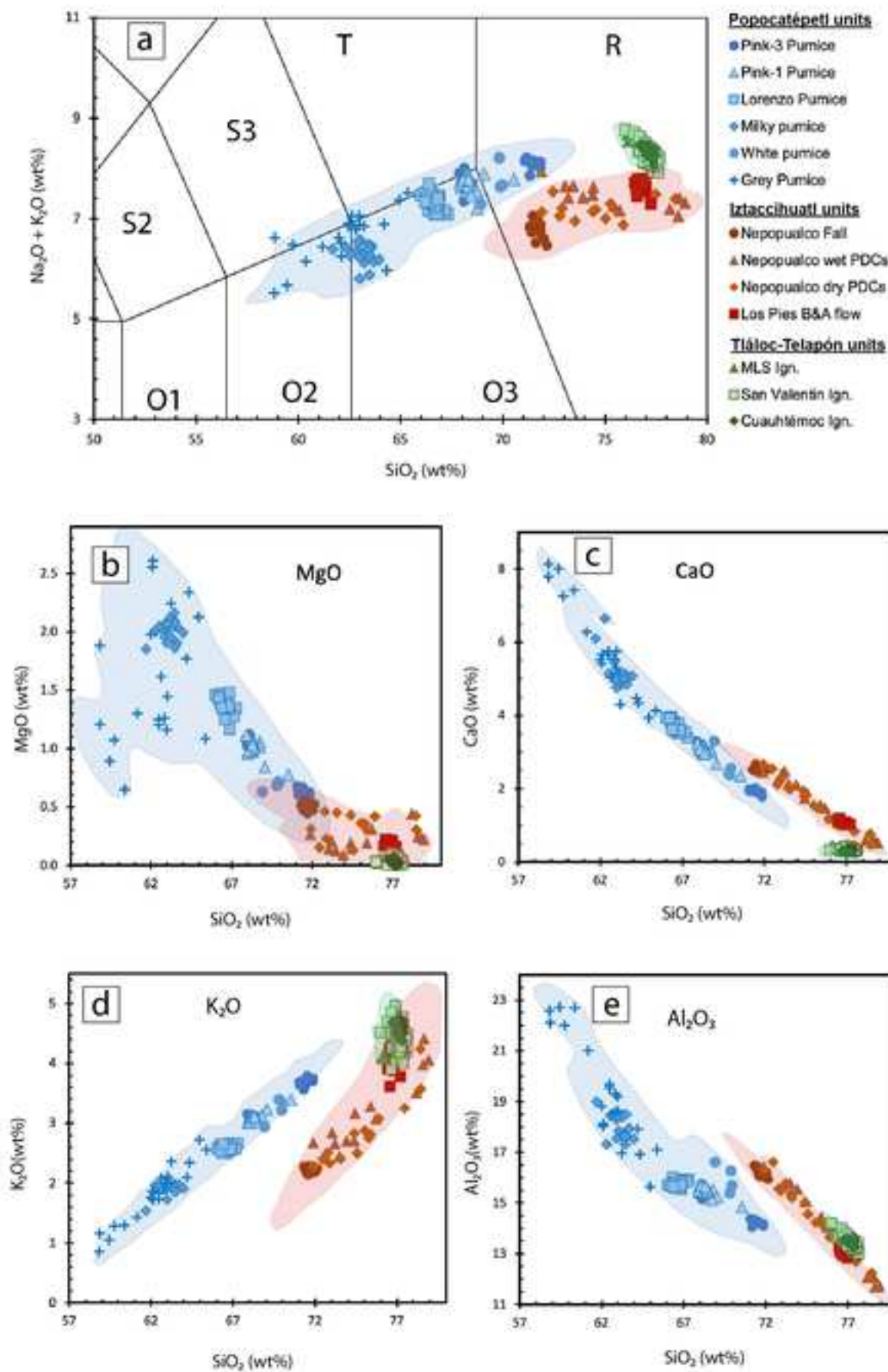


Fig 10



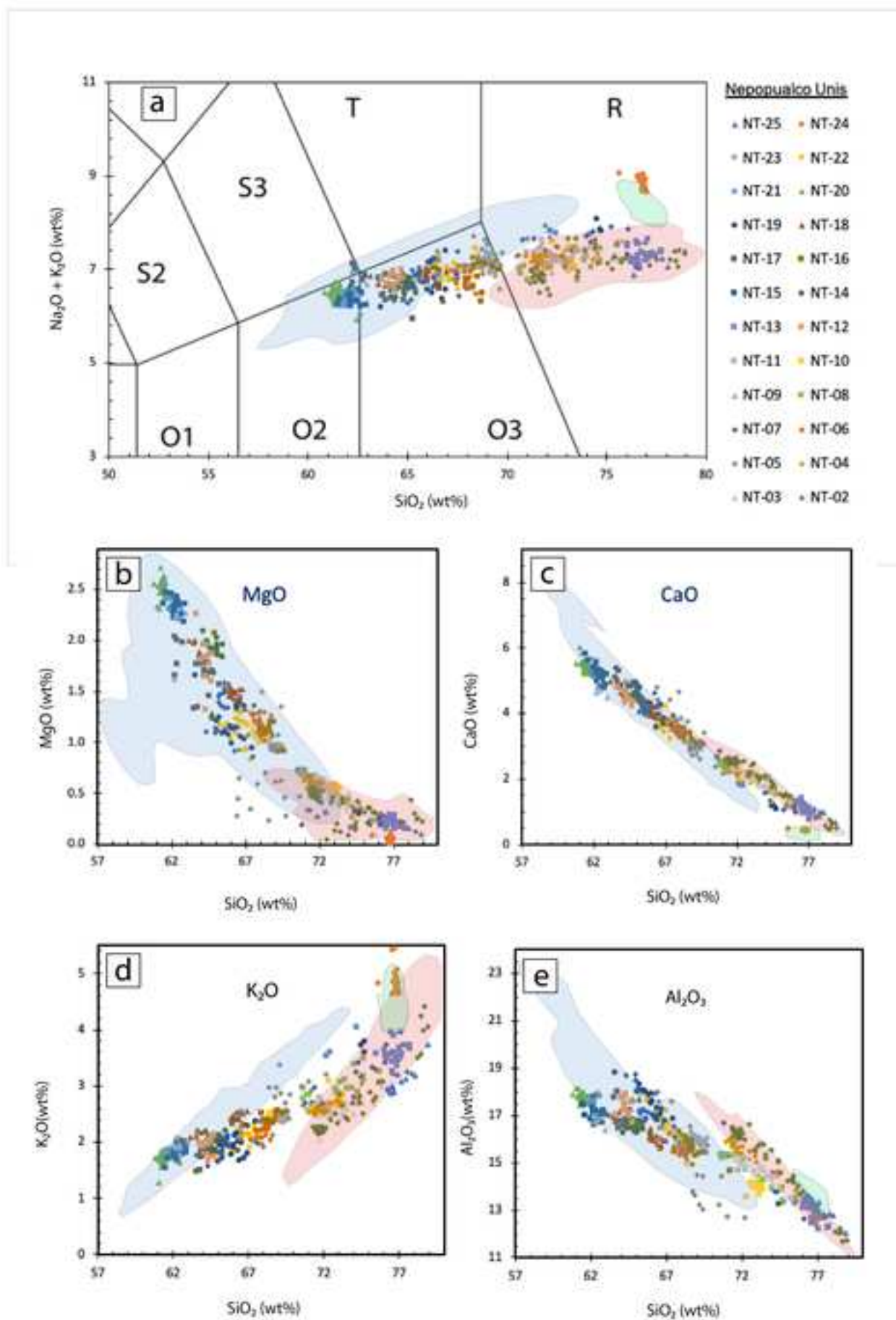


Fig 12

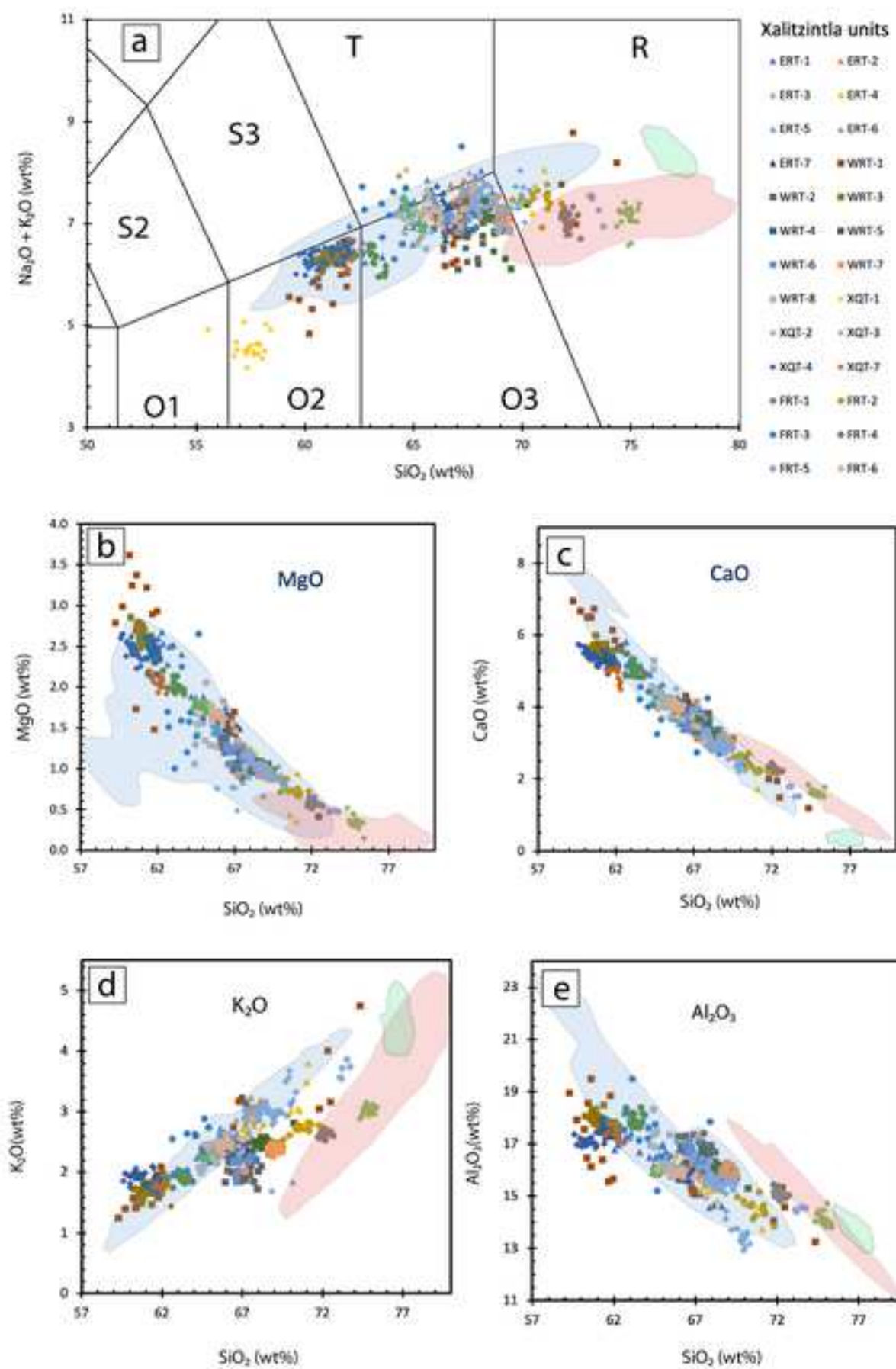


Fig 13

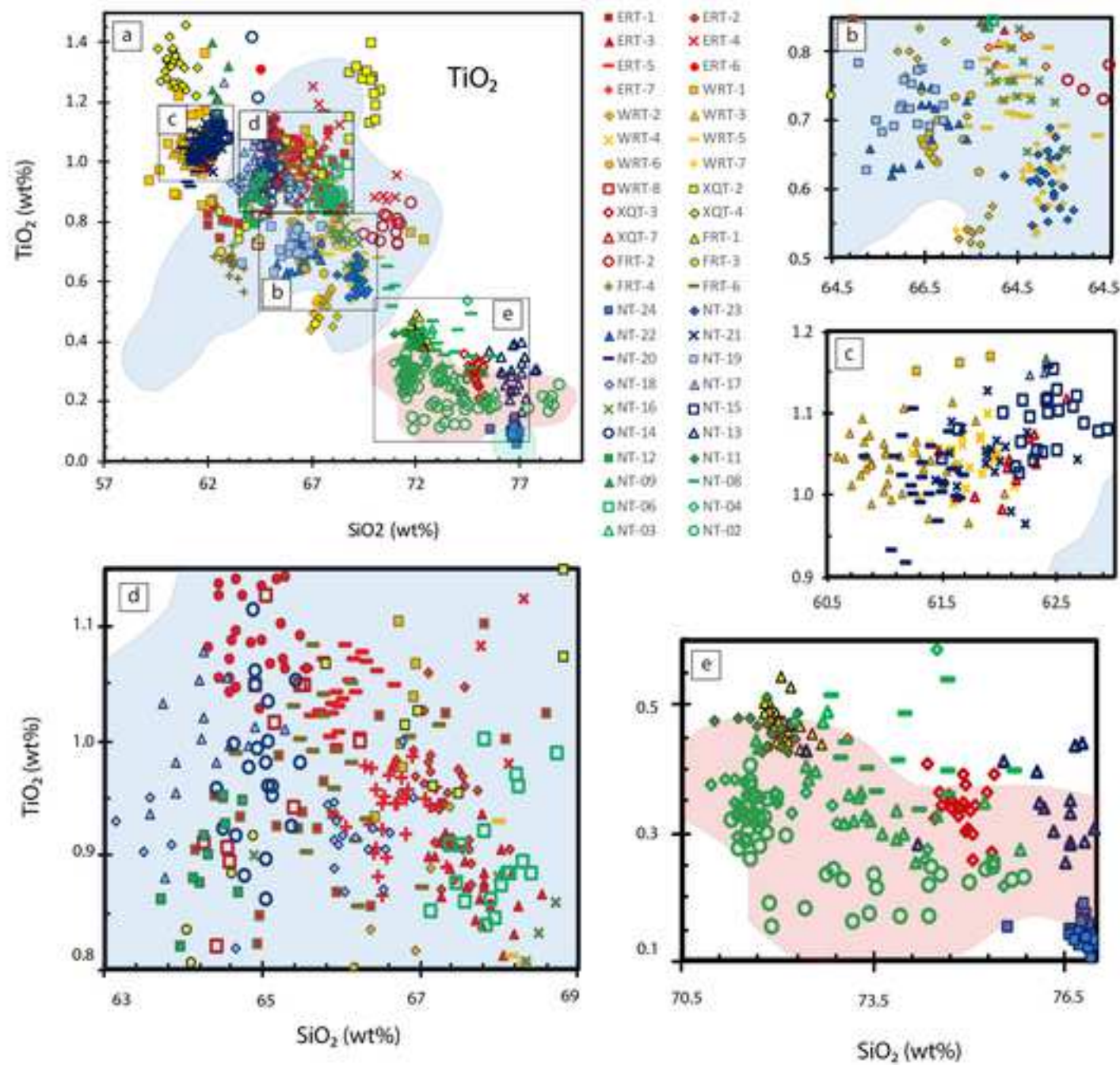


Fig 15

[Click here to access/download;Figure;Fig.15_volcanic history of SNVR.png](#)

